Model for the Viscosity of Particle Dispersions

Jozef Bicerano[a]; Jack F. Douglas[b]; Douglas A. Brune[a]

[a] Dow Chemical Company, M. E. Pruitt Research Center, Midland, MI, U.S.A. [b] Polymers Division, Polymer Blends and Processing Group, National Institute of Standards and Technology, Gaithersburg, MD, U.S.A.

PLEASE SCROLL DOWN FOR ARTICLE

Model for the Viscosity of Particle Dispersions

JOZEF BICERANO,[1,*] JACK F. DOUGLAS,[2,*] and
DOUGLAS A. BRUNE[1]

[1]Dow Chemical Company
M. E. Pruitt Research Center
1702 Building
Midland, MI 48674

[2]National Institute of Standards and Technology
Polymers Division
Polymer Blends and Processing Group
Gaithersburg, MD 20899

*To whom correspondence should be addressed.

1. INTRODUCTION

The difficulty in processing filled materials is often a limiting factor in advanced materials development because of the large changes in fluid viscosity observed in these materials. It is widely appreciated that the shear viscosity η tends to rise rapidly with increasing filler aspect ratio A_f and volume fraction Φ [1–4]. Moreover, the increase in η for fluids containing highly anisotropic filler particles can sometimes be much larger than the increase in stiffness (Young's modulus) for these same filler particles dispersed at the same Φ in a solid polymer matrix [5, 6]. Such large viscosity increases cause important limitations in the processing of filled polymers. (These limitations have been discussed specifically in the case of polyurethane elastomers filled with cellulosic microfibers [5, 6].) It is also important for process modeling to account for the large shear thinning effects found in anisotropic particle dispersions. These shear thinning effects have their origins in particle orientation, in the breakup of particle clusters under flow conditions, and in the non-Newtonian flow properties of the entangled polymer fluid matrix.

A predictive model of the viscosity of filled polymers is evidently a significant challenge for theory as well as for engineering practice. Such a model, with broad potential applicability to dispersions of fillers of different shapes dispersed in different types of fluids, is developed in the present work. Particular emphasis is given to dispersions of platelet-shaped particles because of their wide availability in the form of clays and the commercial interest in dispersing such anisotropic particles in polymers.

The literature relevant to describing the viscosity of filled polymers is both multidisciplinary and vast in scope. It includes publications in mathematics (especially percolation theory and fractals), geology (especially structures and interlayer energies of clays) and biology (especially the movement of microorganisms in various environments) and the more familiar types of resources in

physics, chemistry, rheology, and polymer science. Hundreds of empirical, semiempirical, and theoretical relationships have been developed for the η of dispersions as a function of the volume fraction, particle shape, and, to a more limited extent, shear rate $\dot{\gamma}$. Although a historical survey of this literature is not attempted in the present paper, we review the literature that was helpful in developing our own model. We also indicate important reference works that we think industrial scientists will find useful. The following publications treat key aspects of dispersion viscosity. In an engineering-oriented review, Mewis and Macosko [1] discussed the rheological constitutive equations for dilute dispersions of fibers and platelets. These authors also considered the influence of particle-particle interactions, which can stabilize a dispersion or lead to flocculation for predominantly repulsive or attractive interparticle forces, respectively. Metzner [2] reviewed the viscosity of particle dispersions in polymeric liquids. These fluid "matrices" can be non-Newtonian even in the absence of fillers, and these dispersions can thus have complications not found in fluids more nearly identified as Newtonian. Russel [3] and Israelachvili [7] discussed the role of interparticle forces in dispersion viscosity. Brenner [4] provided convenient numerical tabulations of intrinsic viscosity data as a function of the shear rate for axisymmetric particles having a range of shapes.

We show below that key information about dispersion shear viscosity can be obtained using simple modeling and the concepts of universality and scaling. The arguments for invoking universality and scaling ideas are based on a number of mathematical and phenomenological observations. Our development of a general expression for η of particle dispersions is based on recent theory that indicates a direct relationship between the electrical conductivity and the shear viscosity of dilute dispersions of particles having general shape [8]. More specifically, it was found that the intrinsic viscosity $[\eta]$ divided by the trace of the average electric polarizability tensor is an invariant to a good approximation, so that $[\eta]$ is roughly proportional to the intrinsic conductivity [8]. (A general relation between conductivity and fluid viscosity was advocated long ago by London [9] in the context of a discussion of the viscosity of liquid helium.) This connection between the conductivity and the viscosity of a dispersion is argued to hold more generally, but in a modified form, at higher particle volume fractions. It is well known that, when the particles are either far more or far less conductive than the dispersing matrix, percolation theory can be applied to describe the conductivity of particle dispersions with "universal" scaling relations in terms of the particle volume fraction relative to a critical "percolation" value of Φ^* and critical exponents. The argued correspondence between the viscosity and conductivity of dispersions predicts that viscosity data can be organized similarly and understood in terms of the concepts of percolation theory. We will thus speak of the "viscosity percolation threshold" and invoke universality

concepts to justify applying these theoretical expressions for η to arbitrarily shaped filler particle dispersions.

It must be admitted at the onset of our development that some difficulties exist in invoking universality ideas from percolation theory to describe real materials. The problem revolves around the translation of results shown to hold in lattice percolation calculations to off-lattice applications. Some authors [10–12] have suggested that the critical exponents describing the conductivity of off-lattice materials are not strictly universal, while Heaney [13] has suggested that "crossover" effects can explain the exponent deviations that are sometimes observed experimentally. (These crossover effects are associated with data taken not sufficiently close to the critical percolation volume fraction of Φ*, at which the critical scaling of the conductivity with the volume fraction difference Φ − Φ* should actually be observed.) Despite this lack of perfect confidence in utilizing lattice percolation properties in modeling real materials, the observed deviations of the conductivity exponent relevant to our discussion of viscosity modeling are commonly small [13]. Thus, we utilize results from lattice percolation theory and ignore these complications in our discussion below, which is devoted to developing a good qualitative description of the viscosity of filled polymer liquids.

A universal expression (with platelets, spheres, and fibers as very important special cases) is obtained for η(dispersion) relative to the dispersing fluid. This reduced viscosity is a function of the reduced volume fraction (Φ/Φ*), where Φ* is the *viscosity percolation threshold*. The maximum packing volume fraction Φ_m is then used as an approximation for Φ* and estimated by scaling arguments relating Φ_m to the geometrical percolation threshold p_c. The model is also extended to treat the effects of shear, temperature, particle flexibility, and particle aggregation in fractal clusters. The results of these model calculations are illustrated with several examples, including comparisons with experimental data for clay-filled polymers.

2. VISCOSITY OF POLYMER FLUIDS

Theoretical expressions for η(dispersion) are usually expressed as a product of the dispersing fluid viscosity with a dimensionless function of the volume fraction Φ of the dispersed particles and of other relevant parameters, such as the dimensionless shear rate and temperature. The description of polymer fluid dispersions is complicated by the strong dependence of η(dispersion) on flow conditions and material parameters. Since we are particularly interested in filled polymer fluids, we summarize briefly some of the basic phenomenology for the viscosity of polymer fluids. This discussion is based on a general description of η(polymer) as a function of material parameters given by Bicerano [14].

The zero-shear viscosity η_0 of a pure polymer is a function of the absolute temperature T and of the weight-average molecular weight M_w.[1] Its behavior is described roughly in terms of three material parameters: the glass transition temperature T_g, the activation energy for viscous flow as defined in the high-T and zero-shear limits $E_{\eta\infty}$, and a critical molecular weight M_{cr}. The η_0 of a pure polymer generally increases roughly linearly with (M_w/M_{cr}) for $M_w \leq M_{cr}$ and roughly proportionally to $(M_w/M_{cr})^{3,4}$ for $M_w > M_{cr}$. The η_0 of a pure polymer decreases rapidly with increasing (T/T_g), following a steep and nearly universal variation as a function of (T/T_g) for $1.0 < (T/T_g) \leq 1.2$. Above this temperature range, it approaches as Arrhenius-like dependence, namely, $\eta_0 \sim \exp(E_{\eta\infty}/RT)$. Although this Arrhenius-like behavior is only approached at very high T, the value of $E_{\eta\infty}$ affects the slope and the curvature of $\ln(\eta_0)$ versus $1/T$ above the region of universal behavior by fixing the slope in the asymptotic high-temperature regime.

Both η_0(polymer) and η(polymer) can decrease by many orders of magnitude as M_w decreases and/or as T increases. However, the lowering of many important performance characteristics in polymers of low molecular weight, along with limitations of practical fabrication equipment, do not allow the lowering of η(polymer) to reduce η(dispersion) sufficiently for many processes.

The viscosities of polymer fluids can manifest significant dependencies on the shear rate $\dot{\gamma}$ and the polydispersity [the M_w/M_n) ratio, where M_n denotes the number-average molecular weight], as well as having a small dependence on the density of the polymer at the temperature of the melt. At low shear rates, η is nearly independent of $\dot{\gamma}$, and this plateau in the variation of η with $\dot{\gamma}$ is termed the *first Newtonian regime*. As $\dot{\gamma}$ is increased further, however, a "shear-thinning" regime is reached, at which η can drop by several orders of magnitude relative to η_0. Fabrication processes are typically performed either in the first Newtonian regime or in the shear thinning regime. At exceedingly high $\dot{\gamma}$ values (achieved in laboratory-scale experiments, but thus far not in any practical polymer fabrication processes), a "second Newtonian regime" (η reaching a new plateau value, generally far below η_0) may be reached unless the polymer degrades first by shear-induced bond rupture. A large drop of η(polymer) obviously can make a large contribution to the overall shear-thinning effect on η(dispersion).

In many dispersions, much of the total shear thinning originates from the breakdown of transient particle clusters. It is unclear whether and how this important source of shear thinning might couple to the entanglement phenomena

---

[1]According to ISO-31-8 [15], the term *molecular weight* has been replaced by the technically more correct term *relative molecular mass*. The older, more conventional notation for number-average and weight-average molecular weights is utilized in this article.

of unfilled polymers. Furthermore, when polymer chains are confined between highly anisotropic platelet-shaped fillers that are closer to each other than the average radius of gyration of a chain, the average conformational characteristics (including the M_{cr}) of the polymer may change relative to the "unperturbed" dimensions even in the zero-shear limit. The standard assumption that η(polymer) enters into all equations for η(dispersion) as a simple factor multiplying an expression consisting of terms dependent only on particle characteristics implies the neglect of such potential perturbations of the polymeric matrix by the particles. While this tremendous simplification is justified in the quest for a preliminary model aimed at reproducing the major trends observed in η(dispersion), the future development of more refined models may require consideration of these complications.

For most commodity polymers, extensive amounts of experimental data are available for the dependence of η(polymer) on material parameters and differing flow conditions. If such a full "viscosity profile" [η(polymer) as a function of all relevant parameters] has not been measured, it can be estimated very roughly using the phenomenological equations of Bicerano [14]. If at least some data are available for η(polymer), the equations can be calibrated with these data to provide more reliable predictions of η(polymer).

3. DISPERSION VISCOSITY AT LOW CONCENTRATIONS

3.1. Viscosity Virial Expansion

The viscosity of a dilute particle dispersion, η(dispersion), can be developed formally in a power series in the particle volume fraction Φ. Since this procedure is completely analogous to the development of a power series describing the pressure of a gas, it is conventional to refer to such expansions as *virial expansions* and to their coefficients as *virial coefficients*. Such power series must be truncated at some finite order (as in Eq. 1) because the difficulty of the calculation of the virial coefficients grows rapidly with increasing order.

$$\eta(\text{relative}) \equiv \frac{\eta(\text{dispersion})}{\eta(\text{dispersing fluid})} \approx 1 + [\eta]\Phi + k_H \cdot \Phi^2 + \ldots \tag{1}$$

In the limit of infinitesimal particle volume fraction ($\Phi \rightarrow 0$), the term linear in Φ dominates so that the effect of the filler on the change in η is proportional to [η]. As Φ increases, higher-order terms become important. [The expansion then becomes generally less useful since the lower-order terms are no longer sufficient to reproduce η(relative), and it is exceedingly difficult to develop nonempirical models to estimate the coefficients of the higher-order terms.] The first virial coefficient [η] is usually called the *intrinsic viscosity* in the rheology

literature, while the next virial coefficient k_H is termed the *Huggins coefficient*. These quantities are dimensionless, given the dimensionless nature of the property ratio and the concentration units. The reader should be aware of the fact that virial expansions usually are expressed in the polymer solution literature (and occasionally also in the dispersion literature) in terms of powers of the mass concentration (grams of dispersed phase per unit volume of solution) instead of powers of Φ, so that $[\eta]$ and k_H often have units of specific volume and specific volume squared, respectively. Moreover, there are several conventions for these mass concentration units that have been introduced as a matter of experimental convenience or historical usage.

3.2. Dilute Concentration Regime

The dilute concentration regime is limited to Φ values for which the linear approximation $\eta(\text{relative}) \approx 1 + [\eta]\Phi$ holds. This designation of the dilute regime range is appropriate because the calculation of this leading order virial expansion does not depend on interparticle interactions. Even for spherical particles, the "crossover volume fraction" Φ_x defining the boundary between the dilute regime and the semidilute regime is small (in the range 0.01 to 0.02 [16]; see Sections 3.5 and 6.3). More generally, we can expect Φ_x to scale roughly in proportion to $k/[\eta]$, where k is a proportionality constant with a value that depends on the units chosen for $[\eta]$. Thus, Φ_x decreases very rapidly for highly anisotropic particles, namely, roughly in proportion to $1/A_f^2$ for rods (fibers) and to $1/A_f$ for disks (platelets) (see Section 3.4), where A_f is the aspect ratio. The dilute regime is limited to very low volume fractions for highly anisotropic particles.

3.3. Concentrated and Semidilute Dispersions

A dispersion of filler particles is defined as "concentrated" for Φ greater than the geometrical percolation threshold p_c. The value of p_c is determined by the random placement of idealized particles that are allowed to overlap and defines the volume fraction of space occupied by the overlapping particles when they first span the region in which they are placed. (Monte Carlo simulations of p_c are discussed below.) This volume fraction is important because particles are expected to form large contracting clusters at $\Phi \approx p_c$. Motions in such dispersions are necessarily collective, but a dispersion continues to be "fluidlike" until interparticle interactions cause contacting particles to become "stuck" into a rigid array. At a value of Φ that we will denote by Φ^* (usually $\Phi^* \gg p_c$), the necessity for collective motions becomes strong enough to cause a transition from a highly viscous fluid to a true solid for which $\eta \to \infty$. The semidilute regime is defined to include the broad volume fraction range between Φ_x (at

which the interparticle interactions first become appreciable) and p_c (at which they begin to predominate). In practice, however, it is difficult to perform equilibrium viscosity measurements for volume fractions Φ greater than a "glass transition" volume fraction of about 0.53 to 0.57 for hard sphere dispersions.

In systems with strong attractive interactions between the particles, flocculation may occur (as discussed below in detail), and a large fraction of the particles may associate into relatively diffuse aggregate structures so that the p_c and the Φ^* of the aggregated particles can be reached at much lower volume fractions than those of the primary particles. Thus, the concentration regimes become dependent on interparticle interactions in these aggregating systems. The effective sizes of the particles can also be modified by long-range coulombic repulsive interactions (see Section 9.2) and by the segregation of the polymer and the other components of a multicomponent fluid to the interfaces of the dispersed particles.

3.4. Intrinsic Viscosity and Influence of Particle Shape on the Viscosity of Dilute Particle Dispersions

Douglas and Garboczi [8] derived an approximation relating the intrinsic viscosity $[\eta]$ for dispersions of anisotropically shaped rigid particles and the leading concentration virial for the conductivity (intrinsic conductivity) of an insulating medium with highly conducting inclusions. In testing this relationship, they tabulated data for the $[\eta]$ of dilute dispersions of ellipsoidal particles over a large A_f range and discussed these data particularly for the special case of ellipsoids of revolution to illustrate the magnitude of the shape dependence of $[\eta]$. We briefly review the results of this analysis.

For a biaxially symmetric ellipsoid, Douglas and Garboczi [8] define the "aspect ratio" $A_f = (c/a)$ as a measure of particle asymmetry. Here, c is the length of the symmetry axis (major axis) of the ellipsoid, and $a = b$ is the length of its two degenerate minor axes, so that $A_f > 1$ for prolate ellopsoids (approximating fibers), $A_f = 1$ for spheres, and $A_f < 1$ for oblate ellipsoids (approximating platelets). Exact results for $[\eta]$ are listed in Table 1 and are shown graphically in Fig. 1. Equation 2 gives a good fit to the data for $0.001 \leq A_f \leq 1000$ and is also shown in Fig. 1.

$$[\eta] \approx \frac{1012 + 2904A_f - 1855A_f^{1.5} + 1604A_f^2 + 80.44A_f^3}{1497A_f + A_f^2} \tag{2}$$

It is emphasized that, while Eq. 2 interpolates $[\eta]$ over the practically important range of $0.001 \leq A_f \leq 1000$, it should not be used to extrapolate too far outside this A_f range since it does not give the correct asymptotic scaling behavior $[\eta] \sim A_f^2/\ln(A_f)$ as $A_f \to \infty$. Equation 2 is adequate for most practical applications,

TABLE 1

Exact Results for Isotropically Averaged [η] of Dilute Dispersions and p_c Calculated by Monte Carlo Simulations of Random Dispersions [73] for Ellipsoids of Revolution [Ellipsoids with Two Symmetrically Equivalent Axes ($a = b$)]

A_f	[η]	p_c	A_f	[η]	p_c
0.0005	—	0.000637	1.5	—	0.2795
0.001	—	0.001275	2	2.908	0.2618
0.003333	204.9	—	3	3.685	0.2244
0.01	69.10	0.01248	4	4.663	0.1901
0.02	35.16	—	5	5.806	0.1627
0.04	18.19	—	6	7.099	—
0.05	14.80	—	7	8.533	—
0.055556	13.45	—	8	10.10	—
0.0625	12.10	—	9	11.80	—
0.071429	10.74	—	10	13.63	0.08703
0.083333	9.391	—	12	17.67	—
0.1	8.043	0.1058	14	22.19	—
0.111111	7.371	—	16	27.18	—
0.125	6.700	0.1262	18	32.63	—
0.142857	6.032	—	20	38.53	0.04150
0.166667	5.367	—	25	55.19	—
0.2	4.708	0.1757	30	—	0.02646
0.25	4.059	0.2003	50	176.8	0.01502
0.333333	3.431	0.2289	100	593.7	0.006949
0.5	2.854	0.2629	200	—	0.003195
0.75	—	0.2831	300	4279	0.002052
1	2.500	0.2854	500	—	0.001205

$A_f = (c/a)$, where c is the length of the third ellipsoidal axis. $A_f < 1$ for oblate ellipsoids, which approximates platelets at large $1/A_f$. $A_f = 1$ for spherical particles. $A_f > 1$ for prolate ellipsoids, which approximates fibers at large A_f.

however, since filler particles with asymmetries outside the specified range are uncommon.

For particles under steady shear, one must consider [η] as a tensor rather than as a scalar quantity because of the tendency of anisotropic particles to orient under shear. The results shown in Fig. 1 for [η] represent the dependence of the shear viscosity on the particle shape in the limit of an infinitely dilute dispersion at low $\dot{\gamma}$ at which the so-called rotary Peclet number Pe is small (not
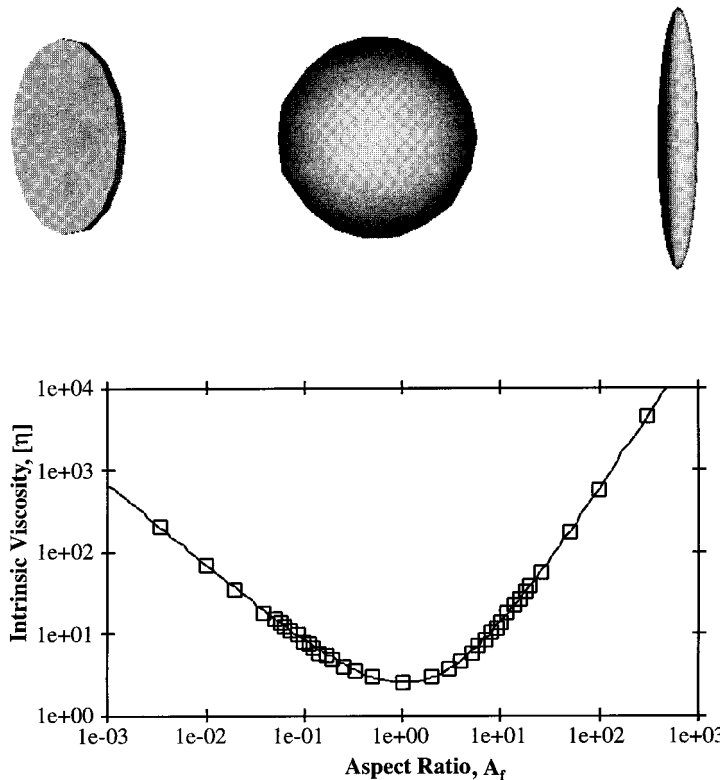
FIG. 1. Isotropically averaged [η] of dilute dispersions of ellipsoids of revolution. The aspect ratio is defined as $A_f = (c/a)$, where c is the length of the ellipsoid along its axis of symmetry and $a = b$ is the length of the ellipsoid in the normal direction. $A_f > 1$ corresponds to prolate ellipsoids (top right, approximating fibers at large A_f), $A_f = 1$ to spherical particles (top middle), and $A_f < 1$ to oblate ellipsoids (top left, approximating platelets at large $1/A_f$). In the bottom figure, squares indicate exact results [8], and the curve represents a fit to the squares (Eq. 2).

larger than 1). *Pe* is a dimensionless shear rate defined as the ratio of the time-scales for rotary Brownian motion and convective motion:

$$Pe = \frac{\dot{\gamma}}{D_r} = \frac{6V \cdot \eta(\text{dispersing fluid}) \cdot F \cdot \dot{\gamma}}{k_B T} \qquad (3)$$

Here, D_r is the rotational diffusion coefficient, k_B is Boltzmann's constant, T is the absolute temperature, V is the particle volume, and F is a particle shape factor (a function of A_f for biaxially symmetric particles [4]). D_r is important because the particle orientation at low Φ is determined by the balance between hydrodynamic forces and rotary Brownian motion. At low Pe, rotary Brownian motion randomizes the particle orientations so that Eq. 2 provides a good description of $[\eta]$. At high Pe, hydrodynamic forces become strong enough to align the particles in the flow direction, reducing their contribution to η(dispersion) in dilute dispersions. This shear thinning effect on $[\eta]$ vanishes for spherical particles and increases with particle shape asymmetry. As $\dot{\gamma} \to \infty$, an anisotropic particle becomes fully aligned with the flow field so that $[\eta]$ levels off to a limiting value of $[\eta]_\infty$. The dependence of $[\eta]$ on $\dot{\gamma}$ for axisymmetric particles such as needles and disks can be estimated using an established formalism developed by Brenner [4]. These useful results are also discussed in an accessible review article by Mewis and Macosko [1].

Figure 2 illustrates $[\eta(\dot{\gamma})]$ for biaxially symmetric particles in terms of its dependence on the dimensionless shear rate Pe. It is seen that the variation of $[\eta(\dot{\gamma})]$ with shear is smooth and gradual, and that it becomes larger with increasing particle asymmetry.

The exact results for $[\eta(\dot{\gamma})]$ are rather cumbersome because the results are given for selected values of A_f in the form of a numerical tabulation. We ob-
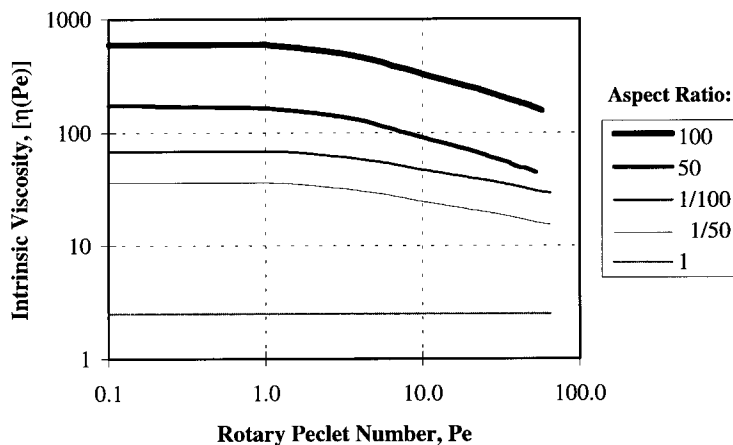
FIG. 2. Effect of shear on intrinsic viscosity $[\eta]$ of ellipsoids of revolution as a function of the rotary Peclet number (Pe). See the legend of Fig. 1 for the definition of A_f. As $Pe \to \infty$, $[\eta]$ decreases slowly to $[\eta]_\infty$ in each case. Curves are labeled by A_f values.

serve, however, that (1) $[\eta(\dot{\gamma})]$ is invariant to the shear direction and is thus always an even function of $\dot{\gamma}$, and (2) $[\eta(\dot{\gamma})]$ approaches constant values as $\dot{\gamma} \rightarrow 0$ and as $\dot{\gamma} \rightarrow \infty$. A useful "Padé approximant" for $[\eta(\dot{\gamma})]$, constructed to be consistent with these mathematical properties, is given in Section 7.6. Our analytic approximation for $[\eta(\dot{\gamma})]$ is extended in Section 7.6 to other properties that share the analytic properties of $[\eta(\dot{\gamma})]$ but cannot currently be calculated exactly.

It is tempting to describe shear thinning by scaling relations based on the dependence of $[\eta]$ on Pe, but this dependence will often not extrapolate well to higher Φ for three reasons:

1. Interparticle collisions may reduce the particle alignment, and thus reduce the amount of shear thinning, in the semidilute regime.
2. Geometrical packing constraints tend to impose some alignment on the particles even in the absence of shear at high Φ values, enhancing the total particle alignment effect in the concentrated regime (see Section 9.2).
3. Attempts to extrapolate from the shear thinning behavior of $[\eta]$ to shear thinning at higher values of Φ must necessarily be restricted to highly anisotropic particles (fibers of aspect ratio A_f and platelets of aspect ratio $1/A_f$, where $A_f \geq 10$) because they neglect some types of much smaller shear-induced ordering effects observed even for spherical particles.

3.5. Huggins Coefficient as a Measure of Interparticle Interaction

While many reliable experimental data and theoretical derivations are available for $[\eta]$ as a function of the particle shape, such information is relatively scarce for the Huggins coefficient k_H. This situation is unfortunate since k_H contains important information about particle shape and interparticle interactions. We begin our discussion by considering spherical particle dispersions for which the understanding of the behavior of k_H is most advanced.

Many attempts have been made to calculate k_H for noninteracting hard spheres. Calculations not taking Brownian motion into account [17–19] underestimate k_H, while the first calculations accounting for Brownian motion [20, 21] overestimated it. Batchelor [22] incorporated both effects by including both open particle trajectories arising from straining motions and closed trajectories arising from simple shear flow and allowing for translational Brownian motion. He found $k_H \approx 6.2$ (with 5.2 from hydrodynamic effects and 1.0 from Brownian motion). Others [23, 24] recently published the revised estimate $k_H = 5.9147$ (with 5.0022 coming from hydrodynamic effects and 0.9125 from Brownian motion).

Furthermore, k_H is also very sensitive to the strength and nature of interparticle interactions. For hard spheres with a short range attractive interaction (some-

times called "sticky hard spheres") it has been proposed [25] that $k_H = (21.4 - 12.2\bar{\Psi})$. Here, $\bar{\Psi}$ is the dimensionless second osmotic virial coefficient. $\bar{\Psi} = 1$ in the limit of a vanishing attractive interparticle contact interaction (i.e., in a good solvent), and $\bar{\Psi} = 0$ at the "theta point" at which attractive interparticle interactions balance the hard core repulsions of the spheres (i.e., a poor solvent). (The results given in Ref. 25 have been converted into a dimensionless form consistent with the conventions of the present paper.) The sticky sphere value of k_H more than triples, from 6.2 for repulsive spherical particles to 21.4 for mildly attractive particles at the theta point, indicating a substantial dependence of k_H on interparticle interactions. The effects of including the $k_H\Phi^2$ term in Eq. 1 are shown in Fig. 3 for hard spheres. The concentration at which these curves separate defines the volume fraction Φ_x. We observe that Φ_x is insensitive to the interparticle interaction, provided that the interparticle interaction is predominantly repulsive.

The trends described above for dilute and semidilute hard-sphere dispersions are rather general. Similar trends are found for flexible polymer chains in solu-
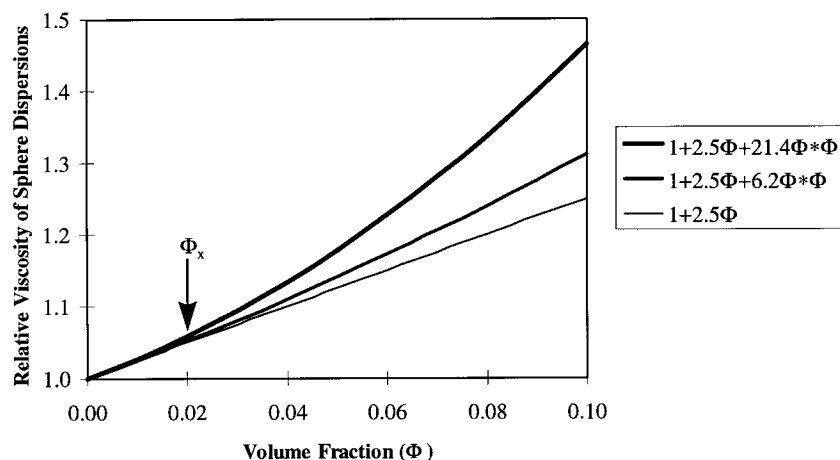
FIG. 3. Effects of the term proportional to Φ^2 in Eq. 1 for the viscosity of dispersions of spherical particles. "Relative viscosity" denotes η(dispersion)/η(polymer). The lowest (thin) curve only considers the first-order term in the virial expansion (Einstein limit). The middle (thick) curve includes the second-order term in the limit of vanishing contact interaction (good solvent). The uppermost (very thick) curve includes the effect of the second-order term at the theta point (poor solvent). The dilute regime extends up to the onset of the semidilute regime at $\Phi_x \approx 0.02$.

tion (obviously a very different type of system than hard spheres), for which k_H increases monotonically with decreasing solvent quality. The decrease for flexible polymers is by more than a factor of two; specifically, k_H changes from a value near $0.3[\eta]^2$ in a good solvent to a value near $0.7[\eta]^2$ under theta conditions [26]. The generality of the solvent quality dependence of k_H suggests some degree of regularity in the interaction dependence of this type of property.

The virial coefficients of other transport properties also depend strongly on the thermodynamic interparticle interaction. For example, the leading virial coefficient k_D for the collective diffusion coefficient D_c of a particle dispersion even changes sign with changing solvent quality, that is, $k_D(\text{spheres}) \approx 4 \Psi - 2.5$, and a similar variation is again found for k_D of polymer solutions [27, 28]. Evidently, k_D and k_H can acquire a significant temperature dependence, especially in mixed solvents near their critical point for phase separation. This sensitivity offers a good way of estimating the basic interparticle thermodynamic interaction parameter Ψ. This parameter can also be estimated by light- or neutron-scattering measurements under favorable circumstances.

Very little work has been done to develop theoretical estimates of k_H for nonspherical particles. Berry and Russel [29] indicate that $k_H \sim 0.5[\eta]^2(1 - 0.0142Pe^2 + \ldots)$ for slender cylindrical fibers. On the other hand, Shaqfeh and Fredrickson [30] found an alternative result as $A_f \to \infty$ for cylindrical fibers; namely, $k_H \sim A_f^4/[\ln(A_f)]^3 \sim [\eta]^2/\ln(A_f)$. Extension of these results to anisotropic particles and particles with attractive interactions is a serious theoretical challenge. More work is needed on this important problem.

Very little work has been done to develop theoretical estimates for the higher-order coefficients of the virial expansion of $\eta(\text{relative})$ for particles of arbitrary shape because of the extreme computational difficulty of this task. In a valiant attempt based on multiple scattering theory (taking only hydrodynamic effects into account), Thomas and Muthukumar [19] estimated a value of 6.4028 for the third virial coefficient (which multiplies Φ^3) of η for hard spheres.

It is clear from the discussion above that the rigorous treatment of the viscosity of particle dispersions is limited to low-order virial expansions, and that even those virial expansion results are generally unavailable for interacting nonspherical particles. Even if we had this kind of information to a few orders in perturbation theory, the concentration range in which these results can be applied becomes increasingly small with increasing particle anisotropy. We clearly need some nonperturbative framework for treating the high-concentration regime, which can be combined with the perturbative virial expansion to treat the viscosity of particle dispersions over a wide concentration range. In the next section, we develop an analogy between the electrical conductivity and the viscosity of particle dispersions that allows us to utilize ideas from percolation theory to develop an expression for $\eta(\text{dispersion})$ for general Φ and particle shape.

4. PERCOLATION MODELING OF DISPERSION VISCOSITY AT HIGH CONCENTRATIONS

4.1. Approximation for Viscosity in Semidilute and Concentrated Dispersions

A good approximation can be obtained for η in the semidilute and concentrated regimes ($\Phi_x \leq \Phi \leq \Phi^*$) in terms of (1) the viscosity of the pure dispersing fluid, (2) the A_f and Φ of the dispersed particles, and (3) a particle-shape-dependent critical volume fraction Φ^*. The formal extension of the relationship found by Douglas and Garboczi [8] between the viscosity of dispersions of rigid particles and the conductivity of dispersions of highly conducting particles leads one to expect (see the discussion in Section 4.2) the following asymptotic relationship for high-volume fractions ($\Phi \rightarrow \Phi^*$):

$$\eta(\text{relative}) \approx K \cdot \left(1 - \frac{\Phi}{\Phi^*} \right)^{-2} \tag{4}$$

In Eq. 4, $\Phi^* \approx \Phi_m \approx 0.64$ for monodisperse spheres [1, 31], Φ^* decreases rapidly with increasing particle anisotropy (discussed below), and K is a proportionality constant on the order of 1, with a value that will be fixed below. See Fig. 4 for a depiction of Eq. 4 over the entire reduced volume fraction range, $0 \leq (\Phi/\Phi^*) \leq 1$, where K is fixed by the approximation $K = 1$ in the present discussion.

4.2. Analogy Between Electrical Conductivity and Viscosity and Its Theoretical Ramifications

The analogy between the hydrodynamics and electrostatics of dilute dispersions [8] can be generalized to finite volume fractions by relying on a phenomenological observation. At intermediate volume fractions $\Phi > \Phi_x$, it is observed that the velocity field of pipe flow characteristically becomes flattened so that a more nearly sliplike boundary condition is obtained for dispersion flow [32, 33]. In the electrostatic problem, this boundary condition would correspond to the problem of insulating particles in a conducting medium. The critical exponent for the particle "fluidity" ($1/\eta$), conductivity in the resulting hydrodynamics-electrostatics analogy at nonvanishing volume fractions, then has the approximate values of 2 and 4/3 in three and two dimensions, respectively. The mean-field value of this "insulator exponent" is 3, so that crossover effects associated with Φ not being sufficiently close to Φ^* might give rise to an effective exponent closer to 3 in Eq. 4 in fits to experimental data restricted to intermediate volume fractions [13].
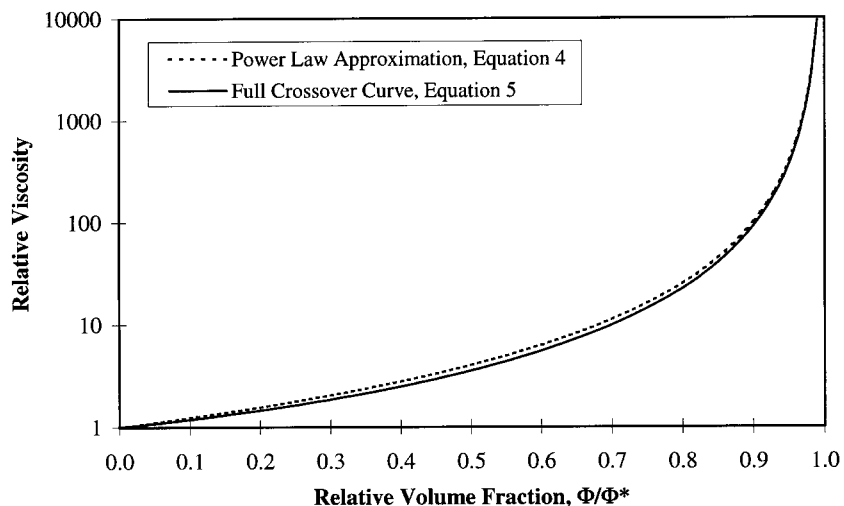
FIG. 4.   Dispersion viscosity "master curves." The "asymptotic form" (Eq. 4) originally developed for the concentrated regime and the "universal form" (Eq. 5) for the full volume fraction range are seen to be almost indistinguishable for most practical purposes. "Relative viscosity" denotes η(dispersion)/η(polymer). "Relative volume fraction" denotes Φ/Φ^*.

Previously, de Gennes [34] made arguments for a hydrodynamic-electrostatic analogy to describe the concentration dependence of dispersion viscosity. He indicated that the percolation exponent for conducting particles in an insulating medium described the fluidity of dispersions, but his predictions were later found to be inconsistent with dispersion viscosity measurements [35]. Experiments on quasi-two-dimensional dispersions obtained by suspending small spherical particles in a thin layer of oil spread on a water surface give an exponent near 4/3 [36], close to the two-dimensional insulating particle percolation exponent for conductivity. This finding is consistent with the prediction for two dimensions mentioned above. A correspondence between [η] for rigid particles and the conductivity virial coefficient for conductive particles is reasonable at low Φ values, however, and the explicit calculations of Douglas and Garboczi [8] confirm this relation.

It is emphasized that the extension of this analogy between the viscosity and the electrical conductivity of concentrated particle dispersions is based on a phenomenological observation (velocity field flattening in concentrated dispersions) that lacks a theoretical explanation. Our extension of the hydrodynamics-electrostatics analogy is thus phenomenological. Further theoretical work is

needed to justify this approximation, but at present we are satisfied that this approximation is physically sensible and is in accordance with observations on these complex fluids.

4.3. Observations Supporting the Percolation Model-Scaling Expression for Dispersion Viscosity

Equation 4 has been invoked for many years as an empirical description of the η of diverse types of dispersions, such as of irregular coal particles and anisotropic particles in polymer fluids, and even of flocculated particle dispersions. Some examples found in the literature are cited below.

Russel and Sperry [37] found that Eq. 4 can be applied to hard sphere dispersions of fractal aggregates if the reducing volume fraction variable Φ^* is modified appropriately. They assumed that Φ^* of the aggregated particles should equal $\Phi^* \approx \Phi_{mp} \cdot N^{1-(3/d)}$ where d is the fractal dimension of the aggregates, N is the average number of particles per aggregate, and Φ_{mp} is the "packing volume fraction" Φ_m of the primary (nonaggregated) particles composing the aggregate. The scaling expression for Φ^*(aggregate) utilized by Russel and Sperry is well known in polymer science literature, in which the power law scaling represents the average inverse segmental density of the fractal aggregates. For specificity, we note that the fractal dimension d equals 2 for flexible polymer chains and slender platelet filler particles, so that we have the nontrivial scaling $\Phi^* \sim N^{-1/2}$. Identical dimensional analysis arguments also apply to the intrinsic viscosity $[\eta]$ of particle aggregates, which scales inversely to the average segmental density of the aggregate, so that we have the approximate scaling relation $\Phi^* \sim 1/[\eta]$. Evidence supporting this scaling relation is discussed in Section 7.2. These trends are also in general agreement with a wide range of observations on the internal structures and dimensions of fractals [38].

It is emphasized that the use of Eq. 4 and the scaling expression of Russel and Sperry for Φ^* has some limitations. The expression is restricted to relatively "strong" aggregates that do not disintegrate at low shear rates. It is also evident that this modeling cannot apply if the aggregates form percolating structures with a scale comparable to the dimensions of the measuring instrument. If Eq. 4 is still to apply even approximately, then Φ^* must saturate for some sufficiently large N value. In our modeling of aggregation effects on η in Section 7.8, we argue that Φ^* saturates to the value p_c, $\Phi^* \to p_c$, and we denote the characteristic number of particles within the aggregate at which this crossover occurs as N_x.

These scaling arguments for Φ^* have ramifications for the concept of "occluded volume" in aggregating dispersions. It is not really the volume of fluid within the aggregate that is important in influencing the viscosity of the dispersion; it is rather the effectiveness of the aggregate to screen its interior from the

flow field that determines $[\eta]$ and thus Φ^*. The occluded volume effect is understood more properly in terms of the screening of hydrodynamic interactions by the aggregate structure.

Wildemuth and Williams [39] showed that Eq. 4 agrees well with data for a remarkable range of materials (irregular-shape coal particles, latex spheres, and aluminum particles). The data covered over two orders of magnitude of variation in solvent viscosity and in particle size and five orders of magnitude in the shear rate $\dot{\gamma}$ variation. They observed that the increase of Φ^* is a direct function of the shear stress $\tau \equiv \eta \, \dot{\gamma}$ rather than the shear rate $\dot{\gamma}$ and represents the effects of τ on Φ^* in terms of a simple model with two adjustable parameters, developed by considering the effects of τ on the relative rates of microstructural breakup and reformation. They also developed a simple model [39] for the yield stress τ_y [40] of concentrated dispersions, which we generalize in Section 7.7 based on our dispersion viscosity model.

Kataoka et al. showed that Eq. 4 represents well the dependence of η on Φ for dispersions in polymeric fluids of spherical particles [41], calcium carbonate and talc particles of unspecified A_f [42], and carbon and glass fibers of A_f up to 28 [42, 43]. Pal and Rhodes [44] showed that the η of emulsions containing dispersed phase volume fractions of less than 0.74 also obeys the concentration scaling relation for the reduced η of hard spheres with appropriate adjustment of Φ^*. De Kruif et al. [45, 46] provided data of high quality for η(dispersion) for model spherical particle dispersions, obtained by both Couette and parallel plate rheometry, for both low and high shear rates. This work is considered in connection with our modeling in the next section. Van Blaaderen et al. [47] used some of these data [46] to show an inverse relationship between η(dispersion) and the long-time self-diffusion coefficient (measured by fluorescence recovery after photobleaching) of dispersed spherical colloidal particles.

Finally, Chong, Christiansen, and Baer [48] collected experimental data for dispersions of spherical particles from many different literature sources and also obtained their own data with an orifice viscometer. They plotted all of these data (which included the effects of the polydispersity of the particle sizes) on a single graph (Fig. 11 of their paper). They then fitted these data with their own empirical expression for η(relative) as a function of (Φ/Φ^*). Their expression differed from Eq. 4, but inspection of Fig. 11 from their paper shows that the data can be described just as well by Eq. 4, especially in the concentrated regime in which Eq. 4 is appropriate.

Brady [49] considered both hydrodynamic and Brownian contributions to the macroscopic stress of a dispersion of Brownian hard spheres to develop a simple model by which Eq. 4 with Φ^* corresponding to random close packing is obtained at high concentrations.

The combined consideration of all of these results shows the broad applicability of Eq. 4 or an equation closely approximating it. This equation appears to

have been introduced first as a phenomenological expression by Maron and Pierce [50], so engineers sometimes refer to it as the "Macron-Pierce equation."

A rough inverse relationship is usually found between the Φ^* and the A_f of dispersed particles [2, 23, 24, 43]. It is commonly assumed that the dependence of Φ^* on the particle shape is similar to the dependence of Φ_m [51]. Within the hydrodynamic-electrostatic analogy discussed above, the characteristic volume fraction at which η(dispersion) approaches infinity is identified as a "viscosity percolation threshold." For a given particle shape, Φ_m is apparently smallest if all particles are of equal size. It increases with increasing polydispersity since the smaller particles can often fit in the gaps between the larger particles, approaching 1 for a very broad particle size distribution. For dispersions of platelet-shaped particles obtained by exfoliating clays, as well as other types of layered materials, the degree of exfoliation of the platelets should also have a major impact on the value of Φ^*. Clumps of platelets (which occur naturally in clays) should have a Φ^* value comparable to compact particles, while Φ^* for dispersed particles must be small for extended platelets. Attractive interparticle interactions can also influence Φ^* if these interactions are strong enough to cause particle aggregation [3]. These effects are discussed below.

4.4.   Influence of Shear on the Viscosity Percolation Threshold Φ^*

Shear can also induce particle ordering, so that Φ^* can increase with shear [39]. For example, for monodisperse hard spheres, the critical volume fraction $\Phi^* \approx 0.63$ for the approach of the viscosity to infinity as $\dot{\gamma} \to 0$ is near the random close packing value of 0.64. However, it increases to $\Phi^* \approx 0.71$ at high shear rates ($\dot{\gamma} \to \infty$), near the maximum close packing value of 0.7405 for a face-centered cubic lattice [45, 46]. This result suggests some degree of shear-induced ordering of the spheres under flow. Notably, Eq. 4 provides a good description of the viscosity under steady shear, provided that the volume fraction is not too high (see the discussion at the end of this section).

Ackerson [52] performed an instructive study of shear-induced ordering. He prepared nearly hard poly(methyl methacrylate) spheres that were sterically stabilized against aggregation by surface modification, dispersed them in a mixture of tetralin and decalin, and used light scattering to observe the interparticle ordering (microstructure) under steady and oscillatory shear flows. He observed four basic types of structures: (1) liquidlike (amorphous), (2) stringlike (disordered layers in which regular spacing of particles persists along the velocity direction), (3) sliding or randomly stacked layers, and (4) face-centered cubic (layers stacked in a specific close-packed pattern). The microstructure depended on Φ, as well as on $\dot{\gamma}$, under steady shear and on the amplitude and the frequency of the shear flow under oscillatory shear. In fact, it could be represented in the

form of microstructural phase diagrams as a function of Φ and $\dot{\gamma}$ under steady shear and as a function of Φ and the shear amplitude under oscillatory shear, both for spherical particle dispersions [45, 46] and for a variety of other particle shapes [39].

As a final point about the influence of $\dot{\gamma}$ on η(dispersion), we note that, for very high shear rates, we can expect interparticle collision processes to have an increasingly disruptive effect on particle ordering, which would lead to a decrease of Φ^*. Shear dilatancy and shear thickening would be symptomatic of this regime. Woodcock [53] has proposed an explanation of shear thickening in dispersions based on this concept of "shear-induced disordering." This effect has important implications for the processing of dispersions of anisotropic particles and deserves further study.

5. GENERAL EXPRESSION FOR DISPERSION VISCOSITY

A crossover formula applicable in the dilute, semidilute, and concentrated regimes ($0 \leq \Phi \leq \Phi^*$), Eq. 5, is next proposed for hard spheres; it is based on the hydrodynamics-conductivity analogy discussed above and the exact virial expansion (Eq. 1). The coefficients of (Φ/Φ^*) and $(\Phi/\Phi^*)^2$ inside the square brackets are fixed by the requirement that Eq. 5 should reduce to Eq. 1 in the dilute regime ($\Phi \to 0$), with $[\eta] = 2.5$, $k_H = 6.2$ [22] and $\Phi^* \approx \Phi_m \approx 0.64$. It also reduces to the asymptotic scaling indicated by the percolation model (with the prefactor modified to $K = 0.94$) in the concentrated regime ($\Phi \approx \Phi^*$). Finally, it can also be extended to dispersions of interacting particles by replacing the coefficient of 0.34 with a more general expression that takes into account the dependence of the Huggins coefficient k_H (Section 3.5) on the dimensionless second-order osmotic coefficient $\bar{\Psi}$.

$$\eta(\text{relative}) \approx \left(1 - \frac{\Phi}{\Phi^*}\right)^{-2} \cdot \left[1 - 0.4 \cdot \left(\frac{\Phi}{\Phi^*}\right) + 0.34 \cdot \left(\frac{\Phi}{\Phi^*}\right)^2\right] \qquad (5)$$

This type of approximant, involving a power law leading term with corrections to the leading power law scaling, is accurate in many applications (e.g., the pressure dependence of the volume of hard sphere fluids [54]). Universality arguments, as well as the experimental evidence summarized above for the validity of the simpler Eq. 4 [which gives similar predictions for η(relative)] in representing experimental data for dispersions of particles having a wide variety of shapes, lead us to expect that Eq. 5 (with the appropriate value of Φ^* inserted to account for particle anisotropy, shear-induced ordering, and any aggregation effects) should be a good approximation for nonspherical particles as well.

In the discussion below, we try to show that Eq. 5 provides a predictive model of broad applicability, satisfying a number of essential characteristics for such a model:

1. It reproduces well the observed trends for η(relative) as a function of the particle shape (for all particle shapes), volume fraction (over the entire range of $0 \leq \Phi \leq 1$), and flow conditions.
2. It goes to the correct asymptotic limits, with η(relative) reducing to the virial expansion (Eq. 1) as $\Phi \rightarrow 0$ and to an expression (in our preference, Eq. 4) that predicts η(relative) $\rightarrow \infty$ at some value of Φ (i.e., Φ^*) at which the dispersion loses its "fluidity."
3. It only uses physically meaningful parameters that can be measured and/ or predicted as a function of the properties of the dispersing fluid or the dispersed material, the dispersion microstructure, and the flow conditions.

Anticipating our further discussion showing the generality of Eq. 5, Table 2 lists η(relative) calculated as a function of (Φ/Φ^*). Figure 4 shows that Eqs. 4 and 5 depend similarly on (Φ/Φ^*) over the volume fraction range $0 < \Phi < \Phi^*$.

It was discussed above that Eq. 4 has been validated experimentally against data [37, 39–48] involving dispersions of fillers with a great diversity of particle shapes, sizes, and size distributions (including fractal aggregates) and obtained at many different shear rates. The fact that Eq. 5 also reduces to the correct limiting form (Eq. 1) in the dilute solution limit is an obvious improvement. Some of the best available experimental data, obtained by de Kruif et al. [45], are plotted in a normalized form in Fig. 5 and compared with Eq. 5. The data were normalized by dividing Φ by the Φ^* values (0.63 for $\dot{\gamma} \rightarrow 0$ and 0.71 for $\dot{\gamma} \rightarrow \infty$) suggested by de Kruif et al. [45] to obtain η(relative) as a function of (Φ/Φ^*) for each data series.

The effects of fractal aggregation, as incorporated into Eq. 5, are illustrated in Fig. 6, which shows the results of calculations at several N and d values. These results were obtained using Russel and Sperry's estimate for Φ^* [37], $\Phi^* = \Phi_{mp} \cdot N^{1-(3/d)}$, where Φ_{mp} is the maximum packing fraction Φ_m of the particles in the absence of aggregation. The limitations of this approximation are discussed in Section 7.8. It is seen that the effect of fractal aggregate size on Φ^* is highly nonlinear. Incorporation of even the very small fractal clusters of $N = 5$ results in a substantial increase of η(relative). As N is increased further, the rate of increase of η(relative) with N slows gradually. The effect of reducing the "fractal dimension" d (more "open" aggregates) is even more drastic.

Next, we make some preliminary comments about the physical meaning of the maximum packing fraction Φ_m and its relation to Φ^*. As discussed above, a dispersion is necessarily considered to be concentrated for $\Phi > p_c$, where p_c is the geometrical percolation threshold, since an "infinite cluster" of dispersed

TABLE 2

Relative Viscosity η(dispersion)/η(polymer) as a Function of
Relative Volume Fraction Φ/Φ* Calculated Using Equation 5

Φ/Φ*	Relative viscosity	Φ/Φ*	Relative viscosity	Φ/Φ*	Relative viscosity	Φ/Φ*	Relative viscosity
0.01	1.016258	0.26	1.678203	0.51	3.683607	0.76	15.49278
0.02	1.033045	0.27	1.720372	0.52	3.836528	0.77	16.89198
0.03	1.050384	0.28	1.764383	0.53	3.999574	0.78	18.48876
0.04	1.068299	0.29	1.810343	0.54	4.173648	0.79	20.32186
0.05	1.086814	0.30	1.858367	0.55	4.359753	0.80	22.44000
0.06	1.105957	0.31	1.908578	0.56	4.559008	0.81	24.90510
0.07	1.125756	0.32	1.961107	0.57	4.772666	0.82	27.79679
0.08	1.146238	0.33	2.016097	0.58	5.002132	0.83	31.21889
0.09	1.167436	0.34	2.073701	0.59	5.248983	0.84	35.30875
0.10	1.189383	0.35	2.134083	0.60	5.515000	0.85	40.25111
0.11	1.212112	0.36	2.197422	0.61	5.802196	0.86	46.29918
0.12	1.235661	0.37	2.263910	0.62	6.112853	0.87	53.80746
0.13	1.260069	0.38	2.333757	0.63	6.449569	0.88	63.28444
0.14	1.285376	0.39	2.407186	0.64	6.815309	0.89	75.48050
0.15	1.311626	0.40	2.484444	0.65	7.213469	0.90	91.54000
0.16	1.338866	0.41	2.565797	0.66	7.647958	0.91	113.2783
0.17	1.367145	0.42	2.651534	0.67	8.123287	0.92	143.7150
0.18	1.396514	0.43	2.741970	0.68	8.644688	0.93	188.1767
0.19	1.427029	0.44	2.837449	0.69	9.218252	0.94	256.7844
0.20	1.458750	0.45	2.938347	0.70	9.851111	0.95	370.7400
0.21	1.491739	0.46	3.045075	0.71	10.55165	0.96	580.8400
0.22	1.526062	0.47	3.158085	0.72	11.32980	0.97	1035.451
0.23	1.561791	0.48	3.277870	0.73	12.19734	0.98	2336.340
0.24	1.599003	0.49	3.404975	0.74	13.16840	0.99	9372.340
0.25	1.637778	0.50	3.540000	0.75	14.26000	1.00	∞

Tables and graphs of η(dispersion) as a function of Φ can be generated for a specific dispersion from this master table by multiplying Φ/Φ* with the value of Φ* and the relative viscosity with the value of η(polymer) appropriate for that dispersion.

particles can be expected to span the fluid at a comparable volume fraction. The fraction of dispersed particles belonging to these particle clusters increases with Φ. At $\Phi = \Phi_m$, the particle mobility has been reduced to such an extent that the dispersion behaves "solid-like," and η(relative) → ∞. Apparently, this is a kind of rigidity percolation threshold [55]. As Φ is increased further (i.e., as solvent molecules are removed, for example, by evaporation during solvent casting of
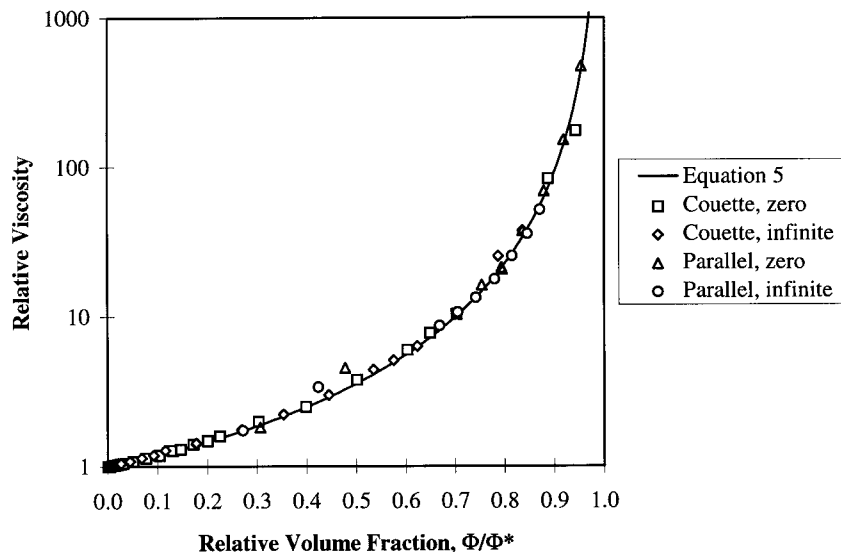
FIG. 5. Comparison of the behavior predicted from the universal form (Eq. 5) developed in this manuscript with the data tabulated by de Kruif et al. [45] for the viscosity of dispersions of sterically stabilized hard silica spheres in cyclohexane. There are no adjustable parameters in Eq. 5. "Relative viscosity" denotes η(dispersion)/η(cyclohexane). "Relative volume fraction" denotes Φ/Φ^*. "Couette" and "parallel" refer to measurements with a Couette rheometer and with a parallel plate rheometer, respectively. "Zero" and "infinite" refer to the limits of $\dot{\gamma} \to 0$ and $\dot{\gamma} \to \infty$, respectively.

fabricated articles), $\Phi > \Phi_m$, and the dispersion becomes an increasingly rigid solid with a nonvanishing shear modulus G. Ultimately, if all remaining solvent is removed, the limit of $\Phi \to 1$ can be approached if the particles are polydisperse in size [56, 57], anisotropic in shape (see below), or deformable [58].

Particle flexibility effects on η(dispersion) can also be important for highly anisotropic particles, such as thin platelets and slender fibers, which are subject to large bending moments. The "flexural rigidity" of such a particle is less than that of more isotropic particles even when the particle is intrinsically very stiff (i.e., has a very high modulus). At the other extreme, we can have dispersions for which the dispersed phase is a fluid and the particle flexibility exerts an evident influence on the dispersion viscosity. These issues are addressed in sections below because of their importance to clay particle dispersions. It is shown that η(dispersion) can still be considered within the framework of Eq. 5 if the flexible dispersed particles retain their structural integrity (do not undergo liq-
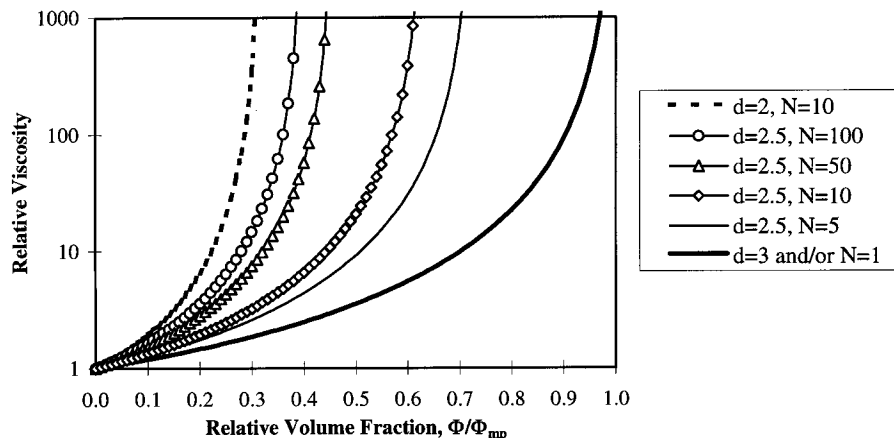
FIG. 6. Effects of fractal aggregation on Φ^* according to Eq. 5 combined with the scaling relationship $\Phi^* \approx \Phi_{\text{maa}} \cdot N^{1-(3/d)}$, which is valid for $N \leq N_x$. N denotes the average number of particles per aggregate, d denotes the fractal dimension, and "relative viscosity" denotes $\eta(\text{dispersion})/\eta(\text{polymer})$. "Relative volume fraction" denotes Φ/Φ_{mp}, where Φ_{mp} is the value of Φ_m in the absence of aggregation. Scaling Φ by Φ_{mp} allows us to illustrate the relative effects of aggregation independently of the particle shape.

uidlike processes such as breakup into smaller particles or coalescence into larger particles).

6. Φ^*, PERCOLATION, AND PARTICLE PACKING

6.1. Geometrical Versus Transport Property Percolation Thresholds

It is important to distinguish purely geometrical quantities, such as the geometrical percolation threshold p_c and the maximum packing fraction Φ_m, from transport property "percolation thresholds" (such as Φ^* for the shear viscosity) measured by observing the onset of a rapid variation of dispersion properties. We recall that p_c is only defined for overlapping particles, while real particles often do not have this property. Interparticle and polymer-particle interactions and the physical properties of the particles relative to their environment also influence the measured transport percolation thresholds. The viscosity and other properties (such as conductivity and dielectric constant) of dispersions tend to change substantially as the dispersed material forms a connected structure so that a relation between p_c and transport percolation thresholds might be ex-

pected. This connection has only been established rigorously for idealized lattice models of conductivity under specialized conditions. Many questions remain open for continuum systems, which often provide a much better description of real materials.

6.2. Background Information on the Geometrical Percolation Threshold p_c

We first cite some basic sources that describe percolation theory and provide information relevant to our model. We then summarize some recent contributions to percolation theory that are useful for understanding properties of dispersions of anisotropic (especially platelet-shaped) particles.

The books by Zallen [59] and Stauffer and Aharony [60] are excellent general references on percolation theory. The former has a more physical emphasis, while the latter has a more mathematical emphasis. The book by Hughes [61] also summarizes much useful information relating to past studies of percolation theory.

Early Monte Carlo simulations of the p_c of fibers with random orientations in the three principal axis directions were performed by Boissonade, Barreau, and Carmona [62] on a simple cubic lattice, and conductivity percolation thresholds of 0.0904 and 0.0635 of highly conducting fillers were found for A_f of 10 and 15, respectively, with the conductivity percolation threshold decreasing roughly in inverse proportion to A_f in the simulated range (1 to 15). This trend is in agreement with the more extensive numerical calculations of p_c summarized in the next subsection.

The percolation of aligned platelets was addressed both experimentally and theoretically by Celzard et al. [63–65]. They studied the electrical conductivity of partially oriented composite films made from an epoxy resin matrix filled with slender micron-size exfoliated graphite platelets of $A_f \approx 100$. They found a low apparent conductivity percolation threshold of 0.013 (i.e., 1.3% by volume) for these anisotropic filler particles. In their latest paper [65], they also addressed the effects of platelet orientation on conductivity percolation threshold due to excluded volume interactions. They showed that this threshold increases rapidly as the maximum angular orientation between the disks is reduced, in other words, as the disks are oriented parallel to each other. Their calculations illustrate a method by which orientation effects potentially could be included in the calculations of the conductivity percolation threshold.

The angular orientation between the platelets can be sensitive to A_f and Φ, to the nature of the dispersing medium, and to the actual sizes of and the total charge on the platelets [66]. Random, highly aligned, and various types of stacked orientations are possible. Furthermore, the imposition of a shear field can result in the alignment of the platelets [32, 67, 68], in depletion of the

platelets from the vicinity of the walls of the flow medium [32], and in damped oscillations of the orientation distribution in the early stages of shearing [69]. Consequently, under favorable combinations of polymer and platelet type and $\dot{\gamma}$, both p_c and Φ^* could increase relative to their values for random dispersions, resulting in shear thinning and extending both the onset of the concentrated regime and the acceptable processability range above the expectation from the values of p_c and Φ^* calculated for a random dispersion.

Balberg [70] indicated that the criteria for the onset of percolation in the continuum are usually based on considering parallel-aligned, equal-size, penetrable, convex objects. He presented criteria for more general macroscopically isotropic or anisotropic systems in which the objects may also be of variable sizes and of totally random orientation (rather than randomly oriented along a few selected directions, such as parallel to the edges and diagonals of a model lattice). He found that percolation could occur at much lower p_c for these model systems.

Fizazi et al. [71] prepared conducting gels of ultrahigh molecular weight polyethylene and a soluble conjugated polymer by thermoreversible gelation from semidilute solutions in decalin and subsequent doping with iodine. They found evidence of connected conducting paths at $\Phi[\text{poly[3-octylthiophene]}] \sim 0.0005$, with no indication of an "ordinary" p_c. They discussed these results in terms of the adsorption of poly(3-octylthiophene) onto a preformed polyethylene gel network that organizes this conductive material into connected paths. Levon, Margolina, and Patashinsky [72] introduced the concept of "multiple percolation." They visualized percolation occurring in the restricted regions allowed to the constrained particles, reducing p_c from its bulk value. In phase-separating blends, this restricted domain is the phase to which the conducting particles segregate.

We next consider trends in the dependence of p_c on particle shape.

6.3. Shape Dependence of p_c and Its Relation to $[\eta]$

The baseline quantity in all of these considerations is the p_c of a dispersion of randomly placed filler particles as a function of A_f. The results of Monte Carlo simulations of p_c by Garboczi et al. [73] for ellipsoids of revolution are tabulated in Table 1 and are represented graphically in Fig. 7. These results are reproduced very well by Eq. 6 [73] over the entire A_f range used in the simulations ($A_f > 1$ for fibers, $A_f = 1$ for spheres, and $A_f < 1$ for platelets):

$$p_c \approx \frac{9.875A_f + A_f^2}{7.742 + 14.61A_f + 12.33A_f^{1.5} + 1.763A_f^2 + 1.658A_f^3} \tag{6}$$
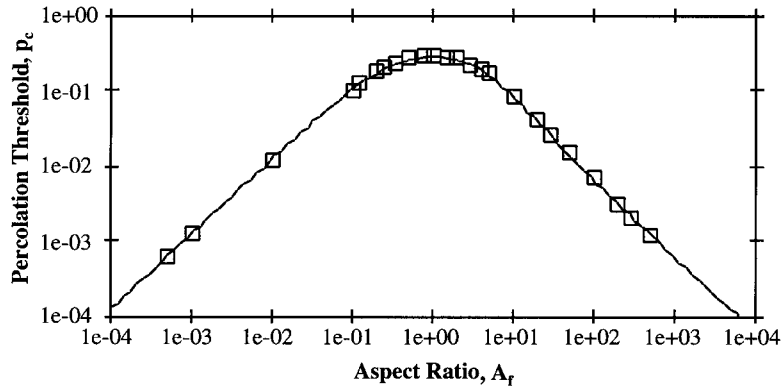
FIG. 7. The p_c of randomly dispersed ellipsoids of revolution [73]. See the legend of Fig. 1 for the definition of A_f. The squares show p_c values calculated by Monte Carlo simulations. The curve represents a fit to the squares (Eq. 6).

The A_f dependence of p_c looks quite symmetric between fibers and platelets, but careful inspection of the results shows that, just as $[\eta]$ increases more rapidly with A_f for fibers (Fig. 1), p_c decreases more rapidly as a function of A_f for fibers. The increase of $[\eta]$ in Fig. 1 is roughly the inverse of the decrease of p_c in Fig. 7. This interesting relation between the infinite dilution quantity $[\eta]$ and the geometric percolation threshold p_c (marking the onset of the concentrated regime) is shown in Fig. 8. It is evident that particle anisotropy both facilitates particle percolation and causes a corresponding increase of η(dispersion) in dilute dispersions.

The rough inverse relation between p_c and $[\eta]$ also follows from the observation that the virial expansion for the conductivity σ of a dispersion of conductive particles has the form of Eq. 1, where $[\sigma]_\infty$ is the intrinsic conductivity (leading virial coefficient for the electrical conductivity of highly conductive particles [8]). We obtain a rough criterion for the conductivity percolation threshold by the condition that the leading-order perturbation term in the expansion $[\sigma]_\infty\Phi$ is on the order of unity. (This estimate of the order of magnitude for the location of the scaling regime is similar to the Ginzburg criterion of critical phenomena [74].) Thus, the conductivity percolation threshold is predicted to scale roughly as $1/[\sigma]_\infty$. Douglas and Garboczi [8] found that $[\eta]$ is proportional to $[\sigma]_\infty$ to a good approximation (this is the basic result of the hydrodynamic-electrostatic analogy discussed in Section 4.2), so that the viscosity percolation threshold Φ^* should likewise scale as $1/[\eta]$ according to this argument [73]. The approximate proportionality between p_c and Φ^* suggests a proportional relation between p_c

(a) p_c as a function of $[\eta]$.

(b) p_c as a function of reciprocal of $[\eta]$.
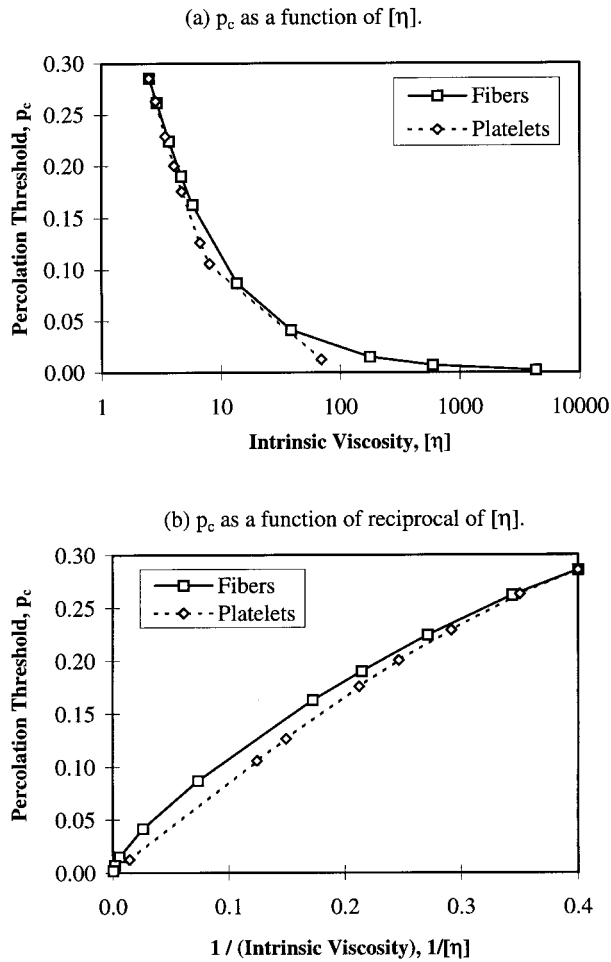
FIG. 8. Correlation between exact results [8] for intrinsic viscosity $[\eta]$ (describing rheological effects of fillers at infinite dilution) and geometrical percolation threshold p_c (defining onset of concentrated regime) values calculated by Monte Carlo simulations [73] for platelets and fibers.

and Φ^* to a reasonable approximation. This approximation is utilized as a working hypothesis in Section 7 for estimating Φ^* of anisotropic particle dispersions.

Finally, it is worth pointing out some preliminary calculations that could form the basis for modeling how the "random close packing fraction" Φ_m relates to the geometrical percolation threshold p_c. Lee and Torquato [75a] considered the p_c of partially overlapping disks, with the "core" of each disk impenetrable while the "shell" can overlap. They found that, as the core size of the disks is increased, p_c increases with the excluded volume interaction and seems to approach the random close packing volume fraction Φ_m as the disks become impenetrable. Bug et al. [75b] also considered whether interactions increase or decrease p_c. They used Monte Carlo simulations to show that increased interaction strength can either increase or decrease p_c. The direction and the magnitude of the change depends in a complex manner on the distance at which two particles are considered to be connected, the dimensionality, and the temperature. Further calculations along these lines would be useful in establishing the mathematical definition of the random close packing volume fraction Φ_m and its variation with shape.

7. VISCOSITY PERCOLATION THRESHOLD Φ^* AND DISPERSION GELATION

7.1. Importance of Φ^* for Dispersion Processing

Although p_c is an indicator of the onset of collective particle motions, the onset of dispersion rigidity manifests itself at a higher volume fraction Φ^* [76, 77]. Hence, while p_c often can provide a good estimate of the upper volume fraction limit of "easy processability" for a dispersion, a more refined estimate for η(dispersion) can be made using Eq. 5 in the concentrated regime of $p_c \leq \Phi < \Phi^*$ if we know Φ^*. The estimation of the viscosity percolation threshold Φ^* as a function of the relevant material and flow parameters is then the basic challenge in developing a predictive model for dispersion shear viscosity for process design. In the discussion that follows, we generally identify Φ^* with the random close packing volume fraction Φ_m. This quantity can be estimated for particles of general shape, in dispersions subjected to a wide variety of flow conditions, by combining geometrical percolation data and experimental particle-packing data.

7.2. Estimating Φ_m from p_c Data and Experimental Particle-Packing Data

It can be expected that Φ_m for randomly distributed particles of arbitrary shape at close packing should correspond to the volume fraction at which the viscosity approaches infinity. Intuitively, the rigidity percolation threshold Φ^*

should decrease with increasing particle asymmetry just as p_c does. These expectations are supported by the numerical results and theoretical arguments given in Section 6.3. An assumption of a proportional relation between p_c and Φ_m and experimental data for certain particle shapes allows us to predict Φ_m in cases for which experimental data are not yet available.

The correlation between Φ_m and A_f was investigated for cylindrical fibers [78, 79]. Using raw spaghetti "fibers" of a single diameter over the range $6.8 \leq A_f \leq 143$ and also including data from other authors for packings of cylindrical glass fibers, chopped glass strands, and wooden rods, Parkhouse and Kelly [79] found experimentally (and rationalized by a mathematical derivation) that Eq. 7 holds, with "ln" denoting the natural logarithm, so that both p_c and Φ_m vary roughly in inverse proportion to the largest particle dimension as $A_f \rightarrow \infty$.

$$\Phi_m \approx \frac{2 \cdot \ln(A_f)}{A_f} \qquad \text{(fibers with } A_f \geq 10\text{)} \tag{7}$$

Since the maximum random packing volume fraction $\Phi_m \approx 0.64 \pm 0.02$ apparently occurs for spherical particles ($A_f = 1$) [80], while $2\ln(A_f)/A_f$ reaches a maximum of 0.736 for $A_f = 2.718$ and goes to zero as $A_f \rightarrow 1$, Eq. 7 cannot be extrapolated much below the A_f range of the data used to develop it. Parkhouse and Kelly [79] suggested that it may be a fair approximation down to $A_f = 6$. In developing our scaling arguments, we assume that Φ_m is proportional to p_c with the same factor for a fiber of aspect ratio A_f and a platelet of aspect ratio $1/A_f$. This assumption gives Eq. 8, which can only be used safely in combination with Eq. 7 down to $A_f \sim 10$ because the asymptotic large-A_f dependence of Eq. 7 is restricted to this range.

$$\Phi_m(\text{platelet}) \approx \Phi_m(\text{fiber}) \cdot \frac{p_c(\text{platelet})}{p_c(\text{fiber})} \tag{8}$$

Values of p_c, calculated by Monte Carlo simulations in many cases (Table 1) and by Eq. 6 otherwise, and Φ_m, calculated by Eq. 7 for fibers of $A_f \geq 10$, can be inserted into Eq. 8 to estimate Φ_m for platelets of $(1/A_f) \leq 0.1$. The results are listed in Table 3 and are shown in Fig. 9, including the result for spheres. It is seen that, at a given anisotropy level, platelets give a somewhat larger Φ_m than fibers. Consequently, Eq. 5 indicates that, if Φ_m is substituted for Φ^*, then as shown in Figs. 10 and 11, a platelet dispersion should have a somewhat lower η than a fiber dispersion at the same anisotropy level. Note that Φ_m is calculated directly for cylindrical fibers, but estimated for cylindrical platelets by a scaling relation based on the p_c values for ellipsoidal particles with biaxial symmetry and the same value of A_f.

TABLE 3

Maximum Packing Volume Fraction Φ_m of Randomly Dispersed
Ellipsoidal Particles with Biaxial Symmetry [Ellipsoidal Particles with
Two Symmetrically Equivalent Axes ($a = b$)]

A_f	Φ_m	A_f	Φ_m	A_f	Φ_m	A_f	Φ_m
0.000100	0.003906	0.01	0.165836	10	0.460517	150	0.066808
0.000500	0.015985	0.02	0.255495	15	0.361073	200	0.052983
0.001000	0.028957	0.025	0.315987	20	0.299573	300	0.038025
0.001563	0.042022	0.033333	0.340745	25	0.257510	400	0.029957
0.002000	0.052440	0.04	0.401921	30	0.226746	500	0.024858
0.003125	0.073876	0.05	0.443958	40	0.184444	640	0.020192
0.003333	0.078293	0.070711	0.508663	50	0.156481	1000	0.013816
0.004419	0.096982	0.1	0.559838	80	0.109551	2000	0.007601
0.005000	0.104772	1	0.640000	100	0.092103	10000	0.001842

In this notation, $A_f = (c/a)$, where c is the length of the third axis of the ellipsoid, so that $A_f > 1$ for prolate ellipsoids (approximating fibers at large A_f), $A_f = 1$ for spherical particles, and $A_f < 1$ for oblate ellipsoids (approximating platelets at large $1/A_f$). The Φ_m values for fibers are calculated using an empirical correlation (Eq. 7). The experimental Φ_m value is used for spheres. A scaling relationship (Eq. 8) is used to calculate Φ_m for platelets.

The hypothesis that Eq. 5 holds for objects of general shape and even for dispersions subject to steady shear provides an interesting prediction for the viscosity percolation threshold Φ^*. This prediction can be checked against packing data, as well as viscosity measurements, if we take $\Phi^* \approx \Phi_m$. To obtain such an approximation, we expand Eq. 5 in the low volume fraction limit to obtain $\eta(\text{relative}) \approx 1 + (1.6)\cdot(\Phi/\Phi^*) + O[(\Phi/\Phi^*)^2]$. Since the leading virial coefficient defines $[\eta]$, consistency requires that $\Phi^* \approx 1.6/[\eta]$. (This prediction of Φ^* is similar in form to that of the "overlap concentration" c^* in polymer solutions that scales as $c^* \sim 1/[\eta]$, where $[\eta]$ is the intrinsic viscosity of the polymer [81–83].) A summary of experimental data on model nonaggregating hard sphere dispersions by Wildemuth and Williams [39b] suggests the empirical relation given by Eq. 9:

$$\Phi^* \approx 1.7/[\eta] \tag{9}$$

This result holds to a good approximation over a wide range of shear stress in which both Φ^* and $[\eta]$ vary [39b] and is in accordance with our hypothesis of "universality." We also recall that the geometrical percolation threshold p_c for ellipsoids of revolution was found to scale roughly as $\sim 1/[\eta]$ over a wide
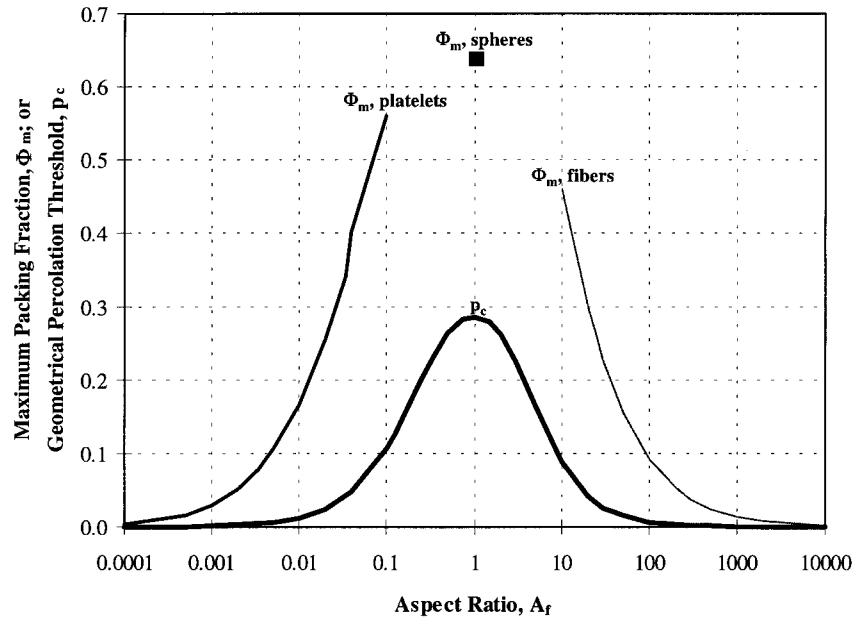
FIG. 9.   Semiempirical estimate for the maximum packing volume fraction Φ_m of randomly dispersed cylindrical particles. $A_f =$ height/diameter for fibers and thickness/diameter for platelets. For comparison, Φ_m for spheres and geometrical percolation threshold p_c for ellipsoids with biaxial symmetry are also shown. Note that Φ_m is calculated directly for cylindrical fibers, but estimated for cylindrical platelets with a scaling relation based on p_c values for ellipsoids.

aspect ratio range (Fig. 8b). This observation provides further support for the near proportionality between p_c and Φ^* suggested above. It would be interesting to check the extent to which Eq. 9 holds for dispersions of monodisperse anisotropic particles.

7.3.   Difficulties in Estimating Φ_m for Anisotropic Particles

It is difficult to determine Φ_m accurately, especially for highly anisotropic particles, because of possibly significant deviations from equilibrium particle configurations in simulation modeling. For example, Buchalter and Bradley [84] analyzed the orientational order in random packings of hard ellipses in two dimensions [84a], as well as hard ellipsoids in three dimensions [84b] by Monte Carlo simulations. These calculations involved "pouring" such objects into a
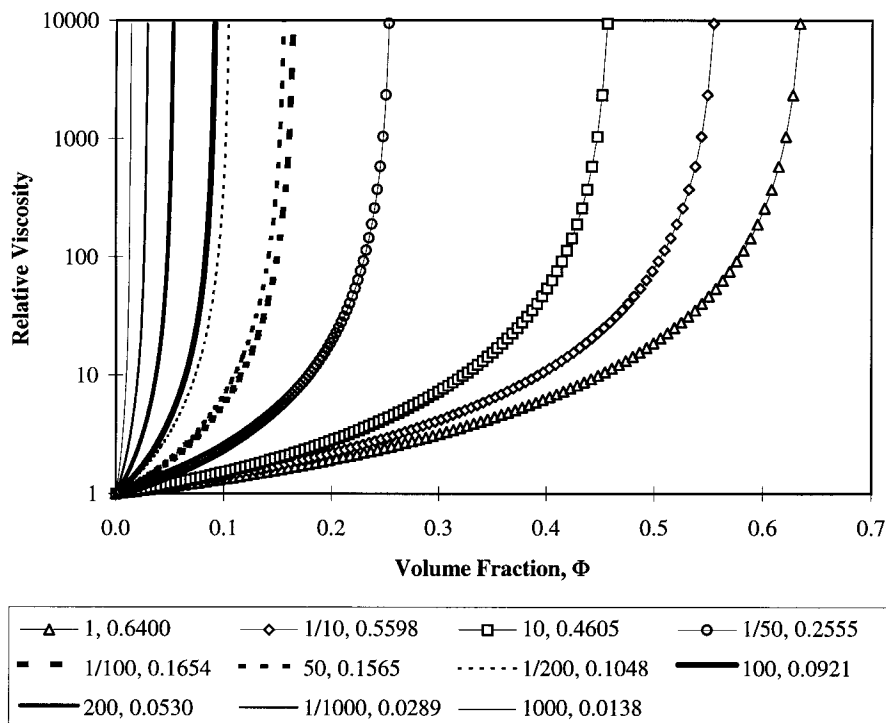
FIG. 10. Examples of viscosity curves calculated as a function of the volume fraction Φ using Eq. 5 with Φ^* replaced by Φ_m for dispersions of spheres, platelets, and fibers. "Relative viscosity" denotes η(dispersion)/η(polymer). Each curve is labeled by the value of A_f (with $A_f > 1$ for fibers, $A_f = 1$ for spheres, and $A_f < 1$ for platelets), followed by the value of Φ_m used in its calculation, in other words, by its (A_f,Φ_m) combination.

container under the influence of a gravitational field. Ellipses packed so that their major axes were aligned preferentially in the horizontal direction. Oblate ellipsoids also packed with their major (symmetry) axes preferentially aligned in the direction of gravity, while the major axes of prolate ellipsoids preferred to lie within the plane perpendicular to gravity. Oriented packings of the ellipses or ellipsoids were thus formed. The orientational alignment effects depended on A_f. For prolate ellipsoids, the orientational order parameter (ranging from 0 for totally isotropic distribution to 1 for a perfectly aligned distribution) reached a maximum of about 0.4 at $A_f \sim 2$ and then decreased to an apparently asymptotic limit of about 0.2. For oblate ellipsoids, this parameter increased rapidly to
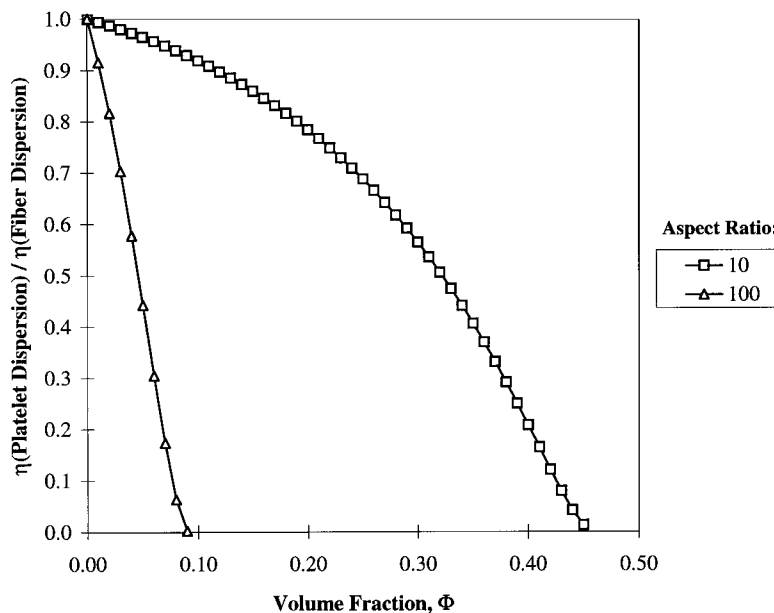
FIG. 11. Relative viscosities as a function of the volume fraction Φ for anisotropic particles. Relative viscosities for dispersions of platelets of aspect ratio $1/A_f$ were divided by those for dispersions of fibers of aspect ratio A_f (see Fig. 10). It is thus shown that, at a given level of particle asymmetry (see curve labels), a dispersion of platelets is expected to have a lower viscosity than a dispersion of fibers. The comparison of the two curves shows that this effect increases with particle asymmetry.

about 0.42 by $A_f \sim (1/4)$ and appeared to level off around that value. The packing fractions at given A_f and $1/A_f$ combinations were always larger for oblate ellipsoids than they were for prolate ellipsoids, as expected. However, these simulated packing fractions were far below the Φ_m values reported by Parkhouse and Kelly [79] for fibers, and the deviations are especially large for prolate ellipsoids. The simulated packing volume fraction also was not found to be maximized for spheres, while experimental values of Φ^* suggest that Φ^* has its maximum value for spheres [85]. These results underscore the difficulties in estimating Φ_m.

7.4. Dispersion Gelation for $\Phi > \Phi^*$

The close-packing concentration Φ_m defines the critical volume fraction Φ^* at which the viscosity approaches infinity in a dispersion at equilibrium. It is

possible for Φ_m to be exceeded through crystallization or other equilibrium ordering processes or through the formation of a "jammed" nonequilibrium state. We define *dispersion gels* as particle dispersions for which $\Phi > \Phi_m$, based on an operational definition of a *gel* as a disordered material for which $\eta \to \infty$.

Kanai et al. [86] investigated the elastic (storage) shear modulus G of flocculating colloidal dispersions, found the onset of elasticity beyond a critical volume fraction of dispersed particles, and used the concept of "rigidity percolation" [55] to interpret their data. The percolation model of dispersion viscosity thus also has some implications in understanding the rigidity of very concentrated particle dispersions ($\Phi > \Phi^*$), which are "solids" rather than "liquids." Figure 12 illustrates dispersion gelation phenomena schematically by showing η and G as functions of Φ and highlighting the role of Φ^* as a critical volume fraction at which a dispersion becomes solid.

The analogy between dispersion rheology and gelation also suggests that the shear relaxation function develops with a power law form above $\Phi \approx \Phi^*$, with exponents governed by percolation theory [87–93]. Such power law scaling is
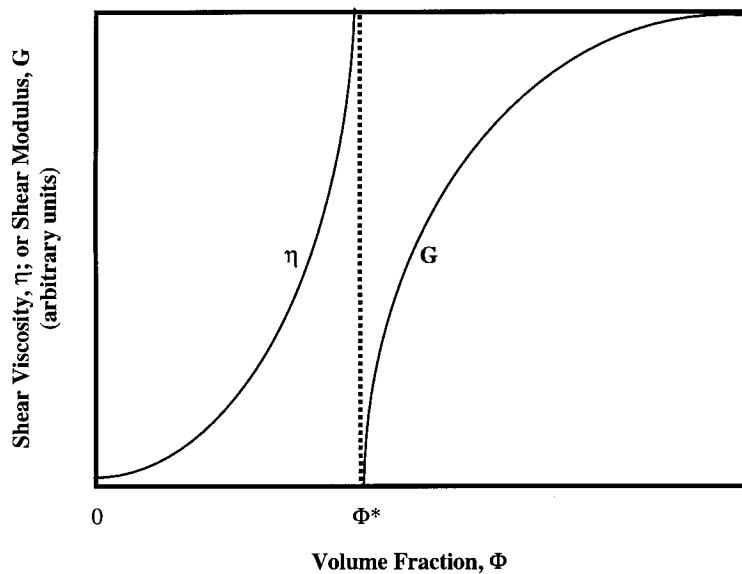
FIG. 12. Schematic illustration of the shear viscosity η and the equilibrium shear modulus G as functions of the particle volume fraction Φ. Note that η approaches infinity as Φ approaches the viscosity percolation threshold Φ^* from below, while the onset of a nonzero G (indicative of the onset of true solidlike rigidity) occurs immediately above Φ^*.

often found in the rheology of soft glassy materials [90] and is naturally associated with the emergence of rigidity through a continuous rigidification transition as occurs in gelation [91]. In de Gennes's "percolation model of gelation" [92], the approach of the viscosity to infinity near the gelation (geometrical percolation) transition is described by the conducting inclusion exponent and the shear modulus by the insulating inclusion exponent. As mentioned above, the viscosity exponent of the gelation problem is reversed relative to the case of particle dispersions. Thus, the viscosity of a gelling sol approaches infinity with the cross-link concentration relative to a critical value, but with the conductor percolation exponent ($\sim$0.8 in three dimensions) rather than the insulator percolation exponent indicated in Eq. 5. These predictions agree with some gelation measurements [88, 89], but universality in the exponents has not generally been observed in gelling systems. It would be interesting to observe in future work whether the shear moduli of dispersions of anisotropic particles scale as $G \sim (\Phi\text{-}\Phi^*)^{0.8}$, where the conductor exponent of about 0.8 replaces the insulator exponent of about 2.0 predicted for the shear modulus in the percolation model of gelation [88, 89, 92]. This conjecture extends the reversal of the conductor and insulator percolation exponents in the dispersion and gelation problems to the shear modulus.

While it is impossible to form a gel from rigid spherical particles with short-range interactions, recent measurements by Roovers [93] have shown that gels can be formed with deformable many-arm star polymers. Dispersion gels have been observed in foams, in which the dispersed air bubbles are deformable [94]. We suggest that dispersion gels of anisotropic particles can be made by exceeding the rigidity percolation threshold ($\Phi > \Phi^*$). For rigid anisotropic particles, this can occur through adjustments in the local particle orientation, which can lead to packing densities greater than those obtained at random close packing under equilibrium conditions. Such a dispersion gel of anisotropic particles can thus be considered a kind of glass. A sol-gel transition has also been observed in colloidal dispersions of platelet-shaped laponite particles [95] that might be related to the concept of dispersion gelation. It seems likely that many soft solids with a colloidal origin may be dispersion gels.

7.5.   Some Phenomenological Observations on the Effects of Filler Polydispersity on Φ_m

Several different types of polydispersity can occur. First, all particles could have the same shape (i.e., platelets of equal A_f), but different sizes. The effect would be to increase Φ_m (and the loose packing volume fraction as shown by Shapiro and Probstein [31]) since smaller particles could fit into the gaps left by the packing of larger particles. This increase of Φ_m remains to be described quantitatively in general as a function of A_f and particle size distribution, but it

has been shown that space can be filled completely (reaching $\Phi_m = 1$) for spherical particles having a power law size distribution [56, 96].

Second, all particles could have the same shape type (i.e., platelets), but have distributions of A_f and of size. The effect of the size distribution should be as described above. It is usually suggested that the distribution of A_f values has a log-normal form. Unless the A_f distribution is extraordinarily broad, its effect should be relatively minor compared to the dominant effect of the most probable value of A_f. This statement was verified for the Young's and shear moduli in the preliminary micromechanical calculations performed as a part of the work of Bicerano and Brewbaker [5, 6] on fiber-reinforced elastomers. Although there are similarities between trends for the elastic moduli and viscosities of materials, the statement has not yet been verified for the viscosity either by calculations or by experiments on well-characterized dispersions and hence must be considered merely as a plausible hypothesis.

Third, the particles could have distributions of shape types (i.e., fibers, platelets, spheres, and/or irregular-shape objects) and of A_f values and sizes for each shape type. In this very complex general case, the trends described above still will influence the overall packing pattern. However, extensive numerical simulations will be needed to estimate Φ_m, and complications such as the tendency of mixtures of objects of different shapes to exhibit "entropy-driven" phase separation will need to be taken into account.

Preliminary attempts to model the shear viscosity of dispersions of mixtures of dissimilar particles, such as the effective medium approach of Tsenoglou and Yang [97], show some progress, but there is much room for improvement.

7.6. Phenomenological Estimate for Shear Rate and Temperature Dependence of Φ^*

A method for the calculation of the effects of shear rate and temperature variation is suggested below. This method will require testing by extensive numerical calculations, as well as by comparisons with shear viscosity measurements, on well-characterized dispersions.

Assume that anisotropic particles in a dispersion are packed in a three-dimensionally isotropic manner in the limit of $\dot{\gamma} \to 0$ and in an ordered closed-packed manner in the limit of $\dot{\gamma} \to \infty$. Then, Eq. 5 can be used with $\Phi^*(\dot{\gamma} \to 0) = \Phi_{m0}$ as the viscosity percolation threshold at vanishing shear rate, where Φ_{m0} is calculated by using Eqs. 6–8 for fibers of aspect ratio $A_f \geq 10$ and platelets of aspect ratio $(1/A_f) \leq 0.1$. Equation 5 can also be used at $\dot{\gamma} \to \infty$, this time with Φ^* estimated by the ordered close-packed volume fraction Φ_{ocp} for particles of a given shape subjected to a flow field of given symmetry.

1. $\Phi_{ocp} \approx 0.7405$ for close-packed spheres [59] and biaxially symmetric ellipsoids.

2. $\Phi_{ocp} \approx 0.9069$ for hexagonal close-packed cylinders [98].
3. $\Phi_{ocp} = 1$ for particles of orthorhombic symmetry (i.e., containing six faces of square and/or rectangular shape, with all edge intersections at an angle of 90°).

The challenge involves estimating how Φ^* increases from Φ_{m0} to Φ_{ocp} as a function of T and $\dot{\gamma}$. We will stipulate that Φ^* increases monotonically and smoothly from Φ_{m0} to Φ_{ocp} as described by Eq. 10, where θ is a characteristic relaxation time specified below. Examples of $\Phi^*(T,\dot{\gamma})$ calculated using Eq. 10 are depicted below after we show how θ can be estimated.

$$\Phi^*(T, \dot{\gamma}) = \Phi_{m0} \cdot \left[1 + \left(\frac{\Phi_{ocp} - \Phi_{m0}}{\Phi_{m0}} \right) \cdot \left(\frac{(\dot{\gamma}\theta)^2}{1 + (\dot{\gamma}\theta)^2} \right) \right] \qquad (10)$$

Before considering model calculations based on Eq. 10, we mention some limitations of this model. The assumption that Φ^* increases monotonically with shear is based on the presumption that shear induces particle alignment and ordering along the fluid flow direction. However, the rotational component of the shear field an have a disruptive effect on this shear-induced particle ordering, especially at high volume fractions, at which interparticle collisions occur with greater frequency. Thus, shear may have a disordering effect at high volume fractions and shear rates, leading to shear thickening instead of shear thinning [53]. Such an effect could create difficulties in processing dispersions. These potential complications of the concentrated regime are neglected here due to the absence of experimental data that support their importance.

In a shear-thinning non-Newtonian dispersing fluid such as a typical polymer melt, shear induces a change in the equilibrium structure of the fluid. In particular, we believe that the large-scale clusters of chains responsible for entanglement phenomena are broken down by the flow process. Since this is a strong effect, the viscosity of a particle dispersion should exhibit a transition to shear-thinning behavior at roughly the same characteristic $\dot{\gamma}$ as the pure polymeric fluid. The breakdown of the cluster structure of the polymer chains is anticipated to facilitate particle orientation. Hence, we propose, as an intuitively appealing hypothesis, that the non-Newtonian flow relaxation of the pure entangled polymer fluid can be identified with the relaxation time θ of Eq. 10. This relaxation time is a function of M_w, M_w/M_n, T, and $\dot{\gamma}$ for a given type of polymeric dispersing fluid. We determine it from the Carreau model type of scaling relation for entangled polymer melts [99] given by Eq. 11, which involves the assumption that the viscous flow relaxation time can be identified with θ.

$$\frac{\eta(\dot{\gamma})}{\eta(0)} = [1 + (\dot{\gamma}\theta)^2]^{-0.35} \qquad (11)$$

Many important fluids (such as water and other small-molecule liquids) are reasonably well described as Newtonian over a wide range of $\dot{\gamma}$. In this case, we identify $\dot{\gamma}\theta$ in Eq. 10 as proportional to the Peclet number Pe in Eq. 3. As a first approximation, we take this proportionality constant to be unity in our present discussion, that is, $\gamma\theta \approx Pe$. We can develop a good approximation for the viscosity of Newtonian dispersions in the dilute filler regime and estimate θ using arguments similar to those proposed for Eq. 10. It is apparent from Fig. 2 that the intrinsic viscosity $[\eta(\dot{\gamma})]$ varies smoothly with $\dot{\gamma}$ and approaches a constant value $[\eta]_\infty$ at large $\dot{\gamma}$. Moreover, since it is a scalar quantity, $[\eta(\dot{\gamma})]$ only depends on the invariants of the rate of deformation tensor, so that it is invariant to the shear direction (an even function of $\dot{\gamma}$). Using Brenner's results [4] for $[\eta]$ as a fuction of Pe (Eq. 3) for the effects of $\dot{\gamma}$, T, and η(dispersing fluid), a "viscous flow relaxation time" θ in a Newtonian fluid can be estimated by fitting $[\eta]$ at low $\dot{\gamma}$ to Eq. 12 (compare approximant to Eq. 10).

$$[\eta(T,\dot{\gamma})] = [\eta]_0 \cdot \left\{ 1 + \left(\frac{[\eta]_\infty - [\eta]_0}{[\eta]_0} \right) \cdot \left(\frac{(\dot{\gamma}\theta)^2}{1 + (\dot{\gamma}\theta)^2} \right) \right\} \tag{12}$$

Equation 12 (in combination with Eq. 10) is only useful in extrapolating from the dilute regime for dispersions in Newtonian fluids of particles with significant anisotropy [e.g., fibers of $A_f \geq 10$ and platelets of $(1/A_f) \leq 0.1$]. We note that $([\eta]_\infty - [\eta]_0) = 0$ for spherical particles, so that shear thinning does not occur in the isotropic (spherical) particle limit at infinitesimal volume fractions, while shear thinning can and does occur in more concentrated dispersions of spherical particles because of particle packing and interparticle interaction effects.

Note that η(dispersing fluid) enters the calculation of $\Phi^*(T,\dot{\gamma})$ in a complicated manner in either Newtonian or non-Newtonian dispersing fluids, so that η(relative) estimated using Eq. 5 always depends implicitly on η(dispersing) in calculating the effects of a $\dot{\gamma}$ and T variation.

Figure 13a depicts Eq. 11 for the $\dot{\gamma}$ dependence of η for a polymeric dispersing fluid with an experimentally measured viscosity at a given T that varies as shown as a function of $\dot{\gamma}$. According to our model assumptions, the value of θ for this shear-thinning fluid is independent of the A_f of the particles dispersed in it, while the θ value of a dispersion in a Newtonian fluid is a function of A_f. A model calculation of η for cylindrical platelets of $A_f = 0.01$ in a Newtonian fluid is shown in Fig. 13b. If extended to higher $\dot{\gamma}$ values, the curve in Fig. 13b would become $\mathcal{S}$ shape and reach an asymptotic limit as $\dot{\gamma} \to \infty$. (Again, we emphasize that further experimental work is needed to verify our assumed form of an appropriate viscous flow relaxation time θ in both types of liquids.) For example, θ can be determined experimentally by light-scattering measurements that monitor particle alignment. Simulation studies can also be used to establish

(a)

(b)
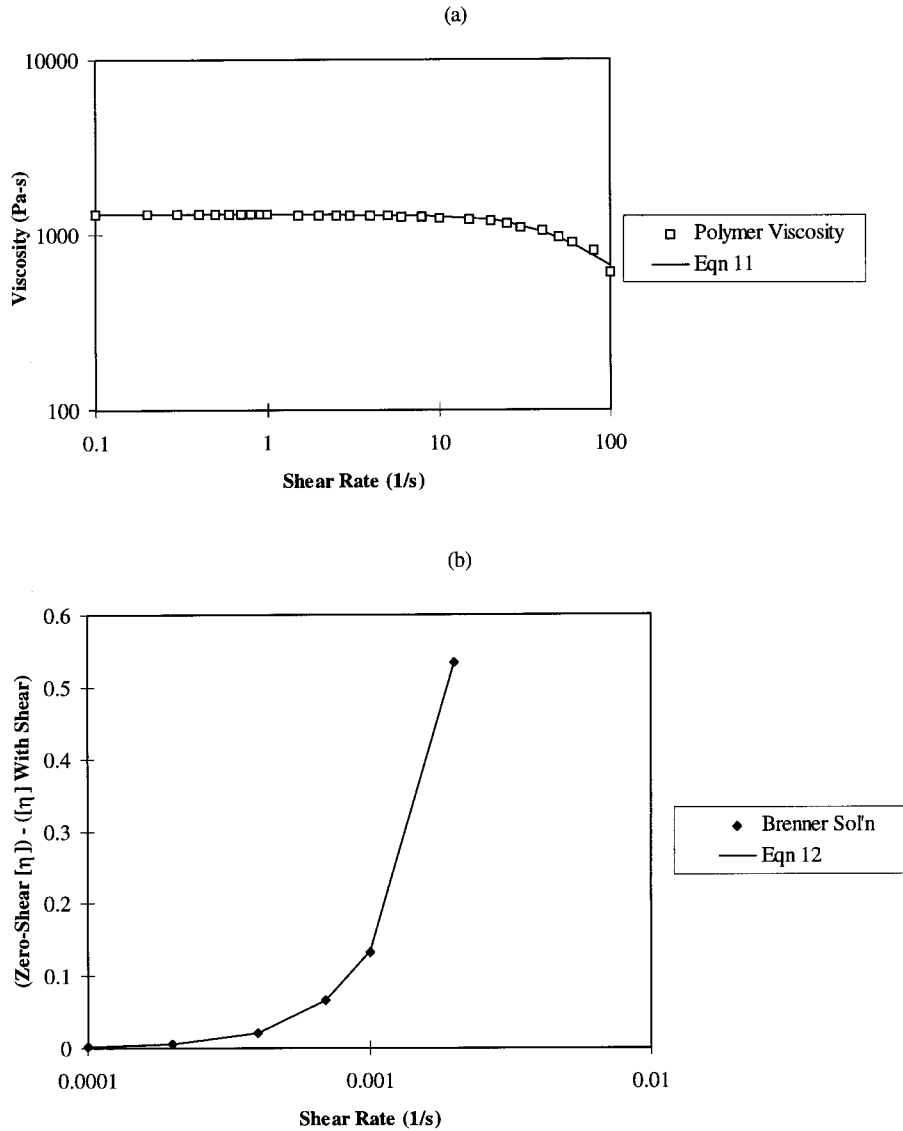
FIG. 13. Examples of calculation of relaxation time θ at a given temperature: (a) fitting of Eq. 11 to viscosity data for a representative non-Newtonian fluid (polymer melt) as a function of shear rate $\dot{\gamma}$; (b) shear-rate dependence of intrinsic viscosity $[\eta]$ of cylindrical platelets of $A_f = 0.01$ in a Newtonian fluid, with the data corresponding to the exact numerical results for $[\eta(\dot{\gamma})]$ and the curve representing Eq. 12.

the value of θ and the validity of our argument for a change in Φ_m with $\dot{\gamma}$ in the case of a Newtonian dispersing fluid.

The results calculated for Φ^* as a function of $\dot{\gamma}$ using Eq. 10 for cylindrical platelets of $A_f = 0.01$ (and hence $\Phi_{m0} \approx 0.177$ by combining Eqs. 6, 7, and 8; and $\Phi_{ocp} \approx 0.907$) are shown in Fig. 14, both for the polymeric fluid and for the Newtonian fluids used in (Fig. 13). The Φ_{m0} values used in Fig. 14 differ from those used in Fig. 10 because p_c values from Monte Carlo simulations were used in Eq. 8 when available in preparing Fig. 10, while all p_c values were calculated using Eq. 6 in preparing Fig. 14. It is seen that, as expected, Φ_m changes substantially as a function of $\dot{\gamma}$. An important difference is seen, however, between the behaviors in the two types of dispersing fluid. In the Newtonian fluid (representative of simple molecular liquids), a small amount of shear is sufficient to induce significant particle alignment, so that Φ_m approaches Φ_{ocp} at a very low value of $\dot{\gamma}$. On the other hand, we expect that particle alignment will be inhibited in polymer fluid dispersions at higher volume fractions by the presence of entangled polymer chains; this is based on measurements (discussed below) of η for these dispersions. Consequently, the onset of the rapid increase of Φ_m should
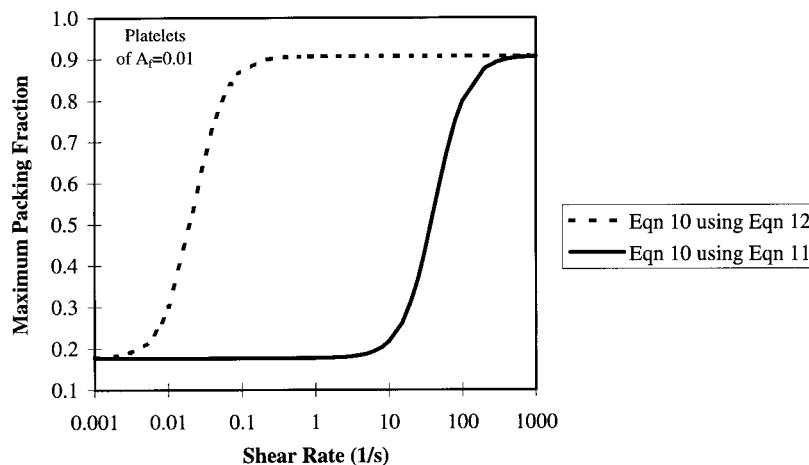
FIG. 14. Maximum packing volume fraction Φ^*. Calculated from Eq. 10 at a given temperature as a function of the shear rate, for cylindrical platelets of $A_f = 0.01$, dispersed in the Newtonian fluid (curve labeled "Eqn 10 using Eqn 12") and in the polymer melt (curve labeled "Eqn 10 using Eqn 11") indicated in Fig. 13.

occur at a much higher $\dot{\gamma}$ value when the dispersing fluid is a polymeric melt. In fact, Φ_m has reached a value very close to Φ_{ocp} in the Newtonian fluid at the $\dot{\gamma}$ range at which significant increases of Φ_m have just begun to manifest themselves in a polymeric fluid in our modeling.

The values of $\Phi_m(\dot{\gamma}) \approx \Phi^*(\dot{\gamma})$ calculated for platelets of $A_f = 0.01$ can be inserted into Eq. 5 to estimate η(relative) as a function of Φ and $\dot{\gamma}$. Figure 15 shows our predictions for these dispersions in the polymeric fluid at each one of a series of $\dot{\gamma}$ values as a function of Φ. It is seen that η(relative) should be lowered substantially with increasing $\dot{\gamma}$, corresponding to shear rates large enough for the pure polymer melt to exhibit shear thinning.

Figure 16 illustrates the increasing sensitivity to the shear rate $\dot{\gamma}$ with increasing volume fraction and with particle aggregation. The curve labeled "0.175" shows the drastic effect of increasing $\dot{\gamma}$ for a dispersion of discrete axisymmetric cylindrical platelets of $A_f = 0.01$ at a volume fraction of $\Phi = 0.175$ (just below $\Phi_{m0} \approx 0.177$); a large η(relative) in the low-shear region and very rapid shear thinning in the high-shear region. The curve labeled "0.175, $d = 2.75$, $N = 5$" shows the effects of very mild fractal aggregation (discussed below in great
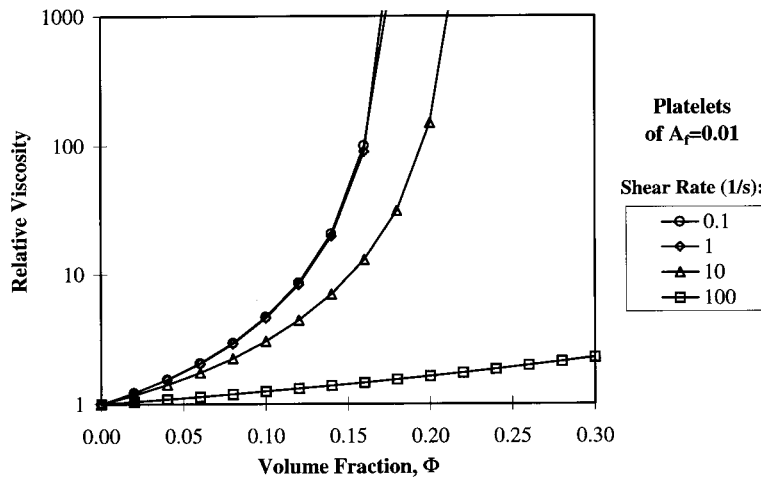
FIG. 15. Relative viscosity [η(dispersion)/η(polymer)]. Calculated as a function of shear rate and volume fraction, for cylindrical platelets of $A_f = 0.01$, in the polymer with a viscosity in the absence of the particles that was shown in Fig. 13a. Curves are labeled by the shear rate in 1/s.
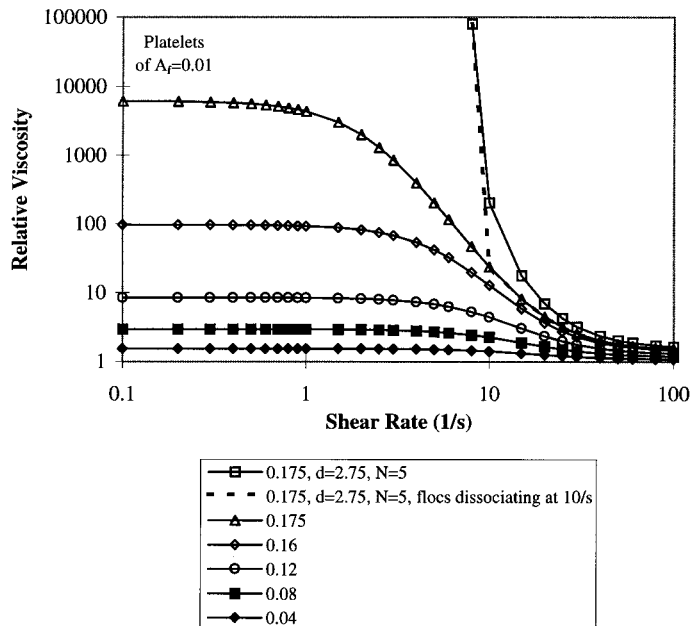
FIG. 16. Relative viscosity of a platelet dispersion as a function of shear rate $\dot{\gamma}$ at fixed volume fraction Φ. This figure illustrates a greater sensitivity to $\dot{\gamma}$ with increasing Φ and fractal aggregation. The cylindrical platelets with an aspect ratio $A_f = 0.01$ are dispersed in a polymer with a shear-dependent viscosity that is indicated in Fig. 13a. "Relative viscosity" denotes $\eta(\text{dispersion})/\eta(\text{polymer})$. The first number labeling each curve is the value of Φ. The curve labeled "0.175, d = 2.75, N = 5" shows the effects of very mild fractal aggregation ($N = 5$ particles per floc, aggregated with fractal dimension $d = 2.75$) for $\Phi = 0.175$. The curve labeled "0.175, d = 2.75, N = 5, flocs dissociating at 10/s" shows what is predicted to happen if the flocs in that dispersion are so weak that they are unable to withstand the shear stress generated at shear rates above 10 s^{-1}.

detail) in this dispersion. Φ_{m0} decreases to 0.153, and η(relative) increases drastically relative to the case of the discrete particles for $\Phi > 0.153$. The curve labeled "0.175, $d = 2.75$, $N = 5$, flocs dissociating at 10/s" indicates what happens if the flocs are so weak that they are unable to withstand the shear stresses generated at $\dot{\gamma} > 10$ s^{-1}, and they thus disintegrate into discrete particles (see Section 7.8). The behavior is similar to that of strong flocs up to $\dot{\gamma} = 10$ s^{-1} and of discrete particles for $\dot{\gamma} > 10$ s^{-1}. The lower curves (for Φ values of 0.16, 0.12, 0.08, and 0.04) show the rapid reduction of the magnitude of shear thinning with decreasing Φ.

7.7. Yield Stress of Dispersion Gels

Dispersion gels ($\Phi > \Phi^*$) exhibit a yield stress τ_y below which they do not flow and above which they flow readily [40]. A semiempirical method for calculating τ_y, originally created by Wildemuth and Williams [39], is summarized in this section because such behavior has important processing implications. Our contribution consists of making the model of Wildemuth and Williams predictive by estimating its two parameters (A and m) from our dispersion viscosity model.

For illustration, we restrict our attention to needle and platelet particles, that is, to fibers of aspect ratio $A_f \geq 10$ and platelets of aspect ratio $(1/A_f) \leq 0.1$. The model of Wildemuth and Williams [39b] is first utilized to estimate the stress dependence of the maximum packing fraction Φ_m given by Eq. 13, with $\Phi_m(T,\dot{\gamma})$ values in Eq. 10 (θ from either Eq. 11 or Eq. 12) and $\eta(T,\dot{\gamma})$ from Eq. 5, to obtain our yield stress estimates. The shear stress is defined as $\tau \equiv \eta \, \dot{\gamma}$. (This relationship is exact for Newtonian fluids. It is often also used in treating a non-Newtonian fluid as a "generalized non-Newtonian fluid" with a shear-rate-dependent viscosity.) We define Φ_{ocp} as the value of Φ_m in the limit of high shear rate ($\dot{\gamma} \to \infty$).

$$1/\Phi_m = \frac{1}{\Phi_{m0}} - \frac{\left(\dfrac{1}{\Phi_{m0}} - \dfrac{1}{\Phi_{ocp}} \right)}{(1 + A\tau^{-m})} \tag{13}$$

The model parameters A and m of the Wildemuth and Williams expression (Eq. 13) can be fixed as follows:

1. Calculate $\Phi_m(T,\dot{\gamma})$ at selected values of $\dot{\gamma}$ and T using Eq. 10.
2. Use Eq. 5 to calculate τ at many different combinations of $\Phi_m(T,\dot{\gamma})$ and Φ.
3. Treat these calculated τ values as a "data set" and fit Eq. 13 to it to fix A and m.

The "yield stress" τ_y is defined by the condition that the shear viscosity approaches infinity ($\eta \to \infty$). It can be seen from Eq. 13 that such a yield stress should occur in the volume fraction range $\Phi_{m0} \leq \Phi \leq \Phi_{ocp}$. Equation 13 can be rearranged to deduce the volume fraction dependence of the critical stress at which the viscosity approaches infinity. If this point is identified with the condition for shear yeilding, this critical stress can be identified with the yield stress τ_y. Equation 14 corresponds to this rearrangement of Eq. 13. See Wildemuth and Williams [39b] for further discussion.

$$\tau_y = \left[A \cdot \left(\frac{\dfrac{\Phi}{\Phi_{m0}} - 1}{1 - \dfrac{\Phi}{\Phi_{ocp}}} \right) \right]^{1/m} \tag{14}$$

In Fig. 17, we show our estimate of the yield stress τ_y for cylindrical platelets of $A_f = 0.01$ dispersed in the polymeric fluid of Fig. 13a. The values of A and m were estimated by fitting Eq. 13 to Eq. 10 at several values of Φ. The fits are not perfect, but the resulting curves of τ_y versus Φ over the range $\Phi_{m0} \leq \Phi \leq \Phi_{ocp}$ all show the same asymptotic behavior ($\tau_y \to 0$ as $\Phi \to \Phi_{m0}$ and $\tau_y \to \infty$ as $\Phi \to \Phi_{ocp}$). Note that the volume fraction Φ at which the platelet dispersion "gels" is small relative to the viscosity percolation threshold Φ^* of a sphere dispersion, and that the rise of τ_y with Φ is predicted to be mild up to rather high volume fractions.
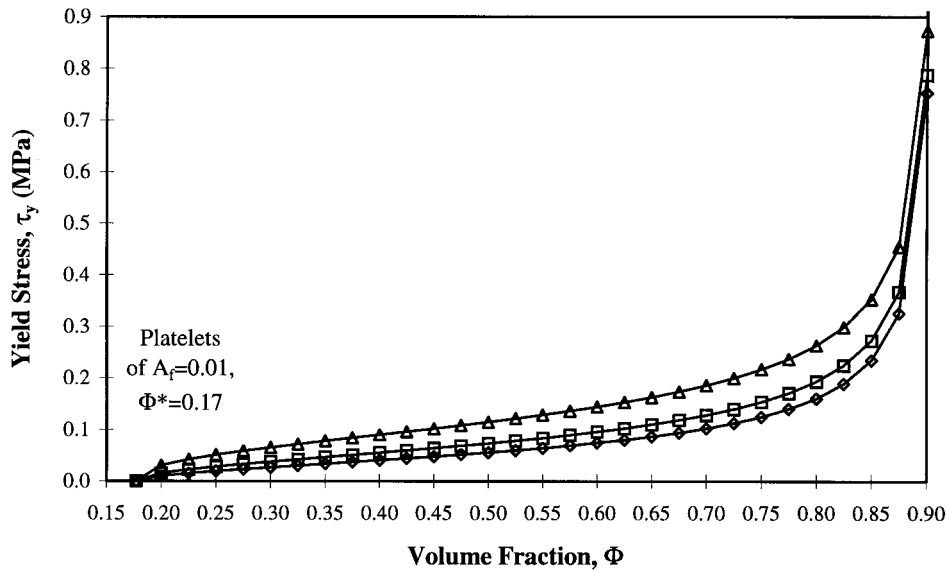
FIG. 17. Yield stress τ_y of a model dispersion gel. Results of τ_y calculations using Eq. 14 for cylindrical platelets of $A_f = 0.01$ dispersed in the polymer with a viscosity in the absence of the particles that was shown in Fig. 13a. The three numbers labeling each curve indicate, respectively, the value of Φ for which Eq. 13 was fitted to Eq. 10 to estimate the parameters A and m and the values of A and m: ($\triangle$) 0.12, $3.7 \cdot 10^{11}$, 2.41; ($\square$) 0.08, $2.4 \cdot 10^9$, 2.05; ($\Diamond$) 0.04, $1.8 \cdot 10^8$, 1.87.

7.8.   Effects of Particle Aggregation on Φ^*

7.8.1.   General Remarks

Readers interested in a broad overview of fractal aggregation are referred to the excellet book by Feder [38]. It is a major challenge to make quantitative a priori predictions of the likelihood and the extent of aggregation in particle dispersions. For example, it has been shown [66] that the angular orientation between platelet-shaped fillers can be sensitive to A_f and Φ, to the nature of the dispersing medium, and to the actual sizes of and the total layer charges on the platelets. Random, orientationally ordered, or stacked configurations are possible.

Although the development of a predictive model of dispersion microstructure remains an elusive goal, some qualitative trends can be anticipated:

1.   The thermodynamics tendency to floc depends on a delicate interplay among solvent-solvent, solvent-particle, and particle-particle interactions. For example, the average number N of particles in a floc tends to increase with increasing Φ, and increased short-range attractive interparticle interactions associated with increasing the salt concentration or lowering the temperature also tend to increase N. However, the formation of structures that have the lowest free energy is often inhibited by kinetic factors, so that the processing history of a dispersion affects its properties.

2.   Aggregate growth far away from equilibrium conditions tends to form especially diffuse fractal structures of low dimension. This type of structure arises because the incoming particles are screened from entering the interiors of the growing aggregates. If particle sticking is not irreversible, the flocs tend to "age" into more compact configurations governed by equilibrium conditions. These equilibrium structures may still be fractal structures having a form similar to branched polymers [100].

3.   Flocs tend to disintegrate into their component particles under vigorous shear flow when the shear stress τ (namely, the magnitude of the stress tensor) becomes sufficiently large. The value of this critical shear stress τ_d directly reflects the magnitude of the attractive interparticle energy. This leads to strongly non-Newtonian flow properties. There can also be a tendency of flocs to form at low shear rates due to increased collision frequency between the particles, leading to shear thickening.

4.   If a flocculated microstructure falls apart as a result of shear or other types of deformation, it may or may not reform after this external perturbation is removed. The breakdown of flocs held together by weaker interparticle interactions (secondary bonds, such as dispersive forces, weak polar forces, and hydrogen bonding) is generally more reversible than the breakdown of flocs held together by stronger interactions (such as ionic, covalent, or metallic bonding).

MARCEL DEKKER, INC.
270 Madison Avenue, New York, New York 10016

The reason is that the reformation of strong bonds (which may have rearranged themselves into new patterns on the surfaces of the particles after a floc fell apart) may require the surmounting of prohibitively large energy barriers.

7.8.2.   *Observations on Flocculated Dispersions*

There is a consdiderable amount of ongoing research, involving experimental work as well as theory and numerical simulations, to elucidate in detail the nature of the flow-induced changes in flocculated dispersions. For example, Pignon, Magnin, and Piau [101] studied the behavior of a thixotropic synthetic clay of the hectorite-type [Laponite] dispersion under steady shear by combining rheometry with light scattering. Their Laponite samples contained disk-shaped particles, 30 nm in diameter and 2 nm thick (and hence with $A_f = 1/15$). In the rest state, the gel structure consisted of micron-size fractal aggregates of extremely "open" structure. The gels had a fibrous texture and $d = 1 \pm 0.05$ close to the sol-gel transition ($0.0035 \leq \Phi \leq 0.0056$). They had a more heterogeneous texture, with zones of lower and lower particle concentration and $d = 1.8 \pm 0.01$ in the higher Φ range ($0.012 \leq \Phi \leq 0.02$). Between these two ranges of Φ values, there was a transition zone (with d gradually increasing from 1 to 1.8), corresponding to entanglement of the micron-size aggregate clusters to produce an increasingly dense microstructure. Under steady shear, these micron-size fractal aggregates contracted and stretched perpendicularly to the shear direction by a mechanism resembling that proposed DeGroot et al. in explaining their own observations [102] of flow-induced anisotropic small-angle light scattering in silica-filled poly(dimethyl siloxane) liquids. There was a critical shear rate [101] above which any additional contraction of the aggregate was impossible. Breakup could be attributed to mechanical stresses.

These experiments [101] also validated earlier theoretical results [103–106]. In particular, they demonstrated the validity of Potanin's theoretical conclusion [104] about the existence of a critical value of $\dot{\gamma}$. While it is not phrased in terms of concepts of fractal geometry, a paper by Tsenoglou [107] on the effects of agglomeration and shear on the fluidity and plasticity of a dispersion of naturally buoyant particles in a Newtonian fluid matrix also provides useful information on these topics.

Some important work has been concerned with the extent of the universality of the fractal dimension of particle aggregates. Aubert and Cannell [108] performed experiments on the aggregation of colloidal silica spheres, showing that slow aggregation always yields clusters of $d = 2.08 \pm 0.05$, while rapid aggregation can produce clusters with either $d = 1.75 \pm 0.05$ or $d = 2.08 \pm 0.05$. However, the clusters with $d = 1.75 \pm 0.05$ were always observed to restructure over time into clusters of $d = 2.08 \pm 0.05$. The lower d values observed under rapid aggregation were ascribed to diffusion-limited aggregation, for which the aggregation rate is limited solely by the time taken by particles and clusters to en-

counter each other by diffusion. The higher d values obtained under slow aggregation or restructuring over time were rationalized in terms of reaction-limited aggregation for which substantial (but surmountable) repulsive barrieres are overcome by thermal activation so that aggregates reach their true equilibrium packing arrangements. Several other studies of different materials also show similar behavior [109], with the d values falling in two narrow ranges.

There has been recent related research on "random surfaces," which include equilibrium cluster models (surfaces with holes) as a part of their description. These random surface models also give $d \approx 2$ for swollen clusters at equilibrium, suggesting that an exponent of about 2 is general for swollen branched polymers, swollen membranes, and swollen equilibrium fractal aggregates at or near equilibrium [100].

7.8.3. A Simple Model for the Viscosity of Aggregated Dispersions

An approximate method for the calculation of aggregation effects is now suggested. We neglect polydispersity effects to simplify the discussion. The equations presented below can be averaged statistically for polydisperse flocs. Furthermore, because their prediction is beyond our scope, we will treat N, d, and τ_d as variables in a parametric study. As discussed above and shown in Fig. 6, Eq. 5 can be used with the scaling relation given by Eq. 15 to account for fractal aggregation. We expect intuitively that the geometrical percolation threshold p_c should be a lower bound to the reduction of Φ^* by aggregation. If this expectation is taken provisionally as a hypothesis, Eq. 15 should hold only for N values of up to a crossover value of N_x, and we take Φ^* to equal p_c for $N > N_x$. N_x is then calculated using Eq. 17, which is obtained by setting Φ^* (Eq. 15) equal to p_c at $N = N_x$.

$$\Phi^* \approx \Phi_m \rightarrow \Phi_{mp} \cdot N^{1-(3/d)} \qquad \text{for } N \leq N_x \tag{15}$$

$$\Phi^* \approx p_c \qquad \text{for } N > N_x \tag{16}$$

$$N_x = \left(\frac{\Phi_m}{p_c} \right)^{\left(\frac{d}{3-d} \right)} \tag{17}$$

N_x is depicted in Fig. 18 as a function of A_f based on p_c values calculated using Eq. 6 and Φ_m values calculated [only for fibers of aspect ratio $A_f \geq 10$ and platelets of aspect ratio $(1/A_f) \leq 0.1$] using Eqs. 7 and 8.

In incorporating fractal scaling into our dispersion shear viscosity model, the forms of Eqs. 2, 5, 10, 11, 12, 13, and 14 should remain invariant; but the values of Φ_m, Φ_{m0}, and Φ_{ocp} prescribed by Eqs. 15, 16, and 17 should be used for the flocculated dispersion.

The model indicates that the viscosities of these flocculated dispersions are sensitive to the value of τ_d, as well as to the shear stress and the temperature:
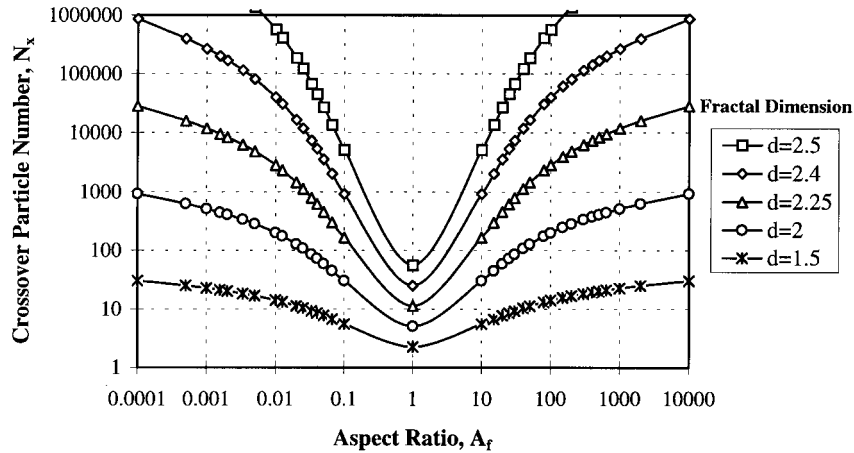
FIG. 18. Crossover particle number N_x of flocculated aggregates. N_x is calculated at several values of the fractal dimension d for ellipsoids of revolution. See the legend of Fig. 1 for the definition of A_f. The curve for $d = 1.5$ shows (Φ_m/p_c), which is taken to powers of 5, 4, 3, and 2 in the calculations for $d = 2.5$, 2.4, 2.25, and 2. These results are approximate because the Φ_m values are more appropriate for cylindrical particles (for which p_c values are not readily available), but the p_c values are for biaxially symmetric ellipsoidal particles (for which Φ_m values are not readily available).

1.   In the idealized "strong floc" limit of $\tau_d \to \infty$, flocs remain intact regardless of the value of τ. Since $d < 3$, Φ^* decreases as described by Eq. 15 for $N \leq N_x$ (with N_x calculated using Eq. 17) and remains constant at $\Phi^* \approx p_c$ (Eq. 16) for $N > N_x$. Since $[\eta]_0$, $[\eta(T,\dot\gamma)]$, Φ_{m0}, and Φ_{ocp} all scale similarly with N, the effect of shear on $\Phi^*(T,\dot\gamma) \approx \Phi_m(T,\dot\gamma)$ is identical to its effect on Φ_{m0} for dispersions in both Newtonian and non-Newtonian fluids according to Eq. 10. Consequently, at any combination of T and $\dot\gamma$, Φ_m, Φ_{m0}, and Φ_{ocp} all decrease by the same factor with increasing N. The dispersion begins to behave like a solid, as shown in Fig. 6 (having $\tau_y > 0$ and τ_y changing more steeply as a function of Φ with increasing N as calculated by combining Eqs. 10, 13, and 14) at a lower Φ_{m0} with increasing N. The range of Φ values ($\Phi_{m0} \leq \Phi \leq \Phi_{ocp}$) at which solid-like behavior can be overcome by shearing narrows because of the reduction of $\Phi_m(T,\dot\gamma)$ and Φ_{ocp} by the same factor. The decrease of Φ_{ocp} implies that the onset of true solid-like rigidity (which cannot be overcome by shear) occurs at a lower Φ value and that the Φ range of solidity ($\Phi > \Phi_{ocp}$) becomes broader.

2.   In the idealized "weak floc" limit of $\tau_d \to 0$, flocs fall apart with a small imposed value of τ. The dispersion then has the values of Φ_m, Φ_{m0}, and Φ_{ocp} scaled as described by Eqs. 15, 16, and 17. It manifests solid-like behavior only

for $\dot{\gamma} \to 0$. At any finite τ value, flocs fall apart so that Φ_m, Φ_{m0}, and Φ_{ocp} jump to their unscaled values for discrete particle dispersions for $\tau > 0$, and the rheological behavior becomes (most likely reversibly if shearing is stopped) that of a discrete particle dispersion.

3. For most real particle dispersions with fractal aggregation, τ_d falls somewhere between these idealized limits for strong and weak flocs. The behavior of a real floc will thus usually resemble that of a strong foc for $\tau < \tau_d$ and that of a weak floc of $\tau > \tau_d$. The effects of fractal aggregation on the shear dependence are illustrated in Fig. 16.

More fundamental calculations of the viscosity of aggregated dispersions are possible in the dilute limit. Mansfield, Douglas, and Garboczi [110] have developed a numerical method to estimate $[\eta]$ for rigid particle aggregates having essentially arbitrary shape complexity. This method involves calculating the electrical polarizability of a conducting form of the aggregate using a Monte Carlo algorithm in which the aggregate is "hit" with random walk paths launched from an enclosing sphere. Douglas and Garboczi [8] showed that $[\eta]$ is proportional to the average electrical polarizability to a very good approximation for particles of general shape. The translational friction coefficient of complex-shaped aggregates has also been shown to be approximately proportional to the electrostatic capacity of a conductor particle having the same shape [111a, 111b]. Furthermore, a probabilistic method involving integrating over random walk paths has also been utilized to estimate the capacity (friction coefficient) for shaped aggregates [111b, 111c]. These random walk methods, in conjunction with the electrostatic-hydrodynamic analogies mentioned above, allow the estimation of $[\eta]$ and of the friction coefficient for particles having essentially arbitrary shape. Moreover, these computational methods become more efficient with increasing particle complexity, allowing the computation of $[\eta]$ in cases that would be prohibitively difficult to simulate by conventional finite-element methods.

The calculation of $[\eta]$ for complex particle aggregates (such as fractal aggregates) allows the estimation of the viscosity of aggregated dispersions if we calculate the average $[\eta]$ for the dispersion and utilize Eq. 5 in conjunction with the approximation given by Eq. 9. This type of calculation should also provide insights into the scaling relation (Eq. 15) observed by Russel and Sperry [37]. More generally, this type of calculation can be utilized to extract further structural parameters describing flocculated aggregates. These methods will be developed further in the near future.

8. DISPERSIONS OF FLEXIBLE PARTICLES AND DROPLETS

8.1. Dispersion Types

Emulsions (soaps, some paints, cosmetics, creams, mayonnaise, milk, and butter) are examples of liquid-in-liquid dispersions, which consist of liquid drop-

lets dispersed in another liquid. Melts of blends, block and graft copolymers of immiscible components; and block and graft copolymer dispersions in a homopolymer matrix are other familiar and technologically important examples of fluid and flexible particle dispersions. The properties of these dispersions depend on the viscosity and deformability of the droplets and their state of dispersion.

The properties of dispersed particles exhibit a wide range, from low viscosity and high deformability to high viscosity and low deformability. For example, *wet foams* are dispersions of gas bubbles in liquids for which Φ is relatively large [112], and the "particle" viscosity is low. The gas bubbles are spherical in early stages of foam expansion, but they distort as they impinge on one another in the later stages of expansion. This deformability makes these dispersed particles pack space more efficiently than hard spheres, and thus a change in Φ_m can be anticipated. In a dilute dispersion of gas bubbles, it is possible to consider the dispersion as a liquid droplet for which the viscosity of the dispersed phase is usually relatively small. Thus, the viscosity of the droplet relative to the matrix fluid, $z_\eta = [\eta(\text{dispersed phase})/\eta(\text{dispersing fluid})]$, can often be approximated as zero ($z_\eta \rightarrow 0$). This is the opposite extreme of the "hard" droplet limit ($z_\eta \rightarrow \infty$), which is appropriate for modeling very viscous or solid dispersed particles.

One often encounters dispersions of particles having intermediate flexibility and viscosity. The influence of these factors on the dispersion viscosity is a problem of great interest. The following are some examples for which such effects are expected to be important:

1. Exfoliated clay platelets of $\sim$1 nm thickness and 100 to 1000 nm lateral dimensions dispersed in polymers were rather flexible and behaved mechanically more like flexible sheets than rigid plates [113, 114]. Numerical simulations showed that internal flexibility affects the detailed orbits of dispersed platelets [115]. Hence, even particles of extremely high modulus can have considerable internal flexibility if they are very anisotropic because of low flexural rigidity arising from large bending moments induced by the very anisotropic geometry.

2. Another example of an inherently rigid, highly anisotropic particle with considerable internal flexibility is xanthan gum (a semirigid biopolymer), which has rheological properties that can be modeled reasonably well by neglecting its flexibility and treating it as a rigid rod [29, 116].

3. Synthetic "rigid-rod" high-performance polymeric fibers of all types, as well as carbon fibers, also have considerable flexibility. Most important, these types of fibers all buckle at the microfibrillar and fibrillar scales of their microstructures under compressive stresses, limiting the range of their potential aerospace applications [117].

4. High-resolution transmission electron microscopy of specimens subjected to mechanical stress, as well as atomistic simulations, showed that carbon nanotubes can be bent reversibly to large angles because of the remarkable flexibility of their hexagonal network, which resists bond breaking and bond switching up to very large strains [118].

5. The flowing or swimming of organisms is an important area of biological research in which the concepts and methods of dispersion rheology of flexible "particles" have been applied for decades [119–122].

In particular, it seems likely that the exfoliation of layered silicates should lead to structures with a significant degree of flexibility and shape irregularity, which could substantially affect the properties of dispersions of these materials. We make some further observations about these materials, which are particularly emphasized in the present paper.

Wen et al. [123] performed static light-scattering measurements on exfoliated graphite materials, showing that graphite sheets adopt a crumpled configuration in solution with a fractal dimension of $d \approx 2.54$. Under poorer solvent conditions, the sheetlike structures collapsed into more compact configurations. These configurational changes are much like the swelling of polymers in solution. Flexible surfaces and membranes, indeed, may be considered as polymers with a connectivity dimension greater than 1 [100]. This interpretation still holds if "sheetlike" or "networklike" polymers are torn in many places so that a "branched polymer" structure is obtained. Douglas [100] introduced a general theoretical treatment of the swelling of membrane and network polymers and the transport properties of these structures in solution, but much more experimental and theoretical work is required in this area.

It is much simpler to understand the effects of the flexibility of solid particles than of liquid particles since complications such as breakup of dispersed domains, changes from one type of dispersed domain shape to another, co-continuity of two or more liquid phases, occlusion of subdomains of one phase within domains of another, and phase inversion are often crucial in dispersions of liquids [124–133]. The present paper only considers liquid dispersions for which the interfacial tension is relatively large and the liquid droplets are dispersed at low concentrations in the suspending fluid.

8.2. Dilute Dispersions of Spherical and Deformable Droplets

The effects of particle flexibility have been studied most extensively for spherical particles, including gas bubbles, liquid droplets, and deformable solid particles. We summarize some results that give insights into the nature of these dispersions.

The importance of both the finite shear modulus G of a flexible sphere [134, 135] and the interfacial tension between the dispersed spheres and the dispersing fluid [112, 136] as sources of the viscoelastic behavior of dispersions of flexible spheres has been established. It has also been shown, by experiments on oil-in-water emulsions [137], that there exists a critical volume fraction at which the viscosity approaches infinity, similar to solid-in-liquid dispersions.

The calculation of the intrinsic viscosity of a dispersion of spherical droplets is a classical hydrodynamic result credited to Taylor [138]. Frankel and Acrivos [139] have elaborated on the theory of the hydrodynamics of dilute emulsions. The intrinsic viscosity of a spherical droplet is given by Eq. 18, where $z_\eta \equiv \eta(\text{droplet})/\eta(\text{dispersing fluid})$ is the relative viscosity of the dispersed particle.

$$[\eta(\text{droplet})] = 1 + \frac{(3z_\eta/2)}{(1 + z_\eta)} \qquad \text{undeformable spherical droplet} \qquad (18)$$

The derivation of this equation assumes that the droplet is undeformable so that $[\eta(\text{droplet})]$ is always greater than zero. Equation 18 reduces to the hard-sphere value of 2.5 for highly viscous droplets ($z_\eta \to \infty$) and to 1 (as originally derived by Taylor [140] in his studies on foam rheology) in the case of a gas bubble in a viscous liquid where $z_\eta \to 0$. Many experimental observations confirm Eq. 18 for dilute droplet dispersions [1, 141], but deviations are observed for very small droplets and also when surfactants are present [142, 143]. Deviations should also be expected when the interfacial tension becomes small (near the critical point and with surfactant emulsions) and the droplets become readily deformable by even very small shear fields. We expect that these values of $[\eta]$ for undeformable spherical droplets are minimal for any object having a fixed shape and z_η.

Some insight into the effects of particle deformation can be obtained from the corresponding calculation of $[\eta(\text{droplet})]$ for droplets with an ideally deformable surface [9]. The intrinsic viscosity of a deformable droplet is given by Eq. 19, which still recovers the hard sphere value of 2.5 at $z_\eta \to \infty$, but shows that $\eta(\text{dispersion})$ becomes reduced relative to the viscosity of the dispersing liquid when the droplet viscosity is lower than the viscosity of the dispersing fluid.

$$[\eta(\text{droplet})] = \frac{(z_\eta - 1)}{[1 + (2/5)\cdot(z_\eta - 1)]} \qquad \text{freely deformable liquid droplet} \qquad (19)$$

We also compare the influence of particle deformability on the shear modulus G to η of a particle dispersion. The effect of the deformable droplets on $\eta(\text{dispersion})$ is equivalent to the modification of $G(\text{dispersion})$ for which the first virial coefficient for the shear modulus G of incompressible materials is

given by Eq. 20 [8], with the relative shear modulus of the dispersed particle being equal to $z_G \equiv G$(elastic particle)$/G$(matrix).

$$[G] = \frac{(z_G - 1)}{[1 + (2/5) \cdot (z_G - 1)]} \qquad \text{deformable elastic droplet} \qquad (20)$$

Intuition suggests, and Eqs. 19 and 20 confirm and quantify, that adding "soft" materials (lower η or G) to a dispersing medium softens the medium as a whole (lowers its η or G). Equation 18 indicates that, if the inclusions are nondeformable, then η(dispersion) generally increases. A similar effect occurs in the elastic case. Imagine the contrasting effects of putting holes in a rubber sheet and of introducing metal grommets. G is reduced in one case, while it can be increased substantially in the other. These simple considerations suggest that it should be possible to increase the viscosities and moduli of filled polymers substantially by simply introducing air in the presence of a surfactant, which introduces rigidity to the matrix-air boundary [144, 145]. We also expect that the addition of salt can substantially affect the rigidity of exfoliated mica "sheet polymers" in solution in a fashion similar to polyelectrolytes in solution. This effect would modify the reinforcing properties of these particles. We can also obtain some qualitative understanding of the effects of particle deformability on the reinforcing effect of fluid and elastic fillers in fluid and elastic matrices, respectively, from these model calculations. These calculations are useful in understanding the general tendency for η(dispersion) and G(dispersion) to drop at higher Φ values of even relatively rigid particles since the particle aggregates that arise inevitably in these systems become "deformable" under shear flow or elastic deformation.

It is apparent from Eqs. 19 and 20 that the η(relative) and G(relative) of dilute dispersions of flexible spheres are equal provided that the boundaries of the spheres are freely deformable. Similar results for these properties should also obtain for ideally rigid boundaries, so that it is tempting to use η and G interchangeably in our theoretical modeling. It is well established that the η(relative) and G(relative) of hard-sphere dispersions are equal [37, 48], assuming an incompressible medium. Then, it is reasonable to suppose this type of relation will hold for general volume fractions and particles of general shape. This assumption is supported somewhat by the empirical Cox-Merz rule [146], which indicates that the frequency dependence of the shear modulus and the shear rate dependence of the viscosity of viscoelastic materials often have a similar form. We develop this elastostatic-hydrodynamic analogy further in the next section after making a few cautionary comments about how these results should be interpreted.

An elastic solid is defined by the condition $G > 0$. This statement applies to systems in thermodynamic equilibrium, but we can generalize this concept to

the common situation of materials that are out of equilibrium. All polymers have some resistance to shear under ordinary processing conditions, and this resistance can be quite persistent. Even if a fluid is in equilibrium at some stage, there are variations in stress associated with the fluid relaxation processes, so that the apparent G depends on the processing rate. For a constant processing rate, however, it is usual to discuss relative values of the material "shear rigidity" G (i.e., shear relaxation modulus at fixed shear rate) in fluids that flow slowly. We can formally apply theoretical results for describing G in elastic solids to describe this transient behavior. For example, as discussed by Bicerano [14], glassy amorphous polymers have $G \sim 10^3$ MPa, while rubbery amorphous polymers have $G \sim 1$ MPa at equilibrium. Substantial variations occur around these orders of magnitude as a function of the polymeric structure and average molecular weight. However, even at the inception of the "terminal zone," a finite $G \sim 10^{-3}$ MPa usually remains over the timescale of a typical fabrication process. This use of G for fluids a well as solids is clearly based on engineering expediency.

8.3.   Dilute Dispersions of Flexible Anisotropic Particles of General Shape

The development of an expression for $[\eta]$ for flexible particles of general shape is facilitated by considering the mathematically closely related problem of the conductivity σ of a dispersion of particles of arbitrary shape and conductivity σ(dispersed particle) in a matrix of conductivity $\sigma_0 = \sigma$(matrix). First, consider the simpler case of a spherical particle. The intrinsic conductivity virial coefficient $[\sigma]$ is given by Eq. 21, for which the relative conductivity of the dispersed particle equals $z_\sigma \equiv \sigma$(dispersed particle)/σ(matrix).

$$[\sigma] = \frac{(z_\sigma - 1)}{[1 + (z_\sigma - 1)/3]} \tag{21}$$

Equation 21 [8], which Maxwell originated, is written in a notation that makes the correspondence with Eqs. 19 and 20 evident. Thus, we make the general observation that adding a soft particle to a viscous fluid or hard matrix is quite similar to adding insulating particles (i.e., particles with a small σ) to a conductive matrix. This analogy between conductivity and viscosity was discussed above in the deduction of the master curve for the viscosity of dispersions of rigid particles. The advantage of this analogy for the present discussion is that accurate approximants of essentially the same form have been developed [147] for (1) $[\sigma]$ for arbitrary shaped particles for which z_σ is also arbitrary and (2) G for arbitrary shaped particles, arbitrary z_G (see Eq. 20), and Poisson's ratio. It is

possible, then, to state a fairly reasonable approximation for $[\eta]$ for deformable particles using these established results.

The intrinsic shear modulus $[G]$ of arbitrary-shaped particles dispersed in an incompressible medium is described well by the approximant given in Eq. 22 [147], where f is given by Eq. 23, $[G]_\infty$ is the intrinsic shear modulus for perfectly rigid particle inclusions ($z_G \to \infty$), and $[G]_0$ is the intrinsic shear modulus for perfectly deformable particles.

$$[G] \approx \frac{[G]_\infty \cdot (z_G - 1)^2 + f \cdot (z_G - 1)}{(z_G - 1)^2 + \{[G]_\infty + (2f/5)\} \cdot (z_G - 1) + f} \tag{22}$$

$$f = \frac{[G]_\infty - [G]_0 + [G]_\infty \cdot [G]_0}{1 + 3[G]_0/5} \tag{23}$$

As for the $[\sigma]$ of insulating particles, $[G]$ for highly extended deformable particles is rather insensitive to particle shape [8, 147]. The exact value of $[G]_0$ for a sphere equals $-5/3$ and only changes to $-28/15$ in the extreme case of needle-shaped flexible inclusions. The average value $[G]_0 \approx 53/30$ should provide a good approximation for deformable particles of modest anisotropy. This approximant is not reliable for extended flat particles, for which $[G]_0$ has a greater variation [147]. Note that $f \to \infty$ in Eq. 23 in the sphere limit, so that Eq. 22 then reduces to the exact result given by Eq. 20. Our approximant for $[\eta]$ for deformable particles involves simply replacing G by η in Eq. 22, a relation that holds exactly for spherical inclusions in an incompressible matrix. Bounds relating conductivity σ and elastic modulus G for general filler concentrations have been discussed rigorously [148], and the electrostatic-elastostatic analogy between G and σ has been employed widely in engineering applications involving inhomogeneous materials [149–151]. The relation between G and σ is certainly not exact as sometimes implied, but the correspondence is often found to be sufficiently strong to make many useful qualitative predictions for the properties of filled materials.

Figure 19 shows that predictions based on Eq. 22 are reasonable:

1. As z_η increases, $[\eta]$ increases monotonically.
2. We obtain $[\eta] \to -5/3$ independently of A_f in the limit of highly elongated deformable low-viscosity particles. Even if one were somehow able to inject a highly anisotropic gas bubble into a fluid, the thermodynamic drive to minimize the interfacial area would result in the rapid conversion of this bubble into a nearly undeformable spherical shape. These reductions of η with deformable particle inclusions should not be met often in practice, but the reduced enhancement of the viscosity for deformable particles of high A_f should be robust.
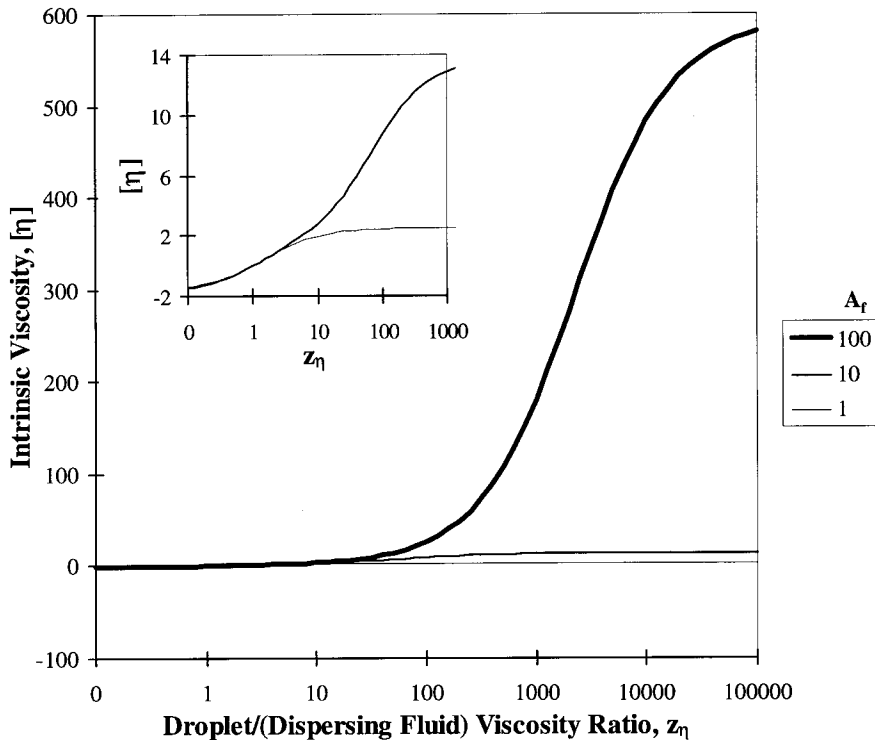
FIG. 19. Intrinsic viscosity $[\eta]$ for anisotropic fluid particles. Estimate of $[\eta]$ as a function of dispersed particle viscosity relative to droplet viscosity, $z_\eta = \eta$(dispersed particles)/η(dispersing fluid), for ellipsoidal particles with biaxial symmetry. Curves are labeled by the values of A_f. The inset shows the more gradual z_η dependence for lower values of the particle asymmetry A_f.

3. At any fixed z_η, the $[\eta]$ values retain the same ordering as a function of A_f.
4. Since $1/[\eta(\text{rigid particle})]$ decreases with increasing anisotropy, $[\eta]$ shows a larger z_η variation with increasing anisotropy.

8.4. Observations on Flexible Particle Dispersions

Nawab and Mason [152] measured the viscosity of dilute dispersions of threadlike (flexible solid) regenerated cellulose (rayon) fibers. They showed that $[\eta]$ is sensitive to a mean particle orientation factor, just like the $[\eta]$ of rigid

anisotropic particles. There was, however, a qualitative difference for rigid fibers of equal A_f in that the mean orientation factor of the flexible rayon fibers was sensitive to the permanent and recoverable deformation of the fibers by the shear gradient. Dispersions with $A_f > 113$ also showed the Weissenberg effect, which is defined as the liquid climbing up the inner cylinder of the Couette rheometer on application of shear. It was also observed that $[\eta]$ decreased with decreasing A_f, but that it increased (rather than decreasing as expected) on the plasticization of the fibers of high A_f by absorbing water.

Eirich and Sverak [153] also measured the effects of the swelling and flexibility of rayon fibers on the viscosity of dilute dispersions; they used several criteria in softening the fibers. They required that (1) the fiber length should change as little as possible; (2) the boundaries should remain sharp; (3) the softened fibers must not stick, fuse with each other, or break up easily; and (4) the softness ought to be such as to allow the fiber to bend readily if held at one end and subjected to a shear rate of about 10 s^{-1}. They were able to swell the fibers by up to a factor of 25 relative to their original volume. Such swelling reduced A_f by a factor of up to 25 since the fiber length essentially remained constant, while softening the fibers parallel to the amount of swelling in a fairly regular and reproducible extent. They found that η(relative) increased with increasing A_f for the rigid fibers. It also invariably decreased with greater swelling, which simultaneously reduced A_f and increased flexibility (making the deconvolution of the relative magnitudes of these two effects difficult). There was no noticeable stretching of the swollen coil-like fibers at the shear rates of 10 to 40 s^{-1} that were used. While some internal movement of the swollen flexible fibers was observed, overall fiber orientation (which was very marked with the rigid fibers) was absent in the swollen flexible fibers.

Zia, Cox, and Mason [154] considered ordered aggregates of rigid spheres, disks, and rods in planar Couette flow as simple physical model systems (for which the experimental data could be analyzed in a straightforward manner) of threads, aggregate of disk-shaped red blood cells, and other flexible particles. They found that chains of spheres formed in an electric field behaved like rigid rods at low shear gradients, but broke up at high gradients, possibly from cavitation of the liquid between the spheres. On the other hand, chains of spheres held together by liquid menisci behaved like flexible threads and formed disordered aggregates at high gradients. Symmetrical (but nonlinear) aggregates of spheres rotated like single spheres at low shear gradients. Aggregates of disks behaved like deformable rods and were easily broken as the disks slid apart.

Forgacs and coworkers [155, 156] studied the flexibility of cylindrical wood pulp fibers by subjecting dilute dispersions to laminar shear and observing the orbits of rotation. They found that the orbits are related to the ability of the fibers to deform under the stresses generated by the liquid. The fibers of greatest rigidity only underwent the types of *rigid rotations* predicted in Jeffery's classic

paper [157]. However, three other types of orbits appeared [158], in the follow-ing order, as fibers of increasing flexibility were considered: springy rotation, flexible rotation, and complex orbits. Some fibers also exhibited a fifth type of orbit, described as a jointed fiber orbit and attributed to the localized fracture of the cell wall. Forgacs and Mason indicated that the shear stress τ determines the types of orbits that are observed. For example, they proposed based, on theoretical considerations [158], that if E denotes the flexural modulus (equal to Young's modulus when a fiber has ideal isotropic elasticity), then the pre-dominant type of fiber orbit will change from rigid rotation to springy rotation at a critical value τ_c that is roughly proportional to E/A_f^4. Note that their proposal incorporates, correctly, the three key factors that affect the flexural rigidity of an anisotropic particle in a flow field. The inherent flexural rigidity increases inherent stiffness (E) and decreases very rapidly with increasing anisotropy (A_f). For example, if A_f is increased 10-fold, the critical shear stress would only remain unchanged if E is increased 10000-fold. The apparent flexural rigidity (whether a particle of given inherent flexural rigidity will actually behave like a rigid particle) also depends on the third important factor, namely, the magni-tude of the applied shear stress. While there was no theory to predict the τ_c values for the onset of flexible particle rotations and complex orbits, the authors also suggested that, by analogy, τ_c should exist for these higher orbit transitions.

8.5.   An Idealized Model for Concentrated Dispersions of Flexible Particles

Let us define a *flexible solid particle* as a flexible dispersed particle that retains its structural integrity (does not undergo breakup into smaller particles or coalescence into larger particles) under flow. We consider next how flexibil-ity alters η(dispersion). The aim here is to develop a working expression for estimating the viscosity of clay dispersions. This application is considered in Section 9.

As discussed above, the viscosity of dispersions of solid particles of consider-able flexibility (such as exfoliated clay platelets and fibers of xanthan gum) can be modeled reasonbly by neglecting the flexibity of the particles. The relatively small deviations between the calculated and observed results are consistent in direction with the errors expected from the neglect of flexibility. These results, as well as the universality of Eq. 5 that allows it to represent the effects of many factors on η(relative) as we showed above, lead us to propose (with some experimental support) that Eq. 5 should be used to estimate η(relative) over $0 \leq \Phi \leq \Phi^*$ for dispersions of solid particles that are somewhat (but not exceed-ingly) flexible. To follow this procedure and obtain results of high accuracy, Φ^* must be increased by the appropriate amount to account for the greater packing efficiency of flexible particles of a given shape. A model is presented

to accomplish this task. It is validated below by comparing its predictions with the experimental data of Krishnamoorti, Vaia, and Giannelis [113]. It should be noted, incidentally, that the data of these authors for poly(dimethyl siloxane) at $T = 301$K were used as the pure dispersing fluid viscosity in all illustrative examples for a polymer melt shown in Figs. 13 to 17.

It is expected that allowing particles to flex should increase Φ_m, so that η(relative) is reduced in comparison to rigid particles. The magnitude of this effect should decrease with increasing $\dot{\gamma}$ since flexibility should not affect Φ_{ocp} nearly as much as it may affect Φ_{m0}. We do not anticipate such a large effect of particle deformability on Φ_{ocp}. We introduce the following hypotheses:

1. The effects of flexibility can be described completely by making Φ_{m0} a function of flexibility, calculated so that as $\dot{\gamma} \to \infty$ the flexibility effects vanish in the same manner as $\Phi^* \to \Phi_{ocp}$.
2. The effects of flexibility on Φ_{m0} for a concentrated dispersion can be predicted from the effects on the $[\eta]_0$ of a dilute dispersion.
3. The results summarized by Bird et al. [159], based on "three-bead, two-rod" model, for the ratio of the $[\eta]_0$ values of flexible and rigid polymer chains can be utilized as a primitive model of flexible particles.

It should be evident that our modeling is highly idealized, but we expect this model to represent the essential features of real flexible particle dispersions. With these three basic assumptions, we obtain Eq. 24, where P is a flexibility parameter ranging from 0 in the limit of infinite rigidity to 1 in the limit of complete flexibility:

$$\frac{\Phi^*_{\text{flex}}}{\Phi^*_{\text{inflex}}} \approx \frac{[\eta]_{\text{inflex}}}{[\eta]_{\text{flex}}} \approx \left(1 - \frac{P}{3} \right)^{-1} \tag{24}$$

For polymer solutions, $P = 0$ describes true rigid-rod polymer chains, $P = 1$ describes freely jointed chains, and P is calculated using Eq. 25, where K_B is the bending energy:

$$P = k_B T / K_B \qquad \text{polymer solutions} \tag{25}$$

Readers interested in the assumptions underlying the derivation of Eqs. 24 and 25 should consult Section 16.4 of Bird et al. [159]. Below, we apply the model formally to dispersions of flexible particles generally.

For dispersions of biaxially symmetric particles, $P = 0$ describes infinitely rigid particles, and $P = 1$ describes completely flexible particles. P can be estimated based on the theory of beam deflection (as discussed below in detail) using Eq. 26, where L is the length of the longest axis of the particle, and r is the minimum radius of curvature of the particles in the dispersion.

$$P = \frac{(L/r)}{[1 + (L/r)]} \qquad \text{dispersions of biaxially symmetric particles} \qquad (26)$$

The radius of curvature in Eq. 26 can be determined by simply matching circular regions of calibrated dimensions with the particle contours in optical micrographs of the particles. This procedure is illustrated schematically in Fig. 20 for the case of a clay dispersion. Using the lateral dimension of a platelet divided by its thickness as their definition of A_f, Krishnamoorti et al. [113] indicated that the platelets in their exfoliated samples had $100 \leq A_f \leq 1000$. With our definition of A_f, we used their electron micrographs to measure r for exfoliated cylindrical platelets, assuming monodisperse platelets of $A_f = (1/100) = 0.01$ for simplicity. These platelets had a thickness of about 1 nm, so that $A_f = 0.01$ implied that their diameter L was 100 nm. We measured $r \approx 225$ nm from the micrographs, so Eq. 26 gave $P \approx 0.31$.

More generally, if the particles are assumed to flex as monolithic beams, it can be shown (see the Appendix) that $(L/r) \sim (A_f^3/E)$, where E is Young's modu-
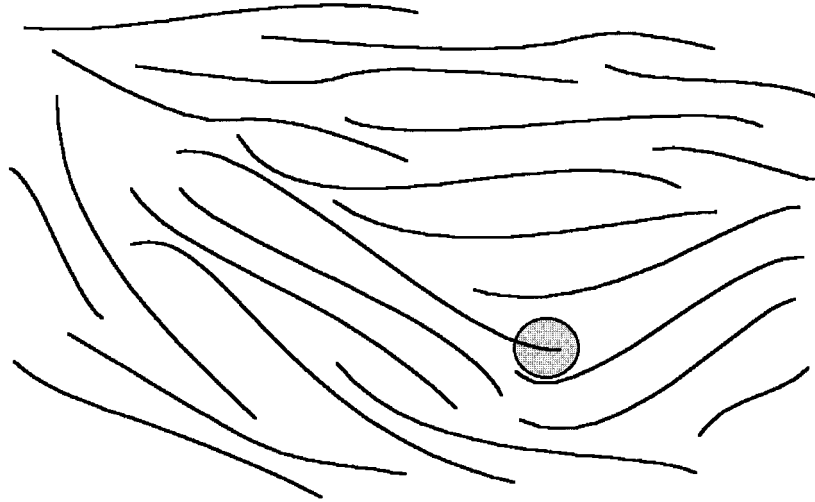
FIG. 20. Schematic image of method for estimating particle radius of curvature from optical micrographs. The minimum observed radius of curvature r of filler particles (curved lines in figure) can be estimated readily from micrographs by matching circles of calibrated size with the contours of the particle image. The estimates of the dispersion viscosity given in Section 9.3 utilize the theoretical model developed therein to account for the effects of particle flexibility on the dispersion viscosity, along with this technique for estimating r.

lus, both for fibers of aspect ratio $A_f > 1$ and for platelets of aspect ratio $(1/A_f)$ < 1. Assuming the silicate platelets of $(1/A_f) \approx 0.01$ used in the experiments [113] to have $E = 10^5$ MPa (a reasonable representative value for such inorganic materials), the proportionality constant can be fixed from the results obtained above. Equation 27 is then obtained and can be used to estimate P for cylindrical fibers and platelets as a function of A_f and E (in MPa) in general, relative to this calibration.

$$P = \frac{A_f^3}{(22.5E + A_f^3)} \qquad \text{cylindrical fibers of } A_f \geq 1$$

and platelets of $(1/A_f) < 1$ \hfill (27)

The ratio of the viscosity percolation thresholds of flexible to inflexible particles $\Phi^*_{\text{flex}}/\Phi^*_{\text{inflex}}$ is calculated as a function of A_f by inserting Eq. 27 into Eq. 24. The results of such calculations for cylindrical fibers and platelets of $E = 10^5$ MPa are shown in Fig. 21. The following observations can thus be made for particles with an intrinsic stiffness of $E = 10^5$ MPa:
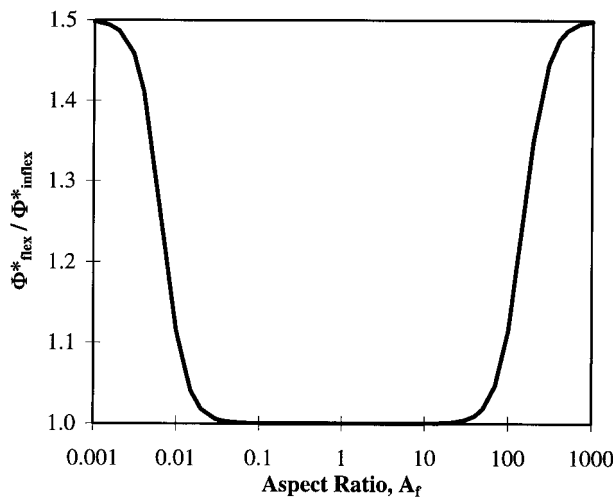
FIG. 21. Relative value of Φ^* for flexible platelets as a function of particle anisotropy A_f. Calculated effects of flexibility of cylindrical fibers and platelets of Young's modulus $E = 10^5$ MPa on the zero-shear maximum packing fraction Φ_{m0}. The factor by which Φ_{m0} increases because of flexibility is shown as a function of the aspect ratio of the cylinder.

1. Φ_{m0} does not begin to increase in a visible manner until $A_f \geq 30$ or $(1/A_f)$ $\leq (1/30)$.

2. At $A_f = 1000$ or $(1/A_f) = 0.001$, P is so close to its limit of 1 for completely flexible particles that Φ_{m0} has almost reached its upper limit of 1.5 times its value for infinitely rigid particles. Cylindrical silicate fibers of $A_f \geq 1000$ and platelets of $(1/A_f) \leq 0.001$, therefore, are expected to behave like totally flexible "ropes" or "sheets" rather than like rigid "needles" or "plates."

3. Since Eq. 27 contains the anisotropy effects in terms of the form A_f^3, while the intrinsic stiffness only enters in a term proportional to E, this conclusion remains valid even if the platelets are assumed to be of far greater stiffness. For example, at $A_f = 1000$ or $(1/A_f) = 0.001$, $(\Phi^*_{flex}/\Phi^*_{inflex}) \approx 1.50$ for both $E = 10^5$ MPa and $E = 2 \cdot 10^5$ MPa.

The results of calculations using our complete model for the viscosity of solid particles in a polymeric fluid (including the effects of particle flexibility) are presented in Section 9.

8.6. Concentrated Dispersions of Liquids and Gases

The breakup of dispersed domains, droplet distortion, co-continuity of two or more liquid phases, occlusion of subdomains of one phase in domains of another, phase inversion, and distinct maxima or minima (rather than a simple monotonic change) as a function of Φ because of the presence of "specific interactions" are often important in the rheology of liquid-in-liquid dispersions [124–133, 160–172]. Although data for the η(relative) of emulsions can sometimes be represented by scaling relationships of the same form as for dispersions of solids after appropriate adjustment of Φ^* [44], the ability to predict the viscosities of liquids or gases dispersed in liquids is very limited. In the absence of good theories, the existing expressions are often based on simple heuristic "rules of mixture." Additional research is needed to address these fundamental materials science problems.

In recent years, the frontiers of such research have moved toward the development of computationally intensive mesoscale simulation software based on methods such as dynamic density functional theory [173], dissipative particle dynamics [174], and lattice Boltzmann theory [175, 176]. While these simulation techniques currently leave out many of the pertinent aspects of the physics of liquid-in-liquid dispersions and hence are not yet ready for routine use as tools for quantitatively predictive rheological modeling, they may be improved sufficiently over the next decade to become adequate for such use.

9. CLAY MINERAL DISPERSIONS IN POLYMERS

9.1. Introduction to Clay Minerals

Clay minerals [66, 177, 178], such as layered aluminosilicates and magnesium silicates, are abundant in nature and hence currently are among the most widely used inexpensive sources of platelet-type fillers. In a study of such natural materials, Hornby, Schwartz, and Hudson [179], in work on complex porous media composed of interpenetrating connected fluid and clay phases, estimated the clay platelet orientation distribution in a specimen from a digitized scanning electron micrograph of model shales, they showed preference for horizontal orientation with the vast majority of the platelets at an angle between −45° and +45° to the horizontal in a roughly normal distribution. See Street [180] and Obiakor and Whitmore [181] for interesting early rheological results on clay dispersions.

The structures and properties of clays, and especially the interlayer forces in them, are obviously relevant to both the dispersion of platelets in a matrix material and the flow of these dispersions. An article by Giese [182] on the calculation of electrostatic interlayer forces in clays, and a review article by Bleam [183], are good starting points in considering these factors at a theoretical and/or computational level. In recent years, great increases in the speed and memory capabilities of computer hardware, and major advances in molecular modeling software, have rendered the very detailed atomistic simulation of these factors feasible.

9.2. Dispersion of Clay Minerals in Polymer Matrices

The reinforcing effects of fillers increase stongly with increasing anisotropy of filler shape, even within the context of traditional composite micromechanics [184–187], in which the filler is assumed to be dispersed in a matrix polymer, but does not modify the inherent properties of the matrix polymer itself. These effects can be dramatic, and they suggest that the thermoelastic properties of the matrix polymer are being modified by the presence of the filler for fillers of great anisotropy. Such synergistic effects involve processes such as the orientation and/or crystallization of polymer chains as a result of their confinement between adjacent platelets [188, 189] or the formation of strongly interacting and/or percolating microfibrillar networks [5, 6, 190]. Consequently, there is a significant experimental research effort to achieve high levels of dispersion of platelets of high A_f in polymer fluids via "exfoliation" [188, 189, 191, 192].

The statistical mechanics of fluids of anisotropic particle dispersions provide some insight into the equilibrium properties of these systems. Onsager [193] showed that a distribution of platelets has an intrinsic tendency toward becom-

ing ordered (aligned) spontaneously with increasing A_f and Φ as a result of geometrical (packing) constraints. This tendency is distinct from any additional extrinsic alignment that can be induced by imposing shear. He also suggested that the effect of long-range interactions can be accounted for by varying the effective size of the particles to include the screening length of these interactions. This effect generally reduces the effective volume fractions defining the dilute, semidilute, and concentrated regimes.

In a recent attempt to model the intrinsic alignment tendency, DiMarzio, Yang, and Glotzer [194] showed how entropic factors are sufficient to expect a phase transition from a three-dimensionally isotropic distribution of platelets to one that is highly ordered. This phenomenon is similar to the well-known liquid crystalline (isotropic to nematic) transition in rigid rod dispersions, which is also expected to occur even in the absence of attractive interparticle interactions [195], but that must be modified when interaction energies are taken into account [196]. Working with platelets of square cross section (for which they defined A_f as the side length divided by the thickness), they [194] showed that, for $A_f < 3.55$, one expects the distribution always to be isotropic. For $A_f > 3.55$, at a given value of A_f the dispersion is isotropic for $\Phi \leq \Phi_{c1}$, where Φ_{c1} is a lower critical volume fraction. There is a mixture of the isotropic and ordered phases for $\Phi_{c1} < \Phi < \Phi_{c2}$, where Φ_{c2} is an upper critical volume fraction and only the ordered phase for $\Phi \geq \Phi_{c2}$. Defining Φ_r as the volume fraction at which equal amounts of the isotropic and ordered phases are expected (i.e., the simple average of Φ_{c1} and Φ_{c2} according to the "lever rule"), they found that $\Phi_r \approx 3.55/A_f$, and a similar variation of Φ_m with particle aspect ratio is found in rods. This scaling is also very similar to the scaling of the p_c of oblate ellipsoids, for which $p_c \approx 1.276/A_f$ in the limit of large platelet asymmetry (as seen by inserting $A_f \to 0$ into Eq. 6, which uses a different notation). The concentration Φ_r is a factor of about 3 larger than p_c for slender plates, and this ratio is about 6 for slender rods. Despite this factor, the Φ range is relevant to experiments on platelet dispersions. For example, $\Phi_r \approx 0.0355$ if $A_f = 100$, and $\Phi_r \approx 0.01$ if $A_f = 355$.

Vaia and Giannelis [197] developed a mean-field model by modifying the Flory-Huggins lattice theory of polymer-monomer mixtures to treat polymer melt intercalation in organically modified layered silicates. They showed how the interplay of entropic and energetic factors, as reflected in the free energy, determines which one of the three possible types of thermodynamic equilibrium states (immiscible, intercalated, or exfoliated) will be favored. In particular, they showed that the entropic penalty for polymer confinement may be compensated for by the increased conformational freedom of the surfactant chain as the layers separate. When the total entropy change is small, small changes in the internal energy of the system determine if intercalation is thermodynamically favored. Exfoliation (complete layer separation) depends on the establishment of favorable interactions between the polymer chains and the organically modified lay-

ered silicate to overcome the entropic penalty of polymer confinement. Vaia and Giannelis then compared the predictions of the model with their experimental results [198] on the effects of silicate functionalization, annealing temperature, polymer molecular weight, and constituent interactions or melt intercalation of polystyrene, poly(3-bromostyrene), poly(vinyl cyclohexane), and poly(2-vinylpyridine). They showed that the predictions of the mean-field model accord reasonably well with experimental predictions and established some general guidelines for selecting potentially compatible combinations of polymers and organically modified layered silicates.

9.3.   Viscosity of Dispersions of Clay Platelets in Polymer Matrices

As stated above, well-tested closed-form expressions can provide first-order estimates of the dispersion viscosity. Such estimates are often all that is needed for engineering applications. However, the detailed treatment of the flow of platelet dispersions in all of its complexities will require large-scale simulations that incorporate the correct physical description of the system. Such an attempt was made recently to model the effects of particle size, shape, internal flexibility, and concentration on the flow of platelet dispersions by coarse-grained molecular dynamics simulations, considering both intraparticle and interparticle hydrodynamic interactions [115]. The calculated orbits for the motion of an isolated rigid symmetrical platelet agreed with the classic solution of Jeffery [157], leading to confidence in the detailed and complex simulation results on the effects of the asymmetry, flexibility, and volume fraction of platelets. For simple shear flow of a concentrated dispersion of platelets with a square cross section, planar orientation of the platelets was induced in the microstructure. For simple shear flow of platelike particles of rectangular cross section with unequal side lengths of the rectangle (and hence a shape that is intermediate between a platelet and a fiber), the major axis of the particles preferentially oriented in the shear direction. The simulations also showed how a platelet with some internal flexibility may deform while undergoing shear flow.

It should also be noted that, as discussed a long time ago by Krieger and Dougherty (as well as by others) in the context of dispersions of hard spheres [199], the most important source of shear thinning in clay dispersions is often the breakdown of the clumps and stacks of platelets rather than platelet orientation. Additional characterization (especially scattering data) are needed on such systems to assess the relative importance of this type of shear thinning.

Krishnamoorti et al. [113, 114] studied some important effects on platelet dispersion viscosity, and we have used their data as a test case to validate our dispersion viscosity model. Their experimental observations and the results of our calculations are now summarized:

1.   Materials with polymer chains intercalated between inorganic platelets manifested shear thinning even at the lowest $\dot{\gamma}$ that they explored and thus did not reach a Newtonian regime.

2.   Materials with platelets exfoliated and dispersed in a polymer matrix manifested Newtonian viscosity at low $\dot{\gamma}$ (with η_0 increasing monotonically with filler weight fraction), followed by shear thinning of magnitude comparable to that of the polymer, but starting at a slightly lower $\dot{\gamma}$. All of these trends are typical of conventional filled polymers and are consistent with Eq. 5. Most of the shear thinning manifested by η(dispersion) originates from the effect of shear on η(polymer). A small amount of additional shear thinning originates from an increase of Φ^* with increasing $\dot{\gamma}$. Contrary to the conventional physical picture of a rigid filler dispersed in a polymer matrix, exfoliated platelets of about 1 nm thickness and 10^3 to 10^4 nm lateral dimensions were rather flexible and behaved mechanically more like flexible sheets of paper than like rigid plates. This low flexural rigidity of platelets of high modulus arises from the large bending moments induced by the very anisotropic geometry.

3.   Grafting polymer chains onto the platelets strengthens matrix-filler adhesion. This effect manifested itself in the shear viscosity of materials in which polymer chains were end-tethered to highly anisotropic exfoliated silicate platelets, which differed significantly from that of the ordinary exfoliated systems. It manifested features reminiscent of block copolymers with lamellar ordering and smectic liquid crystals of small molecules. These features were interpreted by the possible presence, in the end-tethered materials, of a layered long-range domain structure. In such a structure, "grains" in which the silicate layers are oriented in a preferred direction exist, introducing grain boundaries and thus incorporating defects.

4.   The data shown in the first paper [113] for exfoliated platelet dispersions in poly(dimethyl siloxane) were used to validate our model. The authors reported only the weight fractions of the platelets (0.06 and 0.13). Using about 1 g/cm^3 for polymer density and about 2.7 g/cm^3 for platelet density, we estimated $\Phi \approx 0.0231$ at a weight fraction of 0.06 and $\Phi \approx 0.0524$ at a weight fraction of 0.13. The results depicted in Fig. 22 wer obtained using (1) the η(polymer) values shown in Figs. 13a, (2) Eq. 11 to calculate that $\theta \approx 0.0241$ seconds, (3) Eq. 10 (with $\Phi_{m0} \approx 0.242$ obtained by combining Eqs. 6, 7, 8, 24, and 26, and with $\Phi_{ocp} \approx 0.907$, as appropriate for these flexible cylindrical platelets of $A_f \approx$ 0.01) to calculate Φ_m as a function of $\dot{\gamma}$, and (4) Eq. 5 to calculate η(relative). The predictions of our model are in semiquantitative agreement with the experimental data. Most notably, the calculations do not involve any empiricism since they do not use any preexisting data for η(dispersion), as can be seen from the list of the input parameters: T, $\dot{\gamma}$, η(dispersing fluid, Φ, A_f, L, and r. Figure 22 also shows that, since the total shear thinning is a multiplicative superposition of the shear thinning attributable to the polymeric fluid by itself and alignment
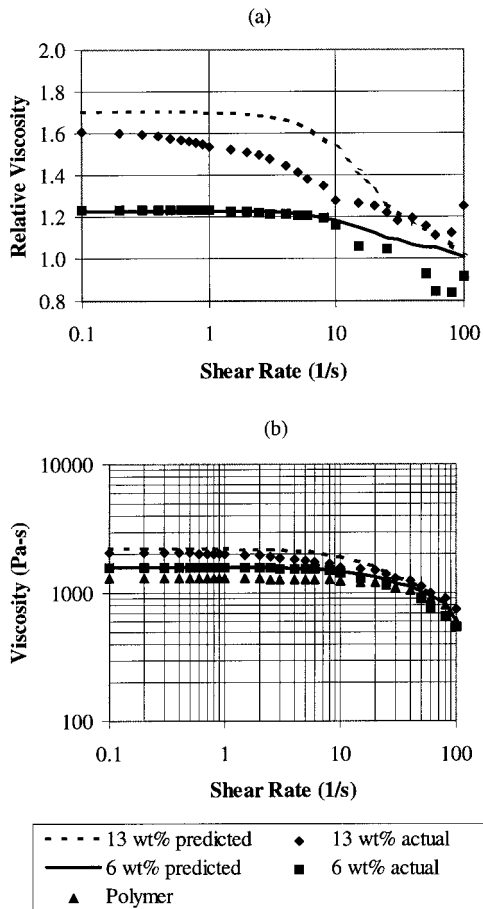
FIG. 22. Comparison between viscosity model and measurements for clays dispersed in polymers. Viscosities observed as a function of shear rate by Krishnamoorti et al. [113] for a dispersion of exfoliated silicate platelets (weight fractions of 0.06 and 0.13) in poly(dimethyl siloxane) at a temperature of $T = 301$K are indicated with symbols. Calculated results, assuming platelets to be monodisperse flexible cylinders with aspect ratio $A_f = $ (thickness/diameter) $= 0.01$, are indicated as lines: (a) relative viscosity $= \eta$(dispersion)$/\eta$(polymer); (b) dispersion viscosity, η(dispersion).

of the platelets, it is significantly greater than each of these separate effects.

5.   An interesting observation from the data is that, at very high shear rates, η(dispersion) may fall below η(polymer), giving η(relative) < 1. It can be seen from Eq. 5 that our model can only give η(relative) ≥ 1. Hence, it is important to consider the additional physical phenomena that may sometimes lower η(relative) below 1. For example, one might imagine that the solid particles increase the shear relaxation time θ of the fluid, causing an increased $\dot{\gamma}\,\theta$ at a fixed $\dot{\gamma}$ value. It is unlikely, however, that this shear thinning at lower shear rates would ever be larger than the increase in viscosity from the presence of the filler. Another possibility, which needs to be evaluated, is that chain clustering associated with entanglements may be diminished at high shear rates by the presence of the filler, so that the filler "plasticizes" the entangled polymeric fluid.

In summary, the modeling of the viscosity of clay dispersions in a polymeric dispersing fluid by Eq. 5 yields a good first approximation to the observed properties of these materials. However, further measurements are needed to validate the modeling. It seems likely that some features not incorporated in the present model, such as the modification of chain entanglement phenomena because of the presence of the filler, will be required for more quantitative estimation of dispersion properties. Our simple model of the viscosity of filled polymers should be useful in its present form, however, both in process design and in interpreting rheological measurements on these dispersions.

10.   SUMMARY AND CONCLUSIONS

A simple unified model (based on the concepts of universality and scaling) for the shear viscosity η of dispersions was presented. Relevant earlier modeling efforts and experimental observations were reviewed in connection with this model.

Some general effects are indicated by our modeling. Filler anisotropy [increasing aspect ratio $A_f > 1$ for fibers and decreasing $(1/A_f) < 1$ for platelets] can lead to substantial increases in the fluid viscosity even in dilute solutions. This effect is reflected in the rapid increase of the intrinsic viscosity $[\eta]$ of particulate fillers with increasing anisotropy. Percolation phenomena at higher volume fractions Φ (reflected in the rapid decrease of the geometrical percolation threshold p_c and the viscosity percolation threshold Φ^*) superimpose on this effect and further increase η. For particles that flocculate into fractal aggregates, there is still a further increase in η when Φ is not too high. The inherent tendency toward alignment of anisotropic particles, especially when augmented by shear, can mitigate these effects to some extent.

The key relationship of our model is Eq. 5, which expresses η(dispersion) relative to η(dispersing fluid) for particles of general shape. Equation 5 incorporates the effects of particle volume fraction, shape, polydispersity, fractal aggregation, and flexibility; dispersing fluid viscosity; and shear rate and temperature on the dispersion viscosity. Much consideration revolves around determining the viscosity percolation threshold Φ^*, which is the volume fraction at which the viscosity approaches infinity.

The value of Φ^* seems to be correlated with the geometrical percolation threshold p_c, and it is suggested that Φ^* is a rigidity percolation threshold. The volume fraction at random close packing Φ_m is identified with Φ^*. As particle asymmetry increases, both Φ_m and p_c decrease rapidly. We obtain first estimates of the limiting conditions for the processability of dispersions of filler particles having general shapes by assuming a proportional relation between Φ_m and p_c for ellipsoids of revolution. Shear-thinning and yielding effects are modeled through phenomenological arguments for how Φ^* is modified under shear. Fractal aggregation and particle flexibility effects on η(dispersion) are estimated by considering how the intrinsic viscosity is modified with particle aggregates and in dispersion of flexible particles.

Our model for η(dispersion) is developed entirely in terms of experimentally accessible parameters, and its use does not require the existence of data on η(dispersion). Consequently, this model is both fundamental and predictive. The following are its parameters:

1. The flow conditions, as described by the temperature and the shear rate.
2. The shear viscosity of the pure dispersing fluid, as described by its viscosity under specified flow conditions. If this fluid is a polymer melt and its viscosity under the flow conditions of interest has not been measured, it can be estimated roughly as described by Bicerano [14].
3. The amount of dispersed particles, as described by their volume fraction Φ.
4. The morphology of the dispersed particles, as described by the aspect ratio, length of longest axis, and minimum radius of the curvature induced by flexibility.

In conclusion, we have developed a simple predictive model for the shear viscosities of dispersions. This model is based on the concepts of universality and scaling. Its implementation relies on a combination of mathematical arguments and phenomenological observations. It is a pragmatic model that will undoubtedly require future refinements and revisions, as discussed in the next section, which describes the remaining challenges. We are confident, however, that it should provide a good starting point for determining the conditions of useful processing in filled polymer liquids when the dispersed particles are highly anisotropic.

11.   REMAINING CHALLENGES

Refinements of our model for the shear viscosity of dispersions of solids in liquids will require improvements in the prediction of Φ^*. A reliable method for obtaining Φ^* by simulations for particles of general shape should hence be sought. In particular, our prediction of Φ^* for platelets needs to be validated by simulations and/or measurements. Simulations may turn out to be especially useful for platelets as it is more difficult to generate truly random equilibrium packings of platelets experimentally than it is for fibers. Furthermore, our estimates of shear-thinning effects, yield stress, fractal aggregation, and particle flexibility effects need to be investigated by simulations and further experiments to validate our often heuristic modeling.

The following additional topics, which fell outside the scope of this manuscript, are also important in developing general rheological models of greater predictive power for disperions:

1. Prediction of dispersion microstructure from fundamental thermodynamic and/or atomistic considerations so that such information can be fed into the rheological model.
2. Prediction of extensional viscosity, which can sometimes be even more important than the shear viscosity. The development of a model for extensional viscosity may be hampered by the scarcity of reliable experimental data (especially at high Φ values).
3. Prediction of time-dependent phenomena such as thixotropy and dilatancy [99, 200–205]. A study of dispersions of black coal in oil as a function of the storage (aging) time [206] shows that η(relative) can be expressed as a function of (Φ/Φ_m) in such time-dependent dispersions as well, provided that the time dependence of Φ_m can be predicted. For example, in the coal dispersions [206], Φ_m decreased aymptotically as a function of time from an initial value to a lower limit, resulting in an increase in η(relative) by a combination of diffusion of oil within the coal and particle agglomeration. The challenge is to predict such kinetic effects.

APPENDIX: VARIATION OF PARTICLE RIGIDITY WITH PARTICLE PROPERTIES

Assume that the particles flex as monolithic beams. Then, as discussed in standard textbooks on mechanics (such as Higdon et al. [207]), the radius of curvature r of the particles at any point is given by Eq. 30 (which is valid for both fibers an platelets), where E is Young's modulus, I is the area moment of the particle cross-section, and M is the bending moment at the point.

$$r = EI/M \tag{30}$$

To estimate the variation of r with particle geometry, we need to estimate how I and M vary with the length L of the long dimension and the thickness t of the particle.

For cylindrical fibers of length L, I is proportional to t^4. If we assume that bending is produced by constant surface tractions, M is proportional to $L^2 t$. Combining these relations, inserting the aspect ratio $A_f = (L/t)$ and denoting the proportionality constant by α, we obtain Eq. 31.

$$L/r = \alpha A_f^3/E \tag{31}$$

For cylindrical platelets of diameter L, I is proportional to Lt^3. If we again assume that bending is produced by constant surface tractions, M is proportional to L^3. Combining these relations and defining the aspect ratio (<1 in our notation) as $(1/A_f) = t/L$, we obtain Eq. 31 again. The particle rigidity parameter P is related to L/r through Eq. 26.

NOTATION

a	one of the two minor axes of an ellipsoid with biaxial symmetry $(a = b)$
A	parameter of "dispersion gel" yield stress model (see Eqs. 13 and 14)
A_f	aspect ratio
b	one of the two minor axes of an ellipsoid with biaxial symmetry $(b = a)$
c	major axis of an ellipsoid with biaxial symmetry $(a = b$; sphere if $c = a = b)$
c^*	"overlap concentration" of polymer solutions; denotes onset of semi-dilute concentration regime
d	fractal dimension
D_c	collective diffusion coefficient
D_r	diffusion coefficient for rotary Brownian motion
E	Young's modulus or flexural modulus
$E_{\eta\infty}$	activation energy for viscous flow, defined in the limits of $\dot{\gamma} \to 0$ and $T \to \infty$
f	dimensionless constant defined by Eq. 23
F	particle shape factor in the definition of the reduced shear rate (Pe)
G	shear modulus
$[G]$	intrinsic shear modulus (leading virial coefficient of shear modulus)

$[G]_0$	intrinsic shear modulus for perfectly deformable particles
$[G]_\infty$	intrinsic shear modulus for perfectly rigid particles
I	area moment of particle cross section
J	compliance
k	a proportionality constant
K	a proportionality constant
k_B	Boltzmann's constant
K_B	force constant for bending
k_D	leading virial coefficient of the collective diffusion coefficient D_c
k_H	Huggins coefficient
L	length of longest axis of a particle
ln	natural logarithm
m	parameter of "dispersion gel" yield stress model (see Eqs. 13 and 14)
M	bending moment
M_{cr}	critical molecular weight
M_n	number-average molecular weight
M_w	weight-average molecular weight
N	average number of particles in a fractal aggregate
N_x	the crossover value of N
p	cross-link concentration
P	particle flexibility parameter
p_c	geometrical percolation threshold
Pe	Peclet number
r	minimum observed radius of curvature of a particle in a dispersion
t	thickness
T	absolute temperature in Kelvin
T_g	glass transition temperature in Kelvin
V	particle volume
z_G	ratio of shear moduli of dispersed particle to matrix; "relative modulus"
z_η	ratio of viscosities of dispersed fluid to dispersing fluid; "relative viscosity"
z_σ	ratio of conductivities of dispersed particle to dispersing particle; "relative conductivity"
$\dot{\gamma}$	shear rate
η	shear viscosity
η_0	shear viscosity in the limit of vanishing shear rate
$[\eta]$	intrinisc viscosity
$[\eta]_0$	value of $[\eta]$ at $Pe \rightarrow 0$
$[\eta]_\infty$	value of $[\eta]$ as $Pe \rightarrow \infty$

$[\eta]_{flex}$	value of $[\eta]$, including effects of particle flexibility
$[\eta]_{inflex}$	value of $[\eta]$ for infinitely rigid particles
θ	viscoelastic relaxation time
σ	conductivity
σ_0	conductivity of matrix material
$[\sigma]$	intrinsic conductivity
$[\sigma]_\infty$	intrinsic conductivity of highly conducting particle relative to suspending matrix
τ	shear stress
τ_c	a critical value of shear stress
τ_d	shear stress at which a fractal aggregate dissociates
τ_y	yield stress of "dispersion gel"
Φ	particle volume fraction
Φ^*	critical volume fraction at which the viscosity approaches infinity, termed *viscosity percolation threshold* in the present paper
Φ_{c1}	lower critical volume fraction for isotropic-to-ordered transition
Φ_{c2}	upper critical volume fraction for isotropic-to-ordered transition
Φ^*_{flex}	value of Φ^*, including effects of particle flexibility
Φ^*_{inflex}	value of Φ^* for infinitely rigid particles
Φ_m	maximum particle packing fraction for disordered particle dispersion
Φ_{mp}	value of Φ_m for primary particles of aggregate in the absence of aggregation
Φ_{m0}	value of Φ_m as $Pe \to 0$
Φ_{ocp}	ordered close-packed maximum volume fraction
Φ_r	arithmetic mean of Φ_{c1} and Φ_{c2}
Φ_x	crossover volume fraction for onset of semidilute concentration regime
$\bar{\Psi}$	dimensionless second osmotic virial coefficient

ACKNOWLEDGMENTS

REFERENCES

1. J. Mewis and C. W. Macosko, Suspension Rheology in *Rheology: Principles, Measurements, and Applications* (C. W. Macosko, Ed.), VCH Publishers, New York, 1994, chap. 10.

2. A. B. Metzner, *J. Rheol.*, *29*, 739–775 (1985).
3. W. B. Russel, *J. Rheol.*, *24*, 287–317 (1980).
4. H. Brenner, *Int. J. Multiph. Flow*, *1*, 195–341 (1974).
5. J. Bicerano and J. L. Brewbaker, *ANTEC '95 Prepr.*, 2542–2546 (1995).
6. J. Bicerano and J. L. Brewbaker, *J. Chem. Soc.*, *Faraday Trans.*, *91*, 2507–2513 (1995).
7. J. N. Israelachvili, *Intermolecular and Surface Forces*, 2nd ed., Academic, New York, 1992.
8. J. F. Douglas and E. J. Garboczi, *Adv. Chem. Phys.*, *91*, 85–153 (1995).
9. F. London, *Phys. Rev.*, *54*, 947–954 (1938).
10. M. Kogut and J. P. Straley, *J. Phys. C*, *12*, 2151–2159 (1979).
11. I. Balberg, *Phys. Rev. Lett.*, *59*, 1305–1308 (1987).
12. I. Halperin, S. Feng, and P. N. Sen, *Phys. Rev. Lett.*, *54*, 2391–2394 (1985).
13. B. Heaney, *Phys. Rev. B*, *52*, 477–480 (1995).
14. J. Bicerano, *Prediction of Polymer Properties*, 2nd ed., Marcel Dekker, New York, 1996.
15. International Organization for Standardization, ISO-31-8.
16. G. J. Kynch, *Br. J. Appl. Phys.*, *3*(suppl. 3), 5–11 (1954).
17. J. M. Peterson and M. Fixman, *J. Chem. Phys.*, *39*, 2516–2523 (1963).
18. B. Cichocki and B. U. Felderhof, *J. Chem. Phys.*, *89*, 3705–3709 (1988).
19. C. U. Thomas and M. Muthukumar, *J. Chem. Phys.*, *94*, 5180–5189 (1991).
20. G. K. Batchelor and J. T. Green, *J. Fluid Mech.*, *56*, 375–400 (1972).
21. G. K. Batchelor and J. T. Green, *J. Fluid Mech.*, *56*, 401–427 (1972).
22. G. K. Batchelor, *J. Fluid Mech.*, *83*, 97–117 (1977).
23. A. R. Altenberger and J. S. Dahler, *J. Colloid Interface Sci.*, *189*, 379–381 (1997).
24. E. Wajnryb and J. S. Dahler, *Adv. Chem. Phys.*, *102*, 193–313 (1997).
25. W. B. Russel, *J. Chem. Soc.*, *Faraday Trans.*, *Part 2*, *80*, 31–41 (1984).
26. M. Muthukumar and K. F. Freed, *Macromolecules*, *10*, 899–905 (1977).
27. J. F. Douglas and K. F. Freed, *Macromolecules*, *27*, 6088–6099 (1994).
28. A. L. Kholodenko and J. F. Douglas, *Phys. Rev. E*, *51*, 1081–1090 (1995).
29. D. H. Berry and W. B. Russel, *J. Fluid Mech.*, *180*, 475–494 (1987).
30. E. S. G. Shaqfeh and G. H. Fredrickson, *Phys. Fluids*, *A*, *2*, 7–24 (1990).
31. A. P. Shapiro and R. F. Probstein, *Phys. Rev. Lett.*, *68*, 1422–1425 (1992).
32. A. Karnis, H. L. Goldsmith, and S. G. Mason, *J. Colloid Interface Sci.*, *22*, 531–553 (1966).
33. H. L. Goldsmith and S. G. Mason, *J. Colloid Sci.*, *17*, 448–476 (1962).
34. P. G. de Gennes, *J. Phys.*, *40*, 783–787 (1979).
35. P. M. Adler, A. Nadim, and H. Brenner, *Adv. Chem. Eng.*, *15*, 1–72 (1990).
36. J. L. Bouillot, C. Camoin, M. Belzons, R. Blanc, and E. Guyon, *Adv. Colloid Interface Sci.*, *17*, 299–305 (1982).
37. W. B. Russel and P. R. Sperry, *Prog. in Org. Coat.*, *23*, 305–324 (1994).
38. J. Feder, *Fractals*, Plenum, New York, 1988.
39. (a) C. R. Wildemuth and M. C. Williams, *Rheol. Acta*, *24*, 75–91 (1985); (b) C. R. Wildemuth and M. C. Williams, *Rheol. Acta*, *23*, 627–635 (1984).
40. N. Q. Dzuy and D. V. Boger, *J. Rheol.*, *27*, 321–349 (1983).
41. T. Kataoka, T. Kitano, M. Sasahara, and K. Nishijima, *Rheol. Acta*, *17*, 149–155 (1978).

42. T. Kitano, T. Kataoka, T. Nishimura, and T. Sakai, *Rheol. Acta*, *19*, 764–769 (1980).
43. T. Kitano, T. Kataoka, and T. Shirota, *Rheol. Acta*, *20*, 207–209 (1981).
44. R. Pal and E. Rhodes, *J. Rheol.*, *33*, 1021–1045 (1989).
45. C. G. de Kruif, E. M. F. van Lersel, A. Vrij, and W. B. Russel, *J. Chem Phys.*, *83*, 4717–4725 (1985).
46. J. C. van der Werff and C. G. de Kruif, *J. Rheol.*, *33*, 421–454 (1989).
47. A. van Blaaderen, J. Peetermans, G. Maret, and J. K. G. Dhont, *J. Chem. Phys.*, *96*, 4591–4603 (1992).
48. J. S. Chong, E. B. Christiansen, and A. D. Baer, *J. Appl. Polym. Sci.*, *15*, 2007–2021 (1971).
49. J. F. Brady, *J. Chem. Phys.*, *99*, 567–581 (1993).
50. S. H. Maron and P. E. Pierce, *J. Colloid Sci.*, *11*, 80–95 (1956).
51. A. P. Philipse, *Langmuir*, *12*, 1127–1133 (1996).
52. B. J. Ackerson, *J. Rheol.*, *34*, 553–589 (1990).
53. L. V. Woodcock, *Chem. Phys. Lett.*, *111*, 455–461 (1984).
54. Y. Song, E. A. Mason, and R. M. Stratt, *J. Phys. Chem.*, *93*, 6916–6919 (1989).
55. (a) M. F. Thorpe, in *Physics of Disordered Materials* (D. A. Adler, H. Fritzsche, and S. R. Ovshinsky, Eds.), Plenum, New York, 1985, pp. 55–61; (b) D. J. Jacobs and M. F. Thorpe, *Phys. Rev. E*, *53*, 3682–3693 (1996).
56. T. Aste, *Phys. Rev. E*, *53*, 2571–2579 (1996).
57. N. Pape, L. Riepe, and J. R. Schopper, *Part. Charact.*, *1*, 66–73 (1984).
58. M. S. Spector, J. A. Zasadzinski, and M. B. Sankaram, *Langmuir*, *12*, 4704–4708 (1996).
59. R. Zallen, *The Physics of Amorphous Solids*, John Wiley and Sons, New York, 1983.
60. D. Stauffer and A. Aharony, *Introduction to Percolation Theory* 2nd ed., Taylor and Francis, London, 1994.
61. B. D. Hughes, *Random Walks and Random Environments*, *Volume 2*: *Random Environments*, Clarendon Press, Oxford, 1996.
62. J. Boissonade, F. Barreau, and F. Carmona, *J. Phys. A*: *Math. Gen.*, *16*, 2777–2787 (1983).
63. A. Celzard, G. Furdin, J. F. Marêché, E. McRae, M. Dufort, and C. Deleuze, *Solid State Commun.*, *92*, 377–383 (1994).
64. A. Celzard, E. McRae, J. F. Marêché, G. Furdin, M. Dufort, and C. Deleuze, *J. Phys. Chem. Solids*, *57*, 715–718 (1996).
65. A. Celzard, E. McRae, C. Deleuze, M. Dufort, G. Furdin, and J. F. Marêché, *Phys. Rev. B*, *53*, 6209–6214 (1996).
66. M. Dijkstra, J.-P. Hansen, and P. A. Madden, *Phys. Rev. E*, *55*, 3044–3053 (1997).
67. E. Anczurowski and S. G. Mason, *J. Colloid Interface Sci.*, *23*, 522–532 (1967).
68. E. Anczurowski and S. G. Mason, *J. Colloid Interface Sci.*, *23*, 533–546 (1967).
69. A. Okagawa and S. G. Mason, *J. Colloid Interface Sci.*, *45*, 330–358 (1973).
70. I. Balberg, *Phys. Rev. B*, *31*, 4053–4055 (1985).
71. A. Fizazi, J. Moulton, K. Pakbaz, S. D. D. V. Rughooputh, P. Smith, and A. J. Heeger, *Phys. Rev. Lett.*, *64*, 2180–2183 (1990).
72. K. Levon, A. Margolina, and A. Z. Patashinsky, *Macromolecules*, *26*, 4061–4063 (1993).

73. E. J. Garboczi, K. A. Snyder, J. F. Douglas, and M. F. Thorpe, *Phys. Rev. E*, *52*, 819–828 (1995).

74. J. Dudowicz, M. Lifschitz, K. F. Freed, and J. F. Douglas, *J. Chem. Phys.*, *99*, 4804–4820 (1993).

75. (a) S. B. Lee and S. Torquato, *Phys. Rev. A*, 5338–5344 (1999); (b) A. L. R. Bug, S. A. Safran, G. S. Grest, and I. Webman, *Phys. Rev. Lett.*, *55*, 1896–1899 (1985).

76. A. R. Boccaccini, *J. Mater. Sci.*, *29*, 4273–4278 (1994).

77. J. Bicerano and D. Adler, *Pure Appl. Chem.*, *59*, 101–144 (1987).

78. M. Nardin, E. Papirer, and J. Schultz, *Powder Technol.*, *44*, 131–140 (1985).

79. J. G. Parkhouse and A. Kelly, *Proc. Roy. Soc. London A*, *451*, 737–746 (1995).

80. (a) J. G. Berryman, *Phys. Rev. A*, *27*, 1053–1061 (1983); (b) M. D. Rintoul and S. Torquato, *Phys. Rev. Lett.*, *77*, 4198–4201 (1996).

81. L. A. Utracki and R. J. Simha, *J. Polym. Sci. A*, *1*, 1089–1098 (1963).

82. W. Burchard, *Macromol. Chem.*, *Macromol. Symp.*, *18*, 1–35 (1988).

83. W. Brown and T. Nicolai, *Colloid Polym. Sci.*, *268*, 977–990 (1990).

84. (a) B. J. Buchalter and R. M. Bradley, Orientational order in random packings of ellipses, *Phys. Rev. A*, *46*, 3046–3056 (1992); (b) B. J. Buchalter and R. M. Bradley, Orientational order in amorphous packings of ellipsoids, *Europhys. Lett.*, *26*, 159–164 (1994).

85. S. W. Churchill, *Viscous Flows*: *The Practical Use of Theory*, Butterworths, Boston, 1988, pp. 504, 505.

86. H. Kanai, R. C. Navarrete, C. W. Macosco, and L. E. Scriven, *Rheol. Acta*, *31*, 333–344 (1992).

87. B. Gauthier-Manuel, E. Guyon, S. Roux, S. Gits, and F. Lefaucheux, *J. Phys.* (*France*), *48*, 869–875 (1987).

88. F. Devreux, J. P. Boilot, F. Chaput, L. Malier, and M. A. V. Axelos, *Phys. Rev. E*, *47*, 2689–2694 (1993).

89. (a) S. Arbabi and M. Sahimi, *Phys. Rev. Lett.*, *65*, 725–728 (1990); (b) M. A. V. Axelos and M. Kolb, *Phys. Rev. Lett.*, *64*, 1457–1460 (1990).

90. P. Sollich, F. Lequeux, P. Hébraud, and M. E. Cates, *Phys. Rev. Lett.*, *78*, 2020–2023 (1997).

91. N. Goldenfeld and P. Goldbart, *Phys. Rev. A*, *45*, 5343–5345 (1992).

92. P. G. de Gennes, *J. Phys.*, *Lett.*, *37*, L1–L2 (1976).

93. J. Roovers, *Macromolecules*, *27*, 5359–5364 (1994).

94. (a) D. J. Durian, *Phys. Rev. Lett.*, *75*, 4780–4783 (1995); (b) M.-D. Lacasse, G. S. Grest, D. Levine, T. G. Mason, and D. A. Weitz, *Phys. Rev. Lett.*, *76*, 3448–3451 (1996).

95. A. Mourchid, A. Delville, and P. Levitz, *Faraday Disc.*, *101*, 275–285 (1995).

96. S. S. Manna and H. J. Herrmann, *J. Phys. A*, *24*, L481–L490 (1991); see also D. Jones, *Nature*, *332*, 310 (1988).

97. C. Tsenoglou and S. Yang, *Polym. Eng. Sci.*, *30*, 1407–1412 (1990).

98. H. M. Princen, *J. Colloid Interface Sci.*, *71*, 55–66 (1979).

99. J. F. Douglas, *Macromolecules*, *25*, 1468–1474 (1992).

100. J. F. Douglas, *Phys. Rev. E*, *54*, 2677–2689 (1996).

101. F. Pignon, A. Magnin, and J.-M. Piau, *Phys. Rev. Lett.*, *79*, 4689–4692 (1997).

102. J. V. DeGroot, Jr., C. W. Macosco, T. Kume, and T. Hashimoto, *J. Colloid Interface Sci.*, *166*, 404–413 (1994).

103. R. C. Sonntag and W. B. Russel, *J. Colloid Interface Sci.*, *115*, 378–389 (1987).

104. A. A. Potanin, *J. Colloid Interface Sci.*, *145*, 140–157 (1991).

105. A. A. Potanin, *J. Colloid Interface Sci.*, *157*, 399–410 (1993).

106. A. A. Potanin, R. de Rooij, D. van den Ende, and J. Mellema, *J. Chem. Phys.*, *102*, 5845–5853 (1995).

107. C. Tsenoglou, *Rheol. Acta*, *28*, 311–315 (1989).

108. C. Aubert and D. S. Cannell, *Phys. Rev. Lett.*, *56*, 738–741 (1986).

109. (a) M. Y. Lin, H. M. Lindsay, D. A. Weitz, R. C. Ball, R. Klein, and P. Meakin, *Nature*, *339*, 360–362 (1989); (b) H. J. M. Hanley, G. C. Straty, and F. Tsvetkov, *Langmuir*, *10*, 3362–3364 (1994); (c) M. Kawaguchi, A. Mizutani, Y. Matsushita, and T. Kato, *Langmuir*, *12*, 6179–6183 (1996).

110. M. L. Mansfield, J. F. Douglas, and E. J. Garboczi, manuscript in preparation.

111. (a) J. B. Hubbard and J. F. Douglas, *Phys. Rev. E*, *47*, R2983–R2986 (1993); (b) J. F. Douglas, H.-X. Zhou, and J. B. Hubbard, *Phys. Rev. E*, *49*, 5319–5331 (1994); (c) H.-X. Zhou, A. Szabo, J. F. Douglas, and J. B. Hubbard, *J. Chem. Phys.*, *100*, 3821–3826 (1994).

112. A. M. Kraynik, *Anu. Rev. Fluid Mech.*, *20*, 325–357 (1988).

113. R. Krishnamoorti, R. A. Vaia, and E. P. Giannelis, *Chem. Mater.*, *8*, 1728–1734 (1996).

114. R. Krishnamoorti and E. P. Giannelis, *Macromolecules*, *30*, 4097–4102 (1997).

115. S. Yamamoto and T. Matsuoka, *J. Chem. Phys.*, *107*, 3300–3308 (1997).

116. P. J. Whitcomb and C. W. Macosco, *J. Rheol.*, *22*, 493–505 (1978).

117. S. Kumar and T. E. Helminiak, in *The Materials Science and Engineering of Rigid-Rod Polymers* (W. W. Adams, R. K. Eby, and D. E. McLemore, (Eds.), *Materials Research Society Symposium Proceedings*, *134*, Materials Research Society, Pittsburgh, PA, 1989, pp. 363–374.

118. (a) S. Iijima, C. Brabec, A. Maiti, and J. Bernholc, *J. Chem. Phys.*, *104*, 2089–2092 (1996); (b) B. I. Yakobson, C. J. Brabec, and J. Bernholc, *Phys. Rev. Lett.*, *76*, 2511–2514 (1996).

119. G. I. Taylor, *Proc. Roy. Soc. A*, *209*, 447–461 (1951).

120. Th. Y.-T. Wu, in *Advances in Applied Mechanics*, Vol. 11 (C.-S. Yih, Ed.), Academic, New York, 1971, pp. 1–63.

121. C. Brennen and H. Winet, *Anu. Rev. Fluid Mech.*, *9*, 339–398 (1977).

122. L. J. Fauci, *J. Comput. Phys.*, *86*, 294–313 (1990).

123. X. Wen, C. W. Garland, T. Hwa, M. Kardar, E. Kokufuta, Y. Li, M. Orkisz, and T. Tanaka, *Nature*, *355*, 426–428 (1992).

124. A. E. Woodward, *Atlas of Polymer Morphology*, Hanser, Munich, 1989.

125. J. A. Manson and L. H. Sperling, *Polymer Blends and Composites*, Plenum, New York, 1976.

126. N. R. Legge, G. Holden, and H. E. Schroeder (Eds.), *Thermoplastic Elastomers*: *A Comprehensive Review*, Hanser, Munich, 1987.

127. I. S. Miles and S. Rostami (Eds.), *Multicomponent Polymer Systems*, Longman Scientific and Technical, Essex, England, 1992.

128. P. M. Subramanian, *Polym. Eng. Sci.*, *25*, 483–487 (1985).

129.   M. W. Matsen and F. S. Bates, *Macromolecules*, *29*, 1091–1098 (1996).
130.   P. K. Janert and M. Schick, *Macromolecules*, *30*, 137–144 (1997).
131.   C. A. Orr, A. Adedeji, A. Hirao, F. S. Bates, and C. W. Macosco, *Macromolecules*, *30*, 1243–1246 (1997).
132.   N. Mekhilef and H. Verhoogt, *ANTEC '97 Prepr.*, 2156–2163 (1997).
133.   V. M. Avila-Garcia, E. Mendizabal, M. Arellano, and R. Gonzalez-Nunez, *ANTEC '97 Prepr.*, 3756–3760 (1997).
134.   R. Roscoe, *J. Fluid Mech.*, *28*, 273–293 (1967).
135.   J. D. Goddard and C. Miller, *J. Fluid Mech.*, *28*, 657–673 (1967).
136.   Y. Otsubo and R. K. Prud'homme, *Rheol. Acta*, *33*, 29–37 (1994).
137.   Y. Otsubo and R. K. Prud'homme, *Rheol. Acta*, *33*, 303–306 (1994).
138.   G. I. Taylor, *Proc. Roy. Soc. London*, *138A*, 41–48 (1932).
139.   N. A. Frankel and A. Acrivos, *J. Fluid Mech.*, *44*, 65–78 (1970); see also S. J. Choi and W. R. Schowalter, *Phys. Fluids*, *18*, 420–427 (1975).
140.   G. I. Taylor, *Proc. Roy. Soc. London*, *226A*, 34–37 (1954).
141.   M. A. Nawab and S. G. Mason, *J. Colloid Sci.*, *13*, 179–187 (1958).
142.   W. N. Bond, *Philos. Mag.*, *4*, 889–898 (1927).
143.   W. N. Bond, *Philos Mag.*, *5*, 794–800 (1928).
144.   R. Bagheri and R. A. Pearson, *Polymer*, *36*, 4883–4885 (1995).
145.   N. P. Louat, M. S. Duesbery, M. A. Imam, V. Provenzano, and K. Sadananda, *Philos. Mag. Lett.*, *63*, 159–163 (1991).
146.   W. P. Cox and E. H. Merz, *J. Polym. Sci.*, *28*, 619–622 (1958).
147.   E. J. Garboczi and J. F. Douglas, *Phys. Rev. E*, *53*, 6169–6180 (1996).
148.   L. V. Gibiansky and S. Torquato, *Phys. Rev. Lett.*, *71*, 2927–2930 (1993).
149.   L. E. Nielsen, *Ind. Eng. Chem. Fund.*, *13*, 17–20 (1974).
150.   G. S. Springer and S. W. Tsai, *J. Comp. Mat.*, *1*, 166–173 (1967).
151.   D. M. Bigg, *Polym. Comp.*, *7*, 125–140 (1986).
152.   M. A. Nawab and S. G. Mason, *J. Phys. Chem.*, *62*, 1248–1253 (1958).
153.   F. Eirich and J. Sverak, *Trans. Faraday Soc.*, *42B*, 57–66 (1946).
154.   I. Y. Z. Zia, R. G. Cox, and S. G. Mason, *Proc. Roy. Soc. A*, *300*, 421–441 (1967).
155.   O. L. Forgacs and S. G. Mason, *Tappi J.*, *41*, 695–704 (1958).
156.   O. L. Forgacs, A. A. Robertson, and S. G. Mason, *Pulp Paper Mag. Canada*, *59*, 117–128 (1958).
157.   G. B. Jeffery, *Proc. Roy. Soc. A*, *102*, 161–179 (1992).
158.   O. L. Forgacs and S. G. Mason, *J. Colloid, Sci.*, *14*, 457–472 (1959).
159.   R. B. Bird, C. F. Curtiss, R. C. Armstrong, and O. Hassager, *Dynamics of Polymeric Liquids*, *Volume 2*: *Kinetic Theory*, 2nd ed., John Wiley and Sons, New York, 1987.
160.   L. E. Nielsen, *Polymer Rheology*, Marcel Dekker, New York, 1977.
161.   R. F. Heitmiller, R. Z. Naar, and H. H. Zabusky, *J. Appl. Polym. Sci.*, *8*, 873–880 (1964).
162.   S. Uemura and M. Takayanagi, *J. Appl. Polym. Sci.*, *10*, 113–125 (1966).
163.   M. Takayanagi, S. Uemura, and S. Minami, *J. Polym. Sci.*, *Part C*, *5*, 113–122 (1964).
164.   L. B. Kandyrin and V. N. Kuleznev, *Kolloid Zhurn.* [English trans.], *36*, 431–436 (1974).

165. C. B. Arends, *Polym. Eng. Sci.*, *32*, 841–844 (1992).

166. J. Lyngaae-Jorgensen and L. A. Utracki, *Makromol. Chem.*, *Macromol. Symp.*, *48/49*, 189–209 (1991).

167. J. Lyngaae-Jorgensen, A. Kuta, K. Sondergaard, and K. Veno Poulsen, *Polym. Network Blends*, *3*, 1–13 (1993).

168. T. I. Ablazova, M. B. Tsebrenko, A. B. V. Yudin, G. V. Vinogradov, and B. V. Yarlykov, *J. Appl. Polym. Sci.*, *19*, 1781–1798 (1975).

169. J. Kolarik, *Polym. Network Blends*, *5*, 87–93 (1995).

170. J. Kolarik, *Polym. Eng. Sci.*, *36*, 2518–2524 (1996).

171. G. I. Taylor, *Proc. Roy. Soc. A London*, *146*, 501–523 (1934).

172. C. Tsenoglou, *J. Rheol.*, *34*, 15–24 (1990).

173. (a) B. A. C. van Vlimmeren, M. Postma, P. Huetz, A. Brisson, and J. G. E. M. Fraaije, *Phys. Rev. E*, *54*, 5836–5839 (1996); (b) J. G. E. M. Fraaije, B. A. C. van Vlimmeren, N. M. Maurits, M. Postma, O. A. Evers, C. Hoffmann, P. Altevogt, and G. Goldbeck-Wood, *J. Chem. Phys.*, *106*, 4260–4269 (1997); (c) N. M. Maurits, B. A. C. van Vlimmeren, and J. G. E. M. Fraaije, *Phys. Rev. E*, *56*, 816–825 (1997).

174. R. D. Groot and P. B. Warren, *J. Chem. Phys.*, *107*, 4423–4435 (1997).

175. N. S. Martys and H. Chen, *Phys. Rev. E*, *53*, 743–750 (1996).

176. (a) X. Shan and H. Chen, *Phys. Rev. E*, *47*, 1815–1819 (1992); (b) X. Shan and H. Chen, *Phys. Rev. E*, *49*, 2941–2948 (1994).

177. R. E. Grim, *Clay Mineralogy*, McGraw-Hill, New York, 1968.

178. R. M. Barrer, *Zeolites and Clay Minerals as Sorbents and Molecular Sieves*, Academic, New York, 1978.

179. B. E. Hornby, L. M. Schwartz, and J. A. Hudson, *Geophys.*, *59*, 1570–1583 (1994).

180. N. Street, *Aust. J. Chem.*, *9*, 467–479 (1956).

181. E. K. Obiakor and R. L. Whitmore, *J. Oil Colour Chem. Assoc.*, *47*, 334–345 (1964).

182. R. F. Giese, *Clays Clay Miner.*, *26*, 51–57 (1978).

183. W. F. Bleam, *Rev. Geophys.*, *31*, 51–73 (1993).

184. R. M. Christensen, *J. Eng. Mater. Tecnnol.*, *101*, 299–303 (1979).

185. T. S. Chow, *J. Mater. Sci.*, *15*, 1873–1888 (1980).

186. J. C. Halpin and J. L. Kardos, *Polym. Eng. Sci.*, *16*, 344–352 (1976).

187. L. A. Utracki and T. Vu Khanh, Filled polymers, in *Multicomponent Polymer Systems* (I. S. Miles and S. Rostami, Eds.), Longman Scientific and Technical, Essex, England, 1992, chap. 7.

188. T. Kurauchi, A. Okada, T. Nomura, T. Nishio, S. Saegusa, and R. Deguchi, *SAE Technical Papers Series*, No. 910584, International Congress and Exposition, Detroit, MI February 25–March 1, 1991.

189. E. P. Giannelis, *JOM*, 28–30 (March 1992).

190. V. Favier, H. Chanzy, and J. Y. Cavaille, *Macromolecules*, *28*, 6365–6367 (1995).

191. E. Giannelis, Nanoscale, two-dimensional organic-inorganic materials, in *Materials Chemistry*: *An Emerging Discipline* (L. V. Interrante, L. A. Caspar, and A. B. Ellis, Eds.), *Adv. Chem. Ser. 245*, American Chemical Society, Washington, DC, 1995, chap. 10.

192. M. Kawasumi, N. Hasegawa, M. Kato, A. Usuki, and A. Okada, *Macromolecules*, *30*, 6333–6338 (1997).
193. L. Onsager, *Ann. New York Acad. Sci.*, *51*, 627–659 (1949).
194. E. A. DiMarzio, A. J.-M. Yang, and S. C. Glotzer, *J. Res. Nat. Inst. Stand. Technol.*, *100*, 173–186 (1995).
195. P. J. Flory and G. Ronca, *Mol. Cryst. Liq. Cryst.*, *54*, 289–310 (1979).
196. P. J. Flory and G. Ronca, *Mol. Cryst. Liq. Cryst.*, *54*, 311–330 (1979).
197. R. A. Vaia and E. P. Giannelis, *Macromolecules*, *30*, 7990–7999 (1997).
198. R. A. Vaia and E. P. Giannelis, *Macromolecules*, *30*, 8000–8009 (1997).
199. I. M. Krieger and T. J. Dougherty, *Trans. Soc. Rheol.*, *3*, 137–152 (1959).
200. W. H. Bauer and E. A. Collins, Thixotropy and dilatancy, in *Rheology*: *Theory and Applications*, Vol. 4 (F. R. Eirich, Ed.), Academic, New York, 1967, chap. 8.
201. A. Parts, *Nature*, *155*, 236–237 (1945).
202. D. C.-H. Cheng, *Nature*, *245*, 93–94 (1973).
203. O. C. C. Lin, *J. Appl. Polym. Sci.*, *19*, 199–214 (1975).
204. R. G. Green and R. G. Griskey, *Trans. Soc. Rheol.*, *12*, 27–37 (1968).
205. H. Freundlich and H. L. Röder, *Faraday Soc. Trans.*, *34*, 308–316 (1938).
206. A. K. Ghosh and S. N. Bhattacharya, *Rheol. Acta*, *23*, 195–206 (1984).
207. A. Higdon, E. H. Ohlsen, W. B. Stiles, J. A. Weese, and W. F. Riley, *Mechanics of Materials*, 3rd ed., John Wiley and Sons, New York, 1976.

Request Permission or Order Reprints Instantly!

Interested in copying and sharing this article? In most cases, U.S. Copyright Law requires that you get permission from the article's rightsholder before using copyrighted content.

All information and materials found in this article, including but not limited to text, trademarks, patents, logos, graphics and images (the "Materials"), are the copyrighted works and other forms of intellectual property of Marcel Dekker, Inc., or its licensors. All rights not expressly granted are reserved.

Get permission to lawfully reproduce and distribute the Materials or order reprints quickly and painlessly. Simply click on the "Request Permission/Reprints Here" link below and follow the instructions. Visit the U.S. Copyright Office for information on Fair Use limitations of U.S. copyright law. Please refer to The Association of American Publishers' (AAP) website for guidelines on Fair Use in the Classroom.

The Materials are for your personal use only and cannot be reformatted, reposted, resold or distributed by electronic means or otherwise without permission from Marcel Dekker, Inc. Marcel Dekker, Inc. grants you the limited right to display the Materials only on your personal computer or personal wireless device, and to copy and download single copies of such Materials provided that any copyright, trademark or other notice appearing on such Materials is also retained by, displayed, copied or downloaded as part of the Materials and is not removed or obscured, and provided you do not edit, modify, alter or enhance the Materials. Please refer to our Website User Agreement for more details.

Order now!

Reprints of this article can also be ordered at

http://www.dekker.com/servlet/product/DOI/101081MC100101428